UNIVERSIDADE FEDERAL DE SANTA CATARINA
TECHNOLOGICAL CENTER
ELECTRICAL ENGINEERING GRADUATE PROGRAM

Kenny Vinente dos Santos

Dual Dynamic Integer Programming Applied to Short-Term Power Generation Scheduling with Detailed Hydropower Production Function

Florianópolis
2022

Kenny Vinente dos Santos

Dual Dynamic Integer Programming Applied to Short-Term Power Generation Scheduling with Detailed Hydropower Production Function

Doctoral Thesis submitted to the Electrical Engineering Graduate Program of the Universidade Federal de Santa Catarina as a requirement for obtaining the Degree of Doctor of Electrical Engineering.
Supervisor:: Prof. Erlon Cristian Finardi, Dr.

Florianópolis
2022

Ficha de identificação da obra elaborada pelo autor,
através do Programa de Geração Automática da Biblioteca Universitária da UFSC.

Vinente dos Santos, Kenny
Dual Dynamic Integer Programming Applied to Short-Term Power Generation Scheduling with Detailed Hydropower Production Function / Kenny Vinente dos Santos ; orientador, Erlon Cristian Finardi , 2022.
140 p.

Tese (doutorado) - Universidade Federal de Santa Catarina, Centro Tecnológico, Programa de Pós-Graduação em Engenharia Elétrica, Florianópolis, 2022.

Inclui referências.

1. Engenharia Elétrica. 2. Programação Linear Inteira Mista. 3. Problema da Programação Diária da Operação Eletroenergética. 4. Programação Dinâmica Dual Determinística Inteira. I. , Erlon Cristian Finardi. II. Universidade Federal de Santa Catarina. Programa de Pós-Graduação em Engenharia Elétrica. III. Título.

Kenny Vinente dos Santos

Dual Dynamic Integer Programming Applied to Short-Term Power Generation Scheduling with Detailed Hydropower Production Function

This Doctoral Thesis has been evaluated and approved by the examining committee composed of the following members:

Prof. André Luiz Diniz Souto Lima, Dr.
Centro de Pesquisas de Energia Elétrica - Eletrobras

Prof. Cláudia Alejandra Sagastizábal, D. Habil.
Instituto de Matemática, Estatística e Computação Científica - Unicamp

Eng. Guilherme Matiussi Ramalho, Dr.
Câmara de Comercialização de Energia Elétrica

We certify that this is **the original and final version** of the Doctoral Thesis, which was deemed suitable to obtain the Doctor of Electrical Engineering degree.

ICP-Edu
Documento assinado digitalmente
Telles Brunelli Lazzarin
Data: 04/11/2022 14:34:33-0300
CPF: ***.400.719-**
Verifique as assinaturas em https://v.ufsc.br

Prof. Dr. Telles Brunelli Lazzarin
Coordinator
Universidade Federal de Santa Catarina

ICP-Edu
Documento assinado digitalmente
Erlon Cristian Finardi
Data: 25/10/2022 13:11:47-0300
CPF: ***.364.749-**
Verifique as assinaturas em https://v.ufsc.br

Prof. Dr. Erlon Cristian Finardi
Advisor
Universidade Federal de Santa Catarina

Florianópolis, 2022.

This thesis is dedicated to my family and my friends.

ACKNOWLEDGEMENTS

I would like to thank my advisor Erlon Finardi, for receiving me as Ph.D. student after so many years before our first conversation. In special, I am very grateful for his mentoring, support, criticism and opportunities to research in power systems, initially an unknown area for me. Obviously, I must to emphasize his good sense of humor and professionalism. Particularly, i feel very honored to be your student along these years, and I hope that our friendship and professional relationship will continue over the years.

Thanks to my advisor, I was able to meet other professors who inspire me. I could not fail to express my deep gratitude to professors Ildemar Decker, Cláudia Sagastizábal and Paulo Silva, who, like my advisor, help me professionally and sometimes personally. All of you are truly inspirations for me.

I am grateful to my thesis committee, Prof. André Diniz, Profa. Cláudia Sagastizábal and Guilherme Matiussi, for their wisdom, patience, guidance and expertise. It was an honor for me to have them in my committee.

I would like to acknowledge the financial support by Universidade Federal do Amazonas for allowing me to be a Ph.D. student and keeping my job without prejudice; this research have financial support of CAPES and Norte Energia through the P&D research project SPARHTACUS II, which I would like to thank.

During the final years of my Ph.D. research, I was fortunate to collaborate with Prof. Victor Zavala. I am very grateful to him for the great ideas and feedbacks which helped me to improve my researches and my thesis. In particular, I would like to thank you for introducing me to the DDiP.

I would like to thank my family, and in particular my mom, Profa. Estrela Vinente for being an inspiration on how education changes lives, and for creating me and taking care of me.

Finally, I thank all my friends of Labplan and Labspot: Brunno Brito, Bruno Colonetti, Clayrton Henrique, Dalton Casamali, Fábio Mantelli, Felipe Béltran, Gabriel Bolacelli, Gilseu Von Muhlen, Guilherme Fredo, Guilherme Matiussi, Larah Ascari, Leonardo Costa, Marcelo Cordova, Pedro Vieira, Renata Pedrini, Rodrigo Vaz, Sandy Tolo, Sara Medeiros, Thiago Santos and Vitor Antunes. A special thanks to Paulo Larroyd and Vitor Matos from Norus Energy, and Murilo Scuzziato from IFSC, which I have the opportunity to work in the SPARHTACUS II project.

“Try not to become a man of success, but rather try to become a man of value.”
(EINSTEIN, 20th century)

RESUMO

O problema da Programação Diária da Operação tem como objetivo estabelecer a geração de energia das usinas hidrotérmicas ao longo de um horizonte de até uma semana a serem utilizadas como referência na operação em tempo real para o dia seguinte. Considerando o sistema elétrico brasileiro, este problema se torna complexo, devido a diversos fatores, como o grande número de usinas hidrelétricas e termelétricas, as dimensões do sistema de transmissão e a participação de fontes intermitentes. Para minimizar as diferenças entre os resultados obtidos na programação diária e a operação em tempo real, faz-se necessário que o modelo da programação diária seja aderente, considerando um alto nível de detalhamento nos componentes do sistema. Desta forma, no caso brasileiro, é importante que este modelo leve em consideração uma formulação detalhada das usinas hidrelétricas, incluindo restrições de *unit commitment* hidráulico. Neste contexto, o problema de otimização resultante será de grande porte e de difícil resolução. Todavia, do ponto de vista do operador do sistema, espera-se que a resolução deste problema seja efetuada em tempo computacional curto. Para contornar estas dificuldades, neste trabalho são apresentadas formulações detalhadas para a função de produção hidrelétrica, levando em consideração características não-lineares e descontínuas, a partir de modelos lineares-inteiros mistos. Em seguida, é proposta uma estratégia de decomposição temporal para o problema da programação diária conhecida como programação dinâmica dual determinística inteira. Ainda, para reduzir a complexidade computacional do problema de otimização resultante, são apresentadas propostas de agregação temporal e simplificação de modelo que quando aplicadas ao final do horizonte de planejamento, causam pequenas distorções nas decisões obtidas para o dia seguinte. A partir dos experimentos computacionais, observou-se: (i) é possível utilizar uma formulação detalhada da função de produção hidrelétrica com base em modelo agregado que apesar de aumentar o esforço computacional, entrega resultados aderentes com a formulação original não-linear; (ii) a programação dinâmica dual determinística inteira é uma estratégia de decomposição válida para este tipo de problema, possibilitando a decomposição temporal do problema e consequentemente, reduzindo o esforço computacional; e (iii) utilizar estratégias de agregação temporal reduzem significativamente o esforço computacional e entregam soluções próximas ao do problema original para o dia seguinte.

Palavras-chave: Programação Diária da Operação. Função de Produção Hidrelétrica. Programação Dinâmica Dual Determinística Inteira. Programação Linear Inteira Mista.

RESUMO EXPANDIDO

Introdução

O problema do Planejamento da Operação Energética (PDE) tem como objetivo estabelecer políticas de operação das usinas do sistema em um horizonte de planejamento plurianual. Normalmente, por se tratar de um problema de otimização de grande porte, com características estocásticas e não-lineares, este problema é dividido em uma série de problemas acoplados entre si. Dentre estes, a Programação Diária da Operação (PDO) é o problema final da cadeia de modelos, que tem como objetivo estabelecer a programação das unidades geradoras e intercâmbios de energia entre sistemas para um horizonte de até uma semana, utilizando as políticas operativas estabelecidas no problema de curto prazo. Neste contexto, na PDE faz-se necessário um nível de detalhamento elevado dos componentes do sistema, uma vez que as decisões obtidas neste problema serão utilizadas como referência para a operação em tempo real. Devido as características do sistema elétrico brasileiro, é importante representar com fidelidade a função de produção hidreléetrica (FPH), sendo esta a primeira contribuição deste trabalho. Uma vez que a PDO é resolvida diariamente pelo operador do sistema, em um esquema de horizonte rolante, é crucial que este problema seja resolvido de maneira rápida e eficiente. Para atender este requisito, neste trabalho aplicamos a estratégia de decomposição conhecida como Programação Dinâmica Dual Determinística Inteira (PDDDi). Por fim, neste trabalho aplicamos estratégias de agregação temporal e simplificação de modelo, que causam pequenas alterações nas decisões obtidas para o dia seguinte, mas que reduzem significativamente o esforço computacional da resolução do problema da PDO.

Objetivos

Propor formulações detalhadas para a função de produção hidrelétrica, além de estratégias eficientes para a resolução do problema da PDO em um sistema hidrotérmico de grande porte.

Metodologia

As metodologias de solução propostas neste trabalho podem ser divididas em técnicas de decomposição temporal e resolução do problema sem decomposição. Para o caso sem decomposição, avaliou-se o esforço computacional para diferentes formulações da FPH que incluem o *unit commitment* hidráulico e faixas operativas, bem como a qualidade da solução obtida em comparação com a formulação não-linear original. Ainda, foram utilizadas técnicas de agregação temporal baseadas em *k*-means, espaçamento uniforme e *diffusing horizon*, além de simplificações de modelo realizadas ao final do horizonte de planejamento, visando reduzir o esforço computacional do problema da PDO com horizonte semanal sem distorcer as soluções obtidas para o dia seguinte. Em termos de decomposição, foi aplicada a PDDDi em casos em que os subproblemas podem conter múltiplos períodos de tempo, podendo ou não ter sobreposição entre estes. Diferentes simulações são apresentadas para os tópicos abordados nesta tese, em que o esforço computacional e a qualidade da solução obtida são analisados e utilizados como critério de avaliação.

Resultados e Discussão

Formulações detalhadas dos principais componentes do sistema e resolução rápida da PDO são objetivos de interesse do operador do sistema. A representação detalhada da FPH, através de um modelo agregado que considera faixas operativas e não-linearidades, apresentou resultados que divergem menos de 5% quando comparados com o modelo não-linear original. Como há um aumento na complexidade computacional, também propomos uma estratégia para escolher um subconjunto das usinas hidrelétricas que tem maior impacto no sistema para possuírem uma representação mais detalhada, em que esta estratégia se mostrou satisfatória nas simulações realizadas. Em termos de decomposição temporal, a DDiP se mostrou eficiente para o sistema utilizado para o caso multiperíodo e com sobreposição, obtendo redução computacional na ordem de até quatro vezes, utilizando *gap* de otimalidade de 0,5%. E em relação as simplificações utilizadas na PDO, quando realizamos relaxações das restrições de integralidade e estratégias de agregação temporal em dois ou mais dias do horizonte final de planejamento, observa-se uma redução no esforço computacional de pelo menos 40%, ao preço de ter distorções médias nas soluções obtidas para o dia seguinte da ordem de 1,5%.

Considerações Finais

O aprimoramento na formulação da FPH traz benefícios na solução obtida, e pode ser implementado para um certo subconjunto de usinas hidrelétricas que causam mais impacto na operação, sem comprometer significativamente o esforço computacional do problema da PDO. Além disso, a decomposição por PDDDi e as estratégias de agregação temporal reduzem significativamente o esforço computacional do problema, possibilitando que formulações mais detalhadas dos componentes do sistema possam ser utilizadas na PDO.

Palavras-chave: Programação Diária da Operação. Função de Produção Hidrelétrica. Programação Dinâmica Dual Determinística Inteira. Programação Linear Inteira Mista.

ABSTRACT

The short-term power generation scheduling (STGS) aims to establish the power generations of the hydro-thermal plants in a planning horizon up to one-week, which will be used as a reference to the day-ahead real-time operation. For the Brazilian power system, this problem is complex due to many factors, such as the high number of hydropower and thermoelectric plants, the dimensions of the transmission system and the participation of the renewable sources. To minimize the differences between the results obtained in the short-term planning and the real-time operation, it is necessary that the short-term power generation model be adherent, considering a high level of details in the system's components. Therefore, for the Brazilian case, it is important that model account a detailed formulation for the hydropower plants, including hydro unit commitment constraints. In this context, the resulting optimization problem will be a large-size problem, which is hard to solve. However, from the point of view of the system operator, it is expected that this problem will be solved in a short computational time. To overcome these difficulties, in this work are presented detailed formulations for the hydropower production function, accounting the nonlinearities and discontinuities characteristics, through mixed-integer linear models. Then, is proposed a temporal decomposition strategy for the STGS problem known as dual dynamic integer programming. In addition, to reduce the computational complexity of the resulting STGS optimization problem, in this thesis are presented temporal aggregation strategies and model simplifications which when applied at the end of the planning horizon, cause slight distortions in the decisions obtained for the day-ahead. From the computational simulations, is possible to observe: (i) it is possible to use detailed formulation for the hydropower production function based in a plant-based model which despite the increase in the computational effort, delivers results more adherent with the original non-linear formulation; (ii) the dual dynamic integer programming is a valid decomposition strategy for this type of problem, allowing temporal decomposition and as consequence, reducing the computational effort; and (iii) the use of temporal aggregation and model simplifications provides significantly reduce in the computational effort and delivers near solutions for the day-ahead when compared with the original STGS problem.

Keywords: Short-Term Power Generation Scheduling. Hydropower Production Function. Dual Dynamic Integer Programming. Mixed-Integer Linear Programming.

LIST OF FIGURES

Figure 1 – Example of variables used in the water balance equation 37
Figure 2 – HPF of a 3-unit plant ignoring the forbidden zones 45
Figure 3 – HPF of a 3-unit plant with forbidden zones 46
Figure 4 – Upper limits of a 3-unit plant using the CH model 48
Figure 5 – Upper limits of a 3-unit plant using the BCH model 48
Figure 6 – Upper and lower limits for HPF of a 3-unit plant using the CH-2 model 49
Figure 7 – Hyperplanes for HPF of a 3-unit plant using the PCH model 51
Figure 8 – HPF for the 3-unit plants as function of Q for fixed volumes 51
Figure 9 – HPF considering fixed volumes V_0, V_1, V_2 52
Figure 10 – Detail of HPF in the turbined outflow range $(415.5, 516)$ m^3/s 53
Figure 11 – Different HPFs for 3-unit plant considering fixed volume 56
Figure 12 – Detail on the turbined outflow range (415.5, 516) m^3/s 57
Figure 13 – Values of objective functions obtained from simulations 62
Figure 14 – Computational time spent of simulations 63
Figure 15 – Thermoelectrical generation in subsystem 2 for $\gamma = 30$ and $\mathbf{Y}_0$ 64
Figure 16 – Scheduled generation of Foz do Chapecó plant 65
Figure 17 – Example of single, multi-period and aggregated stages 69
Figure 18 – Schematic of optimization problems with a particular structure. . . . 70
Figure 19 – Schematic of Benders decomposition 71
Figure 20 – Example of Nested Benders Decomposition 73
Figure 21 – An overview of the DDiP scheme at iteration k 75
Figure 22 – DDIP with a pre-solve step 78
Figure 23 – Some multi-periods stages for a MILP 79
Figure 24 – Illustration of overlap decomposition scheme with no multi-period strategy 80
Figure 25 – Illustration of overlap decomposition scheme with multi-period strategy 80
Figure 26 – Optimality gap and CPU Time for s-DDiP 83
Figure 27 – Optimality gap and CPU Time for a-DDiP 84
Figure 28 – DDiP performance for cases with different values of K. 86
Figure 29 – Optimality gap and CPU time for s-DDiP 87
Figure 30 – Optimality gap and CPU time for a-DDiP 88
Figure 31 – Impact of overlap constraints in the DDiP for cases $K = 12$ and $K = 24$ 90
Figure 32 – DDiP performance for cases with different values of P and $K = 12$. . 90
Figure 33 – DDiP performance for cases with different values of P and $K = 24$. . 91
Figure 34 – Number of active thermal plants for the first 24 hours of the planning horizon, considering cases $K = 168$, s-DDIP, a-DDIP with $K = 24$, $P = 0$ 93

Figure 35 – Thermal plant generation for cases $K = 168$, s-DDiP, a-DDiP with $K = 24$, $P = 0$ 94
Figure 36 – Hydro generation for cases $K = 168$, s-DDiP, a-DDiP with $K = 24$, $P = 0$ 95
Figure 37 – Overview of the different planning horizons in the GS problems of Brazilian case 99
Figure 38 – Original and Quantized Load Curve With 3 Levels 101
Figure 39 – Temporal Resolution of STGS problem 102
Figure 40 – Different time aggregation strategies. 103
Figure 41 – Example of different temporal aggregations performed in a period constituted of 24 hours. 104
Figure 42 – Example of least and most expensive cases when temporal aggregation is performed 105
Figure 43 – Example of temporal aggregation for the thermoelectric uptime constraint. 106
Figure 44 – Thermoelectric generation scheduled in the planning horizon with MS-1, MS-2, and MS-3 for cases with $T = 144$. 108
Figure 45 – Thermoelectric generation for the first 24 hours with MS-1, MS-2, and MS-3 for cases with $T = 144$. 108
Figure 46 – Hydro generation for the first 24 hours with MS-1, MS-2, and MS-3 for cases with $T = 144$. 109
Figure 47 – Thermoelectric generation for the first 24 hours with model simplifications for case MS-1. 110
Figure 48 – Thermoelectric generation for the first 24 hours for case TA-1-ME with $T = 96$. 112
Figure 49 – Thermoelectric generation for the first 24 hours for case TA-1-LC with $T = 96$. 112
Figure 50 – Thermoelectric generation for the first 24 hours for case TA-2-ME with $T = 120$. 114
Figure 51 – Thermoelectric generation for the first 24 hours for case TA-2-LC with $T = 120$. 114
Figure 52 – Thermoelectric generation for the first 24 hours for case TA-3-ME with $T = 96$. 116
Figure 53 – Thermoelectric generation for the first 24 hours for case TA-3-LC with $T = 96$. 116
Figure 54 – Thermoelectric generation for the first 24 hours for cases with model simplifications and temporal aggregations with $T = 120$. 118
Figure 55 – Demand curve of modified IEEE-118 system 133

LIST OF TABLES

Table 1 – Summary of different STGS problems that applied BD 28
Table 2 – Number of variables and constraints in STGS problem 42
Table 3 – HPF models and their characteristics. 56
Table 4 – Characteristics of hydro plants 59
Table 5 – Number of partitions for each NFZ and PWL model chosen 61
Table 6 – Information about the optimization problems 61
Table 7 – Violations due to the operation on forbidden zones for simulations with CH-2 model. 64
Table 8 – Violations due to the operation on forbidden zones for simulations with BCH-2 model. 65
Table 9 – Results for different parameters of PWL formulation. 66
Table 10 – Number of variables and constraints in STGS problem 81
Table 11 – Summary of results obtained for s-DDiP. 83
Table 12 – Summary of results obtained for a-DDiP. 85
Table 13 – Summary of results obtained for s-DDiP with $K = 1$. 88
Table 14 – Summary of results obtained for a-DDiP with $K = 1$. 89
Table 15 – Summary of results obtained of DDiP for different P values with $K = 12$ and $K = 24$. 91
Table 16 – Summary of results obtained of DDiP for case with $\mathbf{Y}^{+}$. 92
Table 17 – Summary of results obtained of DDiP for case with $\mathbf{Y}^{-}$. 92
Table 18 – Summation of all slack variables for simulations with different sizes of stages. 96
Table 19 – Summation of all slack variables for simulations with different overlap sizes. 96
Table 20 – Simplifications that can be applied to the STGS problem 102
Table 21 – Summary of problem statistics for simulations with model simplifications 107
Table 22 – Summary of problem statistics for simulations with temporal aggregations case TA-1-LC 111
Table 23 – Summary of problem statistics for simulations with temporal aggregations case TA-1-ME 111
Table 24 – Summary of statistics problem for simulations with temporal aggregations case TA-2-LC 113
Table 25 – Summary of problem statistics for simulations with temporal aggregations case TA-2-ME 113
Table 26 – Summary of problem statistics for simulations with temporal aggregations case TA-3-LC 115

Table 27 – Summary of problem statistics for simulations with temporal aggregations case TA-3-ME 115
Table 28 – Summary of problem statistics for simulations with model simplifications, temporal aggregations using the *k*-means approach 117
Table 29 – Summary of problem statistics for simulations with model simplifications, temporal aggregations using the equal-spacing approach . . . 117
Table 30 – Summary of problem statistics for simulations with model simplifications, temporal aggregations using the diffusing-horizon approach . . 118
Table 31 – Hourly load data 134
Table 32 – Thermoelectric removed from IEEE 118-bus system 135
Table 33 – Hydroelectric data 135
Table 34 – Coefficients of hydroelectric forebay level polynomials 136
Table 35 – Coefficients of hydroelectric tailrace level polynomials 136
Table 36 – Coefficients of GU yield polynomials referring to hydro *h* 137
Table 37 – Coefficients of GU penstock losses referring to hydro *h* 137
Table 38 – Reservoir data 138
Table 39 – Initial conditions of hydro plants 138
Table 40 – Inflow data (m^3/s) 139
Table 41 – Coefficients of FCF 139

LIST OF ABBREVIATIONS AND ACRONYMS

BD	Benders Decomposition
CH	Convex Hull
DDiP	Dual Dynamic Integer Programming
DH	Diffusing-horizon
EDS	Exponential Decay of Sensitivity
FCF	Future Cost Function
GS	Generating Scheduling
GU	Generating Unit
HPF	Hydropower Production Function
IPWL	Interval Piecewise Linear
LP	Linear Programming
LR	Lagrangian Relaxation
LTGS	Long-term Power Generation Scheduling
MILP	Mixed-integer Linear Programming
MINLP	Mixed-integer Nonlinear Programming
MISOCP	Mixed-integer Second-Order Cone Programming
MP	Master Problem
MPC	Model Predictive Control
MTGS	Medium-term Power Generation Scheduling
NBD	Nested Benders Decomposition
NCHTUC	Network-constrained Hydrothermal Unit Commitment
NFZ	Non-Forbidden Zone
NLP	Nonlinear Programming
ONS	Brazilian Independent System Operator
OPF	Optimal Power Flow
PWL	Piecewise-linear
SDDiP	Stochastic Dual Dynamic Integer Programming
SDDP	Stochastic Dual Dynamic Programming
SDP	Semidefinite Programming
SIN	Brazilian Electric Power System
SOCP	Second-Order Cone Programming
SP	Subproblem
STGS	Short-term Power Generation Scheduling
UC	Unit Commitment

LIST OF SYMBOLS

Indices

b	index of buses.
g	index of thermal plants.
h	index of hydro plants.
i	index of non-forbidden zones.
j	index of hydro generating units.
l	index of transmission lines.
p	index of polytopes.
ref	index of reference bus.
t	index of periods (hours).

Sets

$\mathcal{B}$	buses.
$\mathcal{B}_b$	buses connected to bus b.
$\mathcal{G}$	thermal plants.
$\mathcal{H}$	hydro plants.
$\mathcal{I}$	operating zones of hydropower production function.
$\mathcal{L}$	transmission lines.
$\mathcal{P}$	polytopes used in the PWL model of hydropower production function.
$\mathcal{S}$	points in the volume $\times$ turbine discharge grid.
$\mathcal{T}$	periods.
$\mathcal{U}_b$	hydro and thermal plants connected to bus b.
Ψ	set of reservoirs that are in the FCF.
Ω_h	hydro plants upstream of hydro h.

Variables

fbl_{ht}	forebay level of hydro h in period t (m).
nh_{jht}	net head of unit j, hydro h in period t (m).
php_{ht}	power output of hydro h in period t (p.u. of MW).
php^{*}	value of php in the upper limit (p.u. of MW).
php^{**}	value of php in the lower limit (p.u. of MW).
phu_{jht}	power output of unit j, hydro h in period t (p.u. of MW).
pl_{lt}	active power in transmission line l in period t (p.u. of MW).
pt_{gt}	power output of thermal plant g in period t (p.u. of MW).
q_{jht}	turbine discharge of unit j, hydro h in period t (m^3/s).
Q_{ht}	turbine discharge of hydro h in period t (m^3/s).
S_{ht}	spillage of hydro h in period t (m^3/s).
trl_{ht}	tailrace level of hydro h in period t (m).
u_{gt}	binary variable indicating the on/off status of unit j, hydro h in period t.
V_{ht}	reservoir volume of hydro h at period t (hm^3).

w_{gt} binary variable indicating the shutdown of thermal plant g in period t.
x_{gt} binary variable indicating the on/off status of thermal plant g in period t.
y_{ht} binary variable indicating the on/off status of hydro h in period t.
z_{gt} binary variable indicating the startup of thermal plant g in period t.
α variable related to the future cost function.
β_l correction factor of interval k used to estimate the dependence of volume in the PWL-2 model (p.u. of MW/hm^3).
η_{jht} turbine efficiency of unit j, hydro h in period t.
θ_{bt} voltage angle of bus b in period t (radians).

Parameters

$\mathbf{a}_{mhk}$ approximated upper bound related to hydro production function coefficients for m = {0,1,2}, hydro h and hyperplane k.
$\mathbf{b}_{mhk}$ approximated lower bound related to hydro production function coefficients for m = {0,1,2}, hydro h and hyperplane k.
$\mathbf{C0}_g$ unitary variable cost of thermal plant g ($/p.u. of MW).
$\mathbf{C1}_g$ fixed cost of thermal plant g ($).
$\mathbf{C2}_g$ startup cost of thermal plant g ($).
$\mathbf{C3}_g$ shutdown cost of thermal plant g ($).
$\mathbf{D}_{jh}$ constant related to the hydraulic loss function of unit j and hydro h (s^2/m^5).
$\mathbf{DT}_g$ minimum downtime of thermal plant g (h).
$\mathbf{F}_{mh}$ constant related to the forebay function of hydro h and m = {0,1,2,3,4}.
$\mathbf{G}_{mh}$ constant related to the tailrace function of hydro h and m = {0,1,2,3,4}.
$\mathbf{I}_{mjh}$ constant related to the turbine efficiency function of unit j, hydro h and m = {0,1,2,3,4}.
$\mathbf{K}$ constant that converts water flow (m^3/s) to volume (hm^3).
$\mathbf{M0}_{hk}$ angular coefficient of hydro h concerning the k-th equation of future cost function ($/hm^3).
$\mathbf{M1}_k$ independent term of the k-th linear equation of future cost function ($).
$\mathbf{N1}$ number of hyperplanes used to represent the upper bound of hydro production function.
$\mathbf{N2}$ number of hyperplanes used to represent the lower bound of hydro production function.
$\mathbf{NC}$ number of linear equations used to represent the future cost function.
$\mathbf{NG}$ number of thermal plants.
$\mathbf{NH}$ number of hydro plants.
$\mathbf{NJ}_h$ number of units of hydro h.
$\mathbf{NT}$ number of hours of the planning horizon.
$\mathbf{P}_{bt}$ demand of active power on bus b in period t (p.u. of MW).
$\mathbf{RD}_g$ maximum ramp-down of thermal plant g (p.u. of MW/h).
$\mathbf{RU}_g$ maximum ramp-up of thermal plant g (p.u. of MW/h).
$\mathbf{SR}_t$ system reserve in period t (p.u. of MW).
$\mathbf{UT}_g$ minimum uptime of thermal plant g (h).
$\mathbf{x}_{ab}$ reactance of the transmission line, which connects buses a and b (p.u.).
$\mathbf{Y}_{ht}$ incremental inflow of hydro h in period t (m^3/s).
$\tau_{h_1 h_2}$ water traveling time between hydro plants h_1 and h_2 (h).

CONTENTS

1	**INTRODUCTION**	**20**
1.1	LITERATURE REVIEW IN STGS PROBLEMS AND HPF FORMULATIONS	24
1.2	LITERATURE REVIEW IN SOLVING STGS PROBLEMS VIA PRIMAL DECOMPOSITION	27
1.3	OBJECTIVES	31
1.4	STRUCTURE OF THE WORK	33
2	**MATHEMATICAL FORMULATION OF STGS PROBLEM**	**35**
2.1	HYDROELECTRIC PLANT MODEL	35
2.2	THERMOELECTRIC PLANT MODEL	37
2.3	NETWORK MODEL	38
2.4	FULL FORMULATION OF STGS PROBLEM	40
2.5	FINAL CONSIDERATIONS	42
3	**DETAILED FORMULATIONS FOR PLANT-BASED HPF**	**44**
3.1	THE PLANT-BASED HPF MODEL	44
3.2	ENVELOPE MODELS	46
3.3	PWL MODELS	50
3.4	ASSESSING HPF MODELS	54
3.5	COMPUTATIONAL EXPERIMENTS	57
3.5.1	**Generation of the Set of Polytopes**	**58**
3.5.2	**Results**	**60**
3.6	FINAL CONSIDERATIONS	66
4	**DUAL DYNAMIC INTEGER PROGRAMMING APPLIED TO STGS PROBLEM**	**68**
4.1	DECOMPOSITION METHODS AND BENDERS DECOMPOSITION	68
4.2	NESTED BENDERS DECOMPOSITION AND DUAL DYNAMIC INTEGER PROGRAMMING	72
4.3	IMPROVEMENTS ON DDIP	77
4.3.1	**Pre-solve Strategy for DDIP**	**77**
4.3.2	**Multi-period Strategy and Overlap**	**78**
4.4	COMPUTATIONAL EXPERIMENTS	81
4.4.1	**Data and Initial Setup**	**81**
4.4.2	**Influence of the size of stages**	**82**
4.4.3	**Impact of overlapping constraints**	**86**
4.4.4	**Assessment of primal solutions**	**92**
4.5	FINAL CONSIDERATIONS	96

5 ASSESSING TEMPORAL AGGREGATIONS AND MODEL SIMPLIFICATIONS IN THE STGS PROBLEM 98
5.1 AGGREGATION METHODS 98
5.2 MODEL SIMPLIFICATIONS AND TEMPORAL AGGREGATIONS FOR THE STGS PROBLEM 101
5.3 COMPUTATIONAL EXPERIMENTS 105
5.3.1 Assessing impacts of model simplifications 106
5.3.2 Assessing impacts of temporal aggregations 110
5.3.3 Assessing impacts of model simplifications and temporal aggregations 117
5.4 FINAL CONSIDERATIONS 118
6 CONCLUSIONS 120
REFERENCES 123
APPENDIX A – DATA OF MODIFIED IEEE 118-BUS SYSTEM . . . 133
APPENDIX B – MILP FORMULATION FOR THE PRODUCT BETWEEN A CONTINUOUS AND A BINARY VARIABLE 140

1 INTRODUCTION

Energy production and consumption are important pillars of modern society. Consumption is not only the basis of all industrial activity, but also serves as an indicator of economic growth and social welfare and is needed for fundamental activities such as emergency services and hospitals (BARBIR; ULGIATI, 2008). Thus, energy production standards must adhere to consumers' economic and reliability regulations. In general, large-scale energy production is performed by different types of power plants, such as hydroelectric, thermoelectric, wind, solar, and biomass plants. Depending on the country, energy production is predominantly based on one of these technologies.

Due to hydrological availability and historical aspects, the Brazilian power system is based on hydro generation, complemented by thermoelectric and wind resources. In operational terms, the schedule of energy production is perfoemd by the Brazilian Independent System Operator (ONS). Due to the Brazilian Electric Power System (SIN) being a large-size hydro-thermal-wind system with hydropower plants distributed among several hydrographic basins across the country, often far from the largest loads, the generation scheduling is a complex task, and it is divided in several steps to manage the intrinsic challenges. Also, the hydro plants provide an essential role in energy security (e.g., emergency energy due to an outbreak) and produce renewable and low-cost energy. Finally, there has been a significant increase in wind power generation in the last years in Brazil, mainly located in the northeast and south regions.

All plants and consumption centers are interconnected by a transmission system containing many transmission lines that transport the energy to the main load centers. This transmission system must be robust to ensure continuity of power supply. In quantitative terms, in the Brazilian case, there is a participation of 60.6% from the hydro plants, 22.6% from thermal plants, 12.3% from wind farms, and 4.5% from other sources (ONS, 2021). The ONS employs the Generation Scheduling (GS) problem (PEREIRA, 1985) to coordinate the Brazilian system's cenrtalized dispatch. The GS problem is hard to solve due to several SIN characteristics, as follows:

i. It is a large-scale problem due to the power system dimensions and long planning horizon.

ii. The temporal and spatial coupling is inherent in the problem.

iii. Has uncertainties due to the characteristics of demand, inflows, wind, and equipment failures.

iv. The generation resources have discontinuities, nonlinearities, and non-convexities associated with the operating characteristics.

Due to the features mentioned, the GS problem is divided into coordinated steps. The aim is to find a dispatch of the plants so that the expected cost is minimal, satisfying the requirements of demand supply and reliability of the system. In this context, the GS problem is divided into three subproblems, as described below.

- **Long-term Power GS (LTGS)**: in this subproblem, the study is performed on a 5-years horizon discretized in monthly steps. The LTGS is formulated as a stochastic optimization problem that considers the inflows' uncertainty over the planning horizon. Also, the expansion planning elements and a risk measure are included. Currently, ONS uses the NEWAVE optimization model (MACEIRA, M. et al., n.d.) to solve this problem. In the NEWAVE, the hydropower plants are represented by the energy equivalent reservoirs. The energy interchanges between the subsystems represent the transmission network, and three load levels represent the system demand. As one of the most important outputs, the NEWAVE supplies the future cost function (FCF)[1] (PEREIRA, 1989; PEREIRA; PINTO, L. M. V. G., 1991), which will be used as input data in the medium-term power GS problem.

- **Medium-term Power GS (MTGS)**: in this subproblem, the study is performed in a 2-month horizon, discretized in weekly steps in the first month and a monthly step in the second, taking into account the uncertainties of the inflows. The ONS uses the DECOMP optimization model (DINIZ et al., n.d.), representing the hydro plants individually with an accurate piecewise linear (PWL) model. The FCF obtained in the LTGS represents the operating costs incurred at the end of the second month. In addition, DECOMP considers energy interchanges between subsystems and internal electrical constraints, and the demand modeling is similar to the NEWAVE model. The individual generation of each plant, exchanges between the subsystems, and an FCF are examples of the output of DECOMP.

- **Short-term Power GS (STGS)**: This subproblem performs the day-ahead generation scheduling. The planning horizon is up to 1-week with variable time steps. The ONS uses the DESSEM optimization model (SANTOS et al., 2020) to solve the STGS. In DESSEM, the first day is discretized in half-hour steps, and the following days are discretized in hourly-variable steps. A single scenario represents the inflows, wind generation and demand. A linearized model represents the network. The hydro plants are represented individually by a PWL model obtained through a convex hull (CH) method.

[1] The FCF is a function that represents a value of the expected operational cost of the system as a function of the water stored in the reservoirs at the end of the planning horizon. In the Brazilian case, the FCF is used as a boundary condition to keep the coordination between the different steps of the GS problem.

For the thermal plants, the constraints associated with the unit commitment (UC), as the minimum generation, uptime and downtime, maximum up and down ramp rates, and maximum generation, are represented by a mixed-integer linear model. The value of water stored in the reservoirs is measured by the FCF supplied by DECOMP. The DESSEM solves an optimization problem called network-constrained hydrothermal unit commitment (NCHTUC), a large-scale Mixed-Integer Linear Programming (MILP) model, and provides, as a result, the day-ahead operation of the Brazilian system.

The STGS for the Brazilian case is challenging since the day-ahead scheduled decisions are expected to be close to the employed in real-time operation. This model uses detailed representations of the SIN characteristics from generators and the demand and electrical network. Such features imply a large-scale mixed-integer nonlinear programming (MINLP) problem, which is hard to solve. Thus, currently, simplifications are used to make this problem solvable in a reasonable execution time. Examples of simplifications used in the DESSEM model are the DC formulation for the network, linear approximations for the nonlinear hydropower production function (HPF)[2], and the representation of hydroelectric plants through plant-based models. Therefore, an important point is the quality of these approximations concerning the original nonlinear model.

Many of these challenges present in DESSEM still do not have satisfactory solutions, both from a mathematical and operational aspects. In this context, this work aims to specifically analyze the impact of the nonlinearities (and, as will be seen, the impact of discontinuities) of the HPF on the STGS problem. From this analysis, we intend to answer what are the consequences of using a less adherent model to the original formulation based on operating costs, violation of operational constraints, and computational effort.

The nonlinearities existing in nonlinear programming (NLP) problems can be dealt with in several ways. This thesis shows that a valid strategy to approximate the nonlinear HPF is the approximation through convex constraints, producing lower and upper envelopes. This approach is common in MINLP solvers based on spatial branch-and-bound and branch-and-reduce (BESTUZHEVA et al., 2021; TAWARMALANI; SAHINIDIS, 2005). Another valid approach that has recently been used is the interval piecewise linear (IPWL) approximation (VIELMA, 2015; GEISSLER; MARTIN; MORSI, 2012). In the non-convex case, binary variables are normally used to obtain a high-quality approximation. Both approaches mentioned have advantages and disadvantages, being the IPWL method more interesting when the functions under analysis depend on one or two

[2] The HPF is a key modeling point in the representation of the hydroelectricity, as it relates the amount of water available and the energy produced by the generating units.

variables. The recent improvements in MILP solvers also contribute to the possibility of applying more complex models and strategies.

The computational effort involved in solving the STGS problem, specifically the NCHTUC, is a relevant aspect from the operational point of view. Since ONS needs to run this model daily, the execution time of this model needs to be limited. A two-hour run timeout is currently used in DESSEM (SANTOS et al., 2020). Considering that the NCHTUC contains thousands of continuous and binary variables and thousands of constraints in the Brazilian case, this problem will hardly be solvable by modern optimization solvers within the established runtime without auxiliary solving techniques. In DESSEM, pre-processing strategies based on local branching and feasibility pump are employed. An iterative scheme of addition of violated constraints is used, aiming to find a high-quality feasible solution, near-optimal if possible. Although the results delivered by DESSEM meet the requirement of computational effort and solution quality, some aspects could still be improved, e.g., using binary variables to represent the hydro UC and the consequent computational impacts. Since most SIN generation comes from hydroelectric plants, it makes sense to have more accurate representations of this type of generation.

When solving large-scale MILP problems, the GS typically employs decomposition techniques that help solve the problem (CONEJO et al., 2006). These strategies are normally classified in primal and dual decomposition techniques. While the primal decomposition strategy focuses on complicating variables, the dual decomposition acts on complicating constraints. Dual decomposition techniques aim to break the original problem into a set of subproblems (SP) that are typically easy to solve, finding a set of dual variables that maximizes a dual function. A difficulty associated with this type of strategy is that a primal feasible solution is not obtained at the end of execution of the dual decomposition, being necessary a phase to obtain a primal feasible solution, called primal recovery strategy (BELLONI et al., 2003).

The recovery phase is unnecessary in the primal decomposition strategy; however, the SP obtained is typically harder to solve than those obtained in the dual decomposition. In particular, the Benders Decomposition (BD) (GEOFFRION, 1972) is a classic method used to solve MILP problems that present a subset of continuous and binary complicating variables. When this strategy is applied to a MILP problem, a master problem (MP) contains the complicating variables and a linear programming (LP) SP contains the remaining terms of the original optimization problem not included in the MP. The coordination between the MP and SP is done through Benders cuts obtained in the SP from the dual variables, considering the decisions from the MP for the complicating variables. As a result, the BD is a cutting-plane method and can present convergence issues (BONNANS et al., 2006). Acceleration strategies can be employed to enhance the convergence of BD, aiming to improve the Benders cuts obtained. However, even

with the acceleration strategy, the computational burden in BD is strongly affected by the MP, which usually contains mixed-integer variables.

In GS problems, a variant of BD known as stochastic dual dynamic programming (SDDP) (PEREIRA; PINTO, M. V. G., 1985) is a well-established method applied in multistage stochastic optimization problems, where a nested BD strategy is employed. From specific considerations of the problem (particularly regarding the realization of stochastic variables), the SDDP presents convergence guarantees and obtains the optimal solution (PHILPOTT; GUAN, Z., 2008). In the Brazilian case, SDDP is currently used to obtain a feasible solution of LTGS problem[3], providing the FCF used in subsequent steps. Recently, a strategy known as stochastic dual dynamic integer programming (SDDiP) (ZOU; AHMED; SUN, 2019b) was used to solve STGS problem modeled as a multistage stochastic optimization problem containing mixed-integer variables in the SP, obtaining a satisfactory performance in solving these problems.

The variant of SDDiP to deterministic problems, known as dual dynamic integer programming (DDiP), was recently applied in an LTGS modeled by a multistage optimization problem (LARA et al., 2018). In particular, the DDiP employs a temporal decomposition, aiming to obtain SPs that are easier to solve. The coordination between these SPs is done iteratively through forward and backward steps. As in GS problems, the temporal coupling is significant, and DDiP appears to be a promising method for solving this problem. In addition, when applied to STGS, the temporal decomposition allows more detailed formulations (e.g., detailed HPF) once the SPs obtained have less computational complexity. It is important to note that only a few works in the literature employed the DDiP in GS problems, and usually, the vanilla version of the DDiP is applied. In this sense, this work will implement the vanilla DDiP to obtain high-quality feasible solutions in the STGS problem. Also, different temporal decompositions and overlapping strategies will be used. With this framework, it is expected that high-quality feasible solutions of more complex STGS problems can be obtained in a reasonable computational time due to reduce the computational complexity of the SPs involved.

1.1 LITERATURE REVIEW IN STGS PROBLEMS AND HPF FORMULATIONS

Given that DESSEM uses an hour (or half-hour) time discretization, it is expected that the STGS problem solved needs more detailed information about the hydro-thermal-wind operation. This model has been officially discussed since 1998, and several works related to this model have already been produced over the years. Additionally, considering other countries in the world also solve the STGS problem, there is a vast work contribution in this research area. Regarding the dual decomposition strategy, works (FRANGIONI; GENTILE; LACALANDRA, 2008; MURILLO-SANCHEZ, C.;

[3] in fact, we don' t solve the stochastic optimization problem, instead we used strategies, such as SDDP, to obtain solutions that are considered satisfactory

THOMAS, n.d.; BELLONI et al., 2003; BORGHETTI; FRANGIONI; NUCCI, 2003) uses the Lagrangian decomposition to solve the deterministic version of the STGS problem, whereas in (FINARDI et al., 2020; RAZAVI et al., 2018; COLONETTI; FINARDI, 2021; ANSARI; AMJADY; VATANI, 2014; SCUZZIATO; FINARDI; FRANGIONI, 2018) different strategies are employed to solve the stochastic version of the STGS problem.

The hydrothermal nature of the STGS problem in the Brazilian case brings an additional challenge to this problem. In (FINARDI; SILVA, E. L., 2006), a hydro UC problem considering the nonlinearities of the forebay and tailrace levels, hydraulic losses, and yields of individual generating units is analyzed. The problem is modeled by an MINLP and decomposed via Lagrangian relaxation (LR), obtaining nonlinear subproblems for each hydro generating unit (GU), solved by sequential quadratic programming. The experiments are performed in a test system composed of 21 hydro plants from SIN, and the results show that the LR could be interesting in solving the Brazilian STGS problem.

An approach based on semidefinite programming (SDP) for the STGS problem with individual representation of hydro GUs, nonlinear HPF, and AC network constraints are presented (PAREDES; SOARES, 2015). The authors propose a reformulation of the original problem, replacing the integrality constraints with quadratic constraints and approximating the HPF by a quadratic model. As a result, this leads to a non-convex quadratic programming problem reformulated as an SDP with relaxed rank-1 constraints. Although the results presented in the paper are near-optimal, the SDP reformulation increases the dimension of the problem and significantly increases the computational complexity involved.

Creating a realistic HPF model is a significant challenge to the STGS problem for systems with hydropower predominance. Some difficulties are related to the trilinearity (efficiency $\times$ head $\times$ turbined outflow) and the forbidden operating zones of the GUs (these zones have more impact on plants with few GUs). Furthermore, systems under centralized cost-based dispatch possess hundreds of hydro GUs, and due to execution time limits, the HPF demands some simplification level. In this sense, according to (KONG; SKJELBRED; FOSSO, 2020), the plant-based HPF, where the units in a hydro plant are aggregated as an equivalent one, is the most employed modeling strategy for handling the computational effort even in cases that do not follow a centralized dispatch. The main advantage of using the plant-based concept is that it reduces the optimization problem significantly.

Several studies have used the HPF plant-based approach in UC or STGS problems (HAMANN; HUG; ROSINSKI, 2017; GUEDES et al., 2017; SEGUIN; COTE; AUDET, 2016; MARCHAND et al., 2018). The paper (DINIZ; MACEIRA, M. E. P., 2008) presents a four-dimensional PWL model of HPF as a function of volume (V), plant turbined outflow (Q) and spillage (S), and (DINIZ; SOUZA, 2014) use this same model

and includes the effects of river-level and routing constraints on the STGS problem. The PWL continuous formulation is obtained through a methodology based on CH. From the discretization of $V \times Q$ domain, a grid is built with the tuples (volume, plant turbined outflow, hydropower generated), and then the CH of these points is calculated. After that, the upper limits hyperplanes are selected, i.e., hyperplanes with the generation value consistently above the generation points from the grid. In sequence, a post-processing technique is performed to reduce the average error and to include the spillage.

Although this model considers some nonlinear HPF characteristics, the forbidden zones are not included. Therefore, an infeasible operation might be delivered by this approach. Also, because CH is a concave envelope for the HPF, the model can present a null generation even when Q is not zero. Furthermore, approximating a non-convex function by the convex approximation employed in the CH leads to linearization errors no matter how many segments are added. Despite that, this formulation is currently used in the DESSEM model (SANTOS et al., 2020).

In (CATALAO et al., 2009), a plant-based nonlinear approach is employed to the STGS problem in a deregulated market, where the head-dependency of the HPF is the main subject of study; in (CATALAO; POUSINHO; MENDES, 2010), an extension of this study to include on-off effects of the hydro plants, avoiding generation at forbidden areas is presented, resulting in an MINLP problem. In turn, (CATALAO; POUSINHO; MENDES, 2011) uses this same approach to include the start/stop of the units, discharge ramping constraints, and discontinuous operating regions. These works assume that the HPF has only one discontinuous region to account for the forbidden zones.

A special issue is that MINLP problems are usually hard to solve, even for small instances. Specifically, (CATALAO et al., 2009; CATALAO; POUSINHO; MENDES, 2010) proposes a MILP approach to find a starting point for the MINLP or even an optimal solution. The experiments are performed in a reduced configuration of the Portuguese power system. Although these works do not explicitly comment on why the authors did not use a large-size power system in their simulations, the computational complexity of solving an MINLP may be one of the main reasons.

Continuing the plant-based approach, the work (HAMANN; HUG; ROSINSKI, 2017) proposes a real-time optimization scheme for the Mid-Columbia hydropower system, consisting of seven hydro plants. The CH technique is used to linearize the nonlinear HPF, and auxiliary variables are used to model the generation and discharge of hydro plants. Then, a space-state model with continuous variables is built, and a model predictive control (MPC) problem is formulated. At this point, it is also essential to mention works (GUEDES et al., 2017; SEGUIN; COTE; AUDET, 2016; MARCHAND et al., 2018) that develop a plant-based HPF model considering the different groups of GUs.

With the recent advances in MILP solvers, the strategy to deal with nonlinear

functions as a MILP problem is becoming more popular. This strategy is generally employed (but not restricted) to univariate and bivariate functions due to the number of variables and constraints used in each approximation. Although not all nonlinear functions can be rewritten as PWL functions, this reformulation is valid in many problems. In particular, (KOCH et al., 2015) present this methodology in complex processes arising from the gas-network industry. Another reference where authors apply MILP techniques in PWL functions is (BALAKRISHNAN; GRAVES, 1989). Finally, an overview of different types of formulations for non-convex PWL functions as MILP problems, including non-separable functions, is presented in (VIELMA; AHMED; NEMHAUSER, 2010).

Recently, many works have applied the PWL formulation for the HPF. For example, the work (BRITO; FINARDI; TAKIGAWA, 2020) explores different MILP formulations applied for the HPF in a hydro UC problem with six GUs in a 24-hours horizon. The GUs are represented individually, and the HPF for each GU is linearized in the gross head $\times$ unit turbined outflow plane. Considering that a four-dimensional polynomial represents the Brazilian case's forebay and tailrace levels, the authors approximate the gross head by a linear function depending on volume, individual turbined outflow, and spillage.

Although the results show that the PWL reformulation for HPF can present high-quality solutions, the computational effort is significantly high for the dimension of the problem, and said the approach needs to be applied carefully in a large-size STGS problem with an elevated number of hydro plants or containing several time-periods.

The MILP reformulation for the nonlinear HPF in hydro generation problems is also applied in works (BORGHETTI et al., 2008; TONG; ZHAI; GUAN, X., 2013; LI, X. et al., 2014; JIA; GUAN, X., n.d.). One main concern in these works is the solution quality and the computational time required. Considering that the number of binary variables required to approximate an HPF can be high due to inherent nonlinear characteristics, especially in the bi-dimensional case, this approach can lead to computationally intractable problems. Despite this, the PWL formulation can be interesting to model HPF using the plant-based approach. Also, recently, MILP solvers are including such an approach, which allows for handling certain types of nonlinear optimization problems, including GUROBI (GUROBI, 2022).

1.2 LITERATURE REVIEW IN SOLVING STGS PROBLEMS VIA PRIMAL DECOMPOSITION

The STGS solution is used for several purposes in system operation, particularly as a reference point for real-time operation and determining the day-ahead spot prices. Despite being well-studied and utilized worldwide, the STGS still poses a considerable challenge because it needs to be solved quickly. This time-limit requirement contrasts with the inherent characteristics: the STGS is a large-scale, nonlinear and nonconvex optimization problem. Thus, the STGS needs to be simplified and formulated as a MILP

problem that modern optimization solvers can efficiently tackle when combined with decomposition strategies. This section reviews works that apply primal decomposition (specifically BD) in the STGS problem. Table 1 summarizes some characteristics of different STGS problems that apply BD found in works within the literature.

Table 1 – Summary of different STGS problems that applied BD

(continues)

Optimization Problem	**Characteristics**
Non-convex MINLP (BAI et al., 2015)	- Thermal UC with a 24-hour planning horizon discretized in 1-hour periods - MP: Mixed-integer second-order cone programming (MISOCP) with UC and relaxed AC Optimal Power Flow (OPF) constraints - SP: hourly AC OPF formulated as NLP problems - Benchmarks: IEEE 6-bus, modified 30-bus and 118-bus systems
Non-convex MINLP (AMJADY; ANSARI, 2013)	- Hydrothermal UC with a 24-hour planning horizon discretized in 1-hour periods - MP: MILP with UC constraints - SP: a bilevel problem where the first level is an hourly AC OPF formulated as a relaxed NLP problem and the second is a feasibility problem - Benchmarks: IEEE 9-bus and 118-bus systems - Use strong Benders cuts to improve the convergence of BD
MILP (ALEMANY; MAGNANO, 2015)	- Thermal UC with a 24-hour planning horizon discretized in 1-hour periods - MP: MILP with UC constraints - SP: hourly DC OPF problems - Benchmarks: IEEE 118-bus and RTS 96-bus systems - Use pre-processing strategy to generate initial cuts to improve the convergence of BD
MILP (SUNDAR et al., n.d.)	- Thermal UC with a 24-hour planning horizon discretized in 1-hour periods - MP: MISOCP with UC constraints - SP: scenario-based containing the DC OPF and the contingency probability, formulated as second-order cone programming (SOCP) - Benchmarks: IEEE RTS 96-bus system - Include N-1 security and wind uncertainty
Non-convex MINLP (NICK et al., 2016)	- Thermal UC with a 24-hour planning horizon discretized in 1-hour periods - MP: MILP with UC constraints - SP: hourly linearized AC OPF problems - Benchmarks: 5-bus and IEEE 118-bus systems - Include dynamic thermal line rating (approximated by convex constraints)

Table 1 - Summary of different STGS problems that applied BD

(conclusion)

Optimization Problem	**Characteristics**
Non-convex MINLP (LIU et al., 2019)	- Thermal UC with a 24-hour planning horizon discretized in 1-hour periods - MP: MISOCP with UC and relaxed AC OPF constraints - SP: multiperiod AC OPF problem - Benchmarks: 6-bus, two 24-bus, RTS-79, RTS-96 and a modified IEEE 118-bus systems - Use multi-tree global optimization, optimization-based bound tightening, SOCP relaxations and piecewise outer approximations to guarantee a globally optimal solution
MILP (XU, Y. et al., 2015)	- Thermal UC with a 24-hour planning horizon discretized in 1-hour periods - MP: MILP with UC constraints - SP: hourly DC OPF and transient stability problems - Benchmarks: New England 10-machine and IEEE 50-machine systems - Include transient stability constraints
Non-convex MINLP (NASRI et al., 2016)	- Thermal UC with a 24-hour planning horizon discretized in 1-hour periods - MP: MILP with UC constraints - SP: hourly/wind scenario AC OPF problems - Benchmarks: IEEE RTS-24 bus system - Include uncertainty due to wind
MILP (HEDMAN et al., 2010)	- Thermal UC with a 24-hour planning horizon discretized in 1-hour periods - MP: MILP with UC constraints - SP: hourly DC OPF problems with contingency constraints - Benchmarks: IEEE 7-bus and RTS-96 bus systems - Include transmission switching with N-1 reliability
MILP (FU; LI, Z.; WU, 2013)	- Thermal UC with one up to 7-day planning horizon discretized in 1-hour periods - MP: MILP with UC constraints - SP: a bilevel problem with hourly DC OPF problems with contingency constraints - Benchmarks: 1168-bus system - Solve a real instance large-scale STGS problem
MILP (WU; SHAHIDEHPOUR, 2010)	- Thermal UC with a 24-hour planning horizon discretized in 1-hour periods - MP: MILP with UC constraints - SP: hourly DC OPF problems - Benchmarks: 3-bus and 5663-bus systems - Apply strong Benders cuts based on the DC network to improve the convergence of BD

Source: Author.

As shown in Table 1, most works that apply BD in deterministic STGS problems focus on obtaining SPs containing only the power flow constraints. The reason is due to the inherent temporal decoupling existing in this type of SP, allowing the use of parallelism. In stochastic STGS problems, the BD allows for breaking the original problem into an MP and decoupled SPs for each scenario/realization of the random variable. Also, the BD allows increasing the STGS formulation, including real-time operation constraints, such as contingency or frequency constraints. A point to note is that BD can deal with several optimization problems, including MINLPs where the resulting SP is an LP or a convex NLP. This SP requirement can impose some limits on the applications of BD in STGS problems, particularly the temporal decomposition since STGS problems are normally formulated as non-convex MINLPs.

The concept of temporal decomposition applied to STGS problems is not new but has only recently raised interest among researchers. In (SANTOS; DINIZ, 2009), a multistage BD[4] is proposed to decompose the STGS problem formulated as LP, where each stage comprises several time periods, aiming to find the best trade-off between the number of subproblems to be solved and the computational burden involved. The authors applied this scheme in the Brazilian system in a 168-hour planning horizon discretized in 1-hour periods. In simulations, they observed an optimal aggregation factor between 12 and 14 time periods in computational runtime. Although this work presents some important aspects concerning temporal decomposition and time aggregation, using an LP formulation for this problem is a drawback because it is necessary to use binary variables to represent more realistic characteristics of the hydro and thermal power plants operation.

As expected, the natural extension of the multistage BD is to include subproblems with mixed-integer variables, known as DDiP. It is important to note that only a few works in the literature have applied DDiP to optimization problems. An application of the DDiP to solve a multi-scale mixed-integer MPC is presented in (KUMAR et al., 2021). In this work, the authors decompose the problem into several mixed-integer subproblems that will be solved in the iterative scheme of the DDiP. The simulations are performed to schedule central heating, ventilation, and air-conditioning plant problems considering a 1, 2, 4, 5, 8, 10, and 20-week planning horizon discretized in 1-hour periods. The problem obtained when the planning horizon is 20-weeks contains 188,164 variables, being 67,200 binaries and 184,803 constraints. Although the DDiP lacks the finite convergence property due to mixed-integer variables, the solutions obtained through DDiP are high-quality, with an optimality gap of 0.1%. Thus, in this case, the DDiP outperforms the state-of-the-art solutions MILP solver in terms of the computational burden.

In the context of GS, the work (LARA et al., 2018) apply the DDiP in the long-term planning of electric power infrastructures considering high renewable penetration.

[4] also known as dual dynamic programming

Considering that the problem is a large-scale MILP, due to the multi-year planning horizon discretized in hourly steps, the authors used DDiP for performing aggregations and approximations in the original problem to overcome the computational intractability. For example, a year is modeled using a small number of representative days with hourly resolution. To accelerate the DDiP, they perform a pre-processing step where an aggregated version of the full-space MILP is solved. The solution obtained is used to generate initial cuts before starting the DDiP (warm-starting). Also, they evaluate different types of Benders cuts proposed in (ZOU; AHMED; SUN, 2019b) and observed that despite the classical Benders cuts being the weakest possible cuts, the advantage of being easily and quickly computed overcomes the benefits of other types of cuts in the DDiP scheme.

To overcome the computational complexity due to the temporal resolution of optimization problems, some strategies involving decomposition, aggregation, and approximation can be performed. For example, work (FLAMM et al., 2021) handles the GS problem with the nonlinear hydro model through a two-stage dual dynamic programming approach. Considering that this is a large-scale nonlinear problem, the authors split the problem into two sequential temporal stages. The first is an STGS with an entire nonlinear problem, and the second is an approximated LTGS formulated as an LP problem.

1.3 OBJECTIVES

This work proposes an STGS model with detailed HPF, including nonlinearities and non-convexities. Considering the increase of the computational effort due to the detailed HPF, the decomposition strategy based on DDiP is performed. In this sense, the inherent temporal coupling of the STGS problem brings new possibilities to improve the DDiP, e.g., different block-time aggregations and a particular type of overlap between adjacent SPs. Approximations and aggregations can be performed in the final stages of the planning horizon to overcome the difficulties imposed by the temporal resolution of the STGS problem. Specifically, this thesis aims to:

1) Present different plant-based formulations for the HPF, such as improvements in the CH formulation and other models that includes nonlinearities and discontinuities related to the forbidden operating zones through mixed-integer formulations. The aim is to propose a formulation with reasonable HPF accuracy and a minimal increase in computational effort. In other words, we present an intermediate approach (between the individual unit and the plant-based approaches), which includes details present in the individual representation and the reduced computational effort characteristic of the plant-based approach.

The first formulation proposed is a two-variate mixed-integer model based on the CH for each non-forbidden zone (NFZ). Then, from a detailed analysis of HPF, correlating the state variables dependencies and the planning horizon, two types of PWL models are proposed. The first one is related to the plant's turbined outflow and the second one includes the dependency of the volume.

2) Solve the 1-week STGS problem using DDiP with different block-time aggregations and analyze their effect on DDiP convergence. The critical observation is that DDiP is flexible and enables each SP to have its particular characteristics, such as different time horizons, as long as the information from the original problem is not removed. Compared to a DDiP that operates over single time steps, this approach (i) reduces the number of cost-to-go functions that need to be approximated, and (ii) the block partitioning leads to tight approximations for the cost-to-go functions with a reduced number of iterations. The block representations can also better capture the multiple timescales present in STGS problems (e.g., ramp, minimum uptime, downtime, water balance with coupled reservoir equations).

   The proposed framework employs an overlapping partitioning scheme (known as overlapping Schwarz), which has been recently used in the context of optimal control (NA et al., 2021) and nonlinear dynamic programming problems (NA; ANITESCU; KOLAR, 2021). In this approach, block time partitions incorporate a selected set of constraints of the neighbor partitions. As a result, SPs for the block partitions contain more information on the problem structure, which helps to accelerate the convergence.

3) Analyze the impact of the detailed formulation in all periods in the STGS problem. Considering that in the STGS problem, we are interested in finding the day-ahead scheduled decisions, in which for each day the system operator will execute the STGS problem with new input data, we aim to measure how much the simplifications performed in the last days of the planning horizon impact the decisions for the first day.

   Motivated by the recent studies in MPC problems, our objective is to propose a modified version of the STGS problem that has fewer variables and constraints due to time aggregation, where the decisions of the first day are near to the optimal choices for the original problem. In particular, we evaluate the effects of the diffusing-horizon (DH) strategy on the STGS problem.

In this work, to evaluate the proposals, the experiments are performed in a modified version of the IEEE-118 bus system (IEEE, 2022), where 15 hydros from the Brazilian system replace 14 thermal plants. All the data used in this work is presented in Appendix A.

From the results obtained, we show the following conclusions:

(i) The inclusion of a detailed HPF, with the discontinuities due to the forbidden zones, results in significant changes in the decisions of the STGS problem, with the caveat of an increase in the computational runtime that needs to be taken into consideration;

(ii) The DDiP is a valid strategy to obtain near-optimal solutions for the STGS problem in a reasonable time, and the improvements on the overlapping partitioning accelerate the convergence of the DDiP;

(iii) A detailed formulation on the last days of the planning horizon does not significantly impact the decisions of the first day, allowing for the use of simplified formulations for the last days of the planning horizon.

These contributions are divided into the following papers:

1. **Piecewise Linear Approximations for Hydropower Production Function Applied on the Hydrothermal Unit Commitment Problem**. Authors: Kenny V. Santos and Erlon C. Finardi. Published in *International Journal of Electrical Power and Energy Systems* journal, vol. 135, february 2022, pp. 107464. Link: `https://doi.org/10.1016/j.ijepes.2021.107464`.

2. **Accelerated Multi-period Dual Dynamic Integer Programming Applied to Short-Term Power Generation Scheduling**. Authors: Kenny V. Santos, Bruno R. Colonetti, Erlon C. Finardi, and Victor M. Zavala. Published in *International Journal of Electrical Power and Energy Systems* journal, vol. 145, february 2023, pp. 108689. Link: `https://doi.org/10.1016/j.ijepes.2022.108689`.

3. **Assessing Temporal Aggregations and Model Simplifications in the Short-Term Power Generation Scheduling Problem**. To be submitted.

And as secondary contribution, during this Ph.D., the following paper was published.

1. **Analysis of infeasible unit-commitment solutions arising in energy optimization**. Authors: Leonardo D. Secchin, Guilherme M. Ramalho, Claudia A. Sagastizábal, Paulo J. S. Silva, and Kenny V. Santos. Published in *Mathematics in Industry Reports*, 2022. Link: `http://dx.doi.org/10.33774/miir-2022-ztpbq`.

1.4 STRUCTURE OF THE WORK

This work is organized as follows: Chapter 2 presents the mathematical formulation of the STGS problem used in this work; the different proposed formulations

for detailed HPF are presented in Chapter 3; Chapter 4 presents the DDiP and the overlapping strategy proposed in this work; the study of simplified formulations and temporal aggregations in the STGS problem is presented in Chapter 5; and finally, the conclusions and future directions of research are in Chapter 6.

2 MATHEMATICAL FORMULATION OF STGS PROBLEM

The STGS problem studied in this thesis aims to minimize the cost of operation given a planning horizon (e.g., 24 or 168 hours), taking into account operational constraints for each generator and network constraints. While the horizon of STGS is significantly lower than LTGS and MTGS problems, the plants and the electrical network are modeled with more detail. In this thesis, the STGS problem is considered deterministic, which means that the generation provided by renewable sources is represented by power injections modeled as negative demand on the bus that the renewable source is connected. Furthermore, the inflows and demands for each time-step are known.

The notation used in this thesis is given as follows. Variables are represented by italic letters, except those with lower greek letters. Constant terms are represented by bold letters. Sets are represented by calligraphic letters, except those represented by upper greek letters. The notation $\overline{\mathrm{x}}$ and $\underline{\mathrm{x}}$ are the upper and lower limits of variable x, respectively.

2.1 HYDROELECTRIC PLANT MODEL

Hydroelectric plants generate electricity by converting potential energy into kinetic energy, which is then transformed into electric energy. The difference between upstream and downstream levels allows water to flow through a GU (turbine-generator), producing electrical energy. This section presents the detailed formulation of HPF for a GU.

The active power output of a GU follows the model presented in (FINARDI; SILVA, E. L., 2006). Consider that the plant h has $\mathbf{NJ}_h$ GUs. In this model, the power generation from unit j at instant t, phu_{jt} (in p.u. of MW) is a nonlinear function that depends on the GU turbined outflow q_{jt} [m^3/s], net head nh_{jt} [m], and the turbine-generator efficiency[1] η_{jt} as follows:

$$phu_{jht} = 9.81 \times 10^{-5} \cdot \eta_{jht} \cdot nh_{jht} \cdot q_{jht}. \tag{1}$$

The net head is a function of the forebay level fbl_{ht} [m], tailrace level trl_{ht} [m], and hydraulic losses[2] [m], given by:

$$nh_{jht} = fbl_{ht} - trl_{ht} - \mathbf{D}_{jh} \cdot q_{jht}^2. \tag{2}$$

In Equation (2), the constant $\mathbf{D}_{jh}$ depends on the physical and geometrical characteristics of the penstock [s^2/m^5]. The following gives the forebay level fourth-degree polynomial on the volume of the reservoir [hm^3]:

$$fbl_{ht} = \mathbf{F}_{0h} + \mathbf{F}_{1h} V_{ht} + \mathbf{F}_{2h} V_{ht}^2 + \mathbf{F}_{3h} V_{ht}^3 + \mathbf{F}_{4h} V_{ht}^4. \tag{3}$$

[1] The GU efficiency is evaluated as the product of the hydraulic, mechanical, and generator efficiencies; the last two are considered unitary in this work because they are approximately 100%.

[2] In this work, for each GU, the penstock losses are predominantly caused by hydraulic losses and thus can be considered equal.

The tailrace level is also modeled as a fourth-degree polynomial depending on the plant turbined outflow Q_{ht} [m^3/s] and spillage [m^3/s]:

$$trl_{ht} = \mathbf{G}_{0h} + \mathbf{G}_{1h}(Q_{ht} + S_{ht}) + \mathbf{G}_{2h}(Q_{ht} + S_{ht})^2 + \mathbf{G}_{3h}(Q_{ht} + S_{ht})^3 + \mathbf{G}_{4h}(Q_{ht} + S_{ht})^4, \tag{4}$$

It is also important to note that for some plants, the spillage has no effect in the tailrace; therefore, S_{ht} is zero in Equation (4). The GU efficiency is a nonlinear function expressed in the Hill diagram (FINARDI; SILVA, E. L., 2006). In this work, we use the following polynomial approximation model:

$$\eta_{jht} = \mathbf{I}_{0jh} + \mathbf{I}_{1jh} q_{jht} + \mathbf{I}_{2jh} nh_{jht} + \mathbf{I}_{3jh} q_{jht} nh_{jht} + \mathbf{I}_{4jh} q_{jht}^2 + \mathbf{I}_{5jh} nh_{jht}^2. \tag{5}$$

The power generation php_{ht} of the hydro plant h at time t is the sum of the power output of all GUs:

$$php_{ht} = \sum_{j=1}^{\mathbf{NJ}_h} phu_{jht}. \tag{6}$$

Similarly, the turbined outflow of the hydro plant h is the sum of the individual turbined outflow of all GUs:

$$Q_{ht} = \sum_{j=1}^{\mathbf{NJ}_h} q_{jht}. \tag{7}$$

According to the Hill curve, each Gu has power limits that depend on the net head. The operational limits of the variables involved in the hydro model are given by:

$$\underline{\mathbf{V}}_h \leq V_{ht} \leq \overline{\mathbf{V}}_h;\ 0 \leq S_{ht} \leq \overline{\mathbf{S}}_h;\ \underline{\mathbf{q}}_{jh} u_{jht} \leq q_{jht} \leq \overline{\mathbf{q}}_{jh} u_{jht}, \tag{8}$$

where u_{jht} is a binary variable that represents the status of GU j at time t (1: on, 0: off). Moreover, each generator has a minimum and maximum amount of power that can be produced, restricted by the capability curve[3]. If the capability curve is ignored, the limits for power generation will be given by:

$$\underline{\mathbf{phu}}_{jh} \leq phu_{jht} \leq \overline{\mathbf{phu}}_{jh}. \tag{9}$$

For hydropower operation, the water balance equation relates to how the water is stored in the reservoir in a given time instant. Because hydro plants can be located in the same river basin, the reservoirs are spatially coupled. Therefore, the water balance equation has to consider this coupling with the respective water travel time between coupled reservoirs. In this work, this equation is given by:

$$V_{ht} + \mathbf{K} \cdot \left(Q_{ht} + S_{ht} - \sum_{\forall i \in \Omega_h} Q_{i,t-\tau_{ih}} + S_{i,t-\tau_{ih}} \right) = V_{h,t-1} + \mathbf{K} \cdot \mathbf{Y}_{ht}. \tag{10}$$

[3] The capability curve of a generator defines boundaries for active and reactive power generation, considering restrictions related to overheating of the generators

In Equation (10), the constant $\mathbf{K}$ is responsible for converting flow into volume, $\mathbf{Y}_{ht}$ is the incremental inflow, the set Ω_h contain all reservoirs that are upstream of hydro h, and τ_{ih} is the water travel time between the reservoirs i and h. For example, Figure 1 shows a case where two hydroelectric plants are upstream of hydroelectric h, i.e., Ω = {2,3}, and the decision variables are used in the water balance equation.

Figure 1 – Example of variables used in the water balance equation.

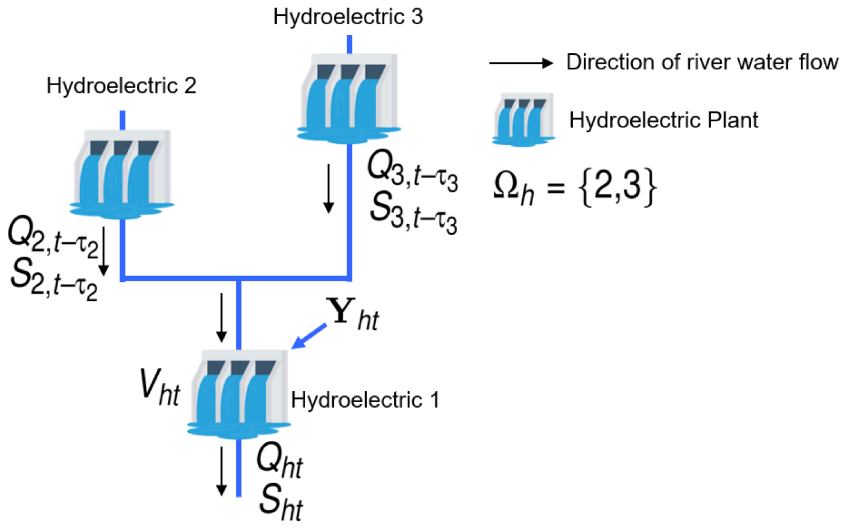

Source: Author.

Finally, in the centralized dispatch of predominant hydro systems, as the Brazilian case, the FCF is used to valuate the water stored at the end of the planning horizon. In this work, the FCF is formulated as a PWL model, given by:

$$\alpha + \sum_{\forall h \in \Psi} \mathbf{M0}_{hi} V_{h,\mathbf{NT}} \geq \mathbf{M1}_i, \tag{11}$$

where α is the expected cost, Ψ is the set of reservoirs that are in the FCF, $\mathbf{M0}_{hi}$ is the angular coefficient and $\mathbf{M1}_i$ is the independent term of the linear approximation. The subscript i concerns the i-th linear equation of FCF, and $\mathbf{NT}$ is the last period of the planning horizon (e.g., $\mathbf{NT}$ = 168 if the planning horizon is 168 hours with hourly steps).

2.2 THERMOELECTRIC PLANT MODEL

The model for the thermoelectric plants used in this work is the 3-binary model (GENTILE; MORALES-ESPAÑA; RAMOS, 2017). In this formulation, in addition to the operational limits of each thermoelectric plant, the UC constraints must be considered, such as the minimum uptime and downtime, ramp up and ramp down, and the minimum power to be turned on/off. These equations are presented as follows:

$$z_{gt} - w_{gt} = x_{gt} - x_{g,t-1}, \tag{12}$$

$$\sum_{\max(i=t-\mathbf{UT}_g+1,1)}^{t} z_{gi} \leq x_{gt}, \tag{13}$$

$$\sum_{\max(i=t-\mathbf{DT}_g+1,1)}^{t} w_{gi} \leq 1 - x_{gt}, \tag{14}$$

$$pt_{gt} - pt_{g,t-1} \leq \mathbf{RU}_g x_{g,t-1} + \underline{\mathbf{pt}}_g z_{gt}, \tag{15}$$

$$pt_{g,t-1} - pt_{gt} \leq \mathbf{RD}_g x_{gt} + \underline{\mathbf{pt}}_g w_{gt}, \tag{16}$$

$$\underline{\mathbf{pt}}_g x_{gt} \leq pt_{gt} \leq \overline{\mathbf{pt}}_g x_{gt},\ x_{gt}, z_{gt}, w_{gt} \in \{0,1\}, \tag{17}$$

In Equations (12)-(18), the subscript g concerns the thermoelectric generator g, the subscript t is the time period, $\mathbf{UT}_g$ is the minimum uptime of g, $\mathbf{DT}_g$ is the minimum downtime of g, $\mathbf{RU}_g$ is the maximum ramp-up allowed for g and $\mathbf{RD}_g$ is the maximum ramp down allowed for g. The variable x_{gt} represents the on/off status of unit g at period t (x_{gt} = 1 if the thermoelectric plant is on, 0 if it is off), z_{gt} is a start-up variable denoting if unit g has been started at period t (i.e., x_{gt} = 1 and $x_{g,t-1}$ = 0), and w_{gt} is a shut-down variable denoting if unit g has been shut down at period t (i.e., x_{gt} = 0 and $x_{g,t-1}$ = 1). The active power produced by unit g at instant t is represented by pt_{gt} [p.u. of MW]. Again, if the capability curve of the thermoelectric generator is ignored, then the active power limits is given by the following constraint:

$$\underline{\mathbf{pt}}_g \leq pt_{gt} \leq \overline{\mathbf{pt}}_g. \tag{18}$$

2.3 NETWORK MODEL

In this thesis, the STGS problem will consider the DC formulation for the network. Due to the linear structure of constraints, this model is a common formulation used in STGS problems (the same formulation employed in the DESSEM model). A detailed network formulation involving nonlinear (AC) constraints and relaxations of AC OPF can be founded in (ZIMMERMAN; MURILLO-SANCHEZ, C. E.; THOMAS, 2011; MOLZAHN; HISKENS, 2019; KORUK; DEY; SUN, 2016). The DC formulation considers the following hypothesis:

H.1. The angular difference between two connected buses is small, such that $\text{sen}(\theta_a - \theta_b) \approx \theta_a - \theta_b$ and $\cos(\theta_a - \theta_b) \approx 1$, $\forall(a,b) \in \mathcal{L}$;

H.2. The conductance of all transmission lines is approximated 0, i.e., $\mathbf{g}_{ab} \approx 0, \forall (a,b) \in \mathcal{L}$;

H.3. All the reactive power is ignored;

H.4. All voltage magnitudes of buses are equal to 1 p.u.

Considering hypotheses H.1. to H.4., the DC network formulation (DC OPF) is given by:

$$\sum_{\forall g \in \mathcal{U}_b} pt_{gt} + \sum_{\forall h \in \mathcal{U}_b} php_{ht} - \sum_{l \in \mathcal{B}_b} pl_{lt} = \mathbf{P}_{bt} \tag{19}$$

$$pl_{lt} = (\theta_{at} - \theta_{bt})/\mathbf{x}_{ab} \tag{20}$$

$$\underline{\mathbf{pl}}_l \leq pl_{lt} \leq \overline{\mathbf{pl}}_l \tag{21}$$

$$\underline{\theta}_b \leq \theta_{bt} \leq \overline{\theta}_b \tag{22}$$

$$\theta_{\text{ref},t} = 0. \tag{23}$$

In Equations (19)-(23), the following notation was used: the network is composed of b buses belonging to set $\mathcal{B}$ and l transmission lines belonging to set $\mathcal{L}$. $\mathcal{B}_b$ is the set of all buses that are connected with bus b. $\mathbf{P}_{bt}$ represents the active power demand at bus b in time t. A transmission line that connects buses a and b has reactance $\mathbf{x}_{ab}$ [p.u.]. The active power through line l at time t is represented by pl_{lt} [p.u. of MW], and if l connects buses a and b, we use the notation $l : (a,b)$, and the power flow is from a to b. The set $\mathcal{U}_b$ contains all generators connected to bus b, where $g \in \mathcal{U}_b$, and $h \in \mathcal{U}_b$ are thermoelectric and hydro plants belonging to this set, respectively. The variable θ_{bt} is the voltage angle of the bus b at instant t, and the subscript *ref* represents the reference bus.

In STGS problems, it is common to impose a system reserve constraint, which is formulated by:

$$\sum_{g=1}^{\mathbf{NG}} \left(\overline{\mathbf{pt}}_g x_{gt} - pt_{gt} \right) + \sum_{h=1}^{\mathbf{NH}} \sum_{j=1}^{\mathbf{NJ}_h} \left(\overline{\mathbf{phu}}_{jh} u_{jht} - phu_{jht} \right) \geq \mathbf{SR}_t, \tag{24}$$

where $\mathbf{NG}$ is the number of thermoelectric plants, $\mathbf{NH}$ is the number of hydro plants and $\mathbf{SR}$ is the system reserve [p.u. of MW].

2.4 FULL FORMULATION OF STGS PROBLEM

Combining equations presented in Sections 2.1, 2.2 and 2.3, we formulate the STGS problem studied in this thesis, modeled as an MINLP problem and mathematically described in Equation (25) as follows:

$$\min \quad \sum_{t=1}^{\mathbf{NT}} \sum_{g=1}^{\mathbf{NG}} \left(\mathbf{C0}_g pt_{gt} + \mathbf{C1}_g x_{gt} + \mathbf{C2}_g z_{gt} + \mathbf{C3}_g w_{gt}\right) + \alpha \tag{25a}$$

$$\text{s.t.} \quad z_{gt} - w_{gt} = x_{gt} - x_{g,t-1}, \quad \forall g \in \mathcal{G}, \forall t \in \mathcal{T} \tag{25b}$$

$$\sum_{i=\max(t-\mathbf{UT}_g+1,1)}^{t} z_{gi} \leq x_{gt}, \quad \forall g \in \mathcal{G}, \forall t \in \mathcal{T} \tag{25c}$$

$$\sum_{i=\max(t-\mathbf{DT}_g+1,1)}^{t} w_{gi} \leq 1 - x_{gt}, \quad \forall g \in \mathcal{G}, \forall t \in \mathcal{T} \tag{25d}$$

$$pt_{gt} - pt_{g,t-1} \leq \mathbf{RU}_g x_{g,t-1} + \underline{\mathbf{pt}_g} z_{gt}, \quad \forall g \in \mathcal{G}, \forall t \in \mathcal{T} \tag{25e}$$

$$pt_{g,t-1} - pt_{gt} \leq \mathbf{RD}_g x_{gt} + \underline{\mathbf{pt}_g} w_{gt}, \quad \forall g \in \mathcal{G}, \forall t \in \mathcal{T} \tag{25f}$$

$$phu_{jht} = 9.81 \times 10^{-5} \cdot \eta_{jht} \cdot nh_{jht} \cdot q_{jht}, \quad \forall j \in \mathcal{J}_h, \forall h \in \mathcal{H}, \forall t \in \mathcal{T} \tag{25g}$$

$$nh_{jht} = fbl_{ht} - trl_{ht} - \mathbf{D}_j \cdot q_{jht}^2, \quad \forall j \in \mathcal{J}_h, \forall h \in \mathcal{H}, \forall t \in \mathcal{T} \tag{25h}$$

$$fbl_{ht} = \mathbf{F}_{0h} + \mathbf{F}_{1h} V_{ht} + \mathbf{F}_{2h} V_{ht}^2 + \mathbf{F}_{3h} V_{ht}^3 + \mathbf{F}_{4h} V_{ht}^4, \quad \forall h \in \mathcal{H}, \forall t \in \mathcal{T} \tag{25i}$$

$$trl_{ht} = \mathbf{G}_{0h} + \mathbf{G}_{1h}(Q_{ht} + S_{ht}) + \mathbf{G}_{2h}(Q_{ht} + S_{ht})^2 + \mathbf{G}_{3h}(Q_{ht} + S_{ht})^3 + \mathbf{G}_{4h} \cdot (Q_{ht} + S_{ht})^4, \quad \forall h \in \mathcal{H}, \forall t \in \mathcal{T} \tag{25j}$$

$$\eta_{jht} = \mathbf{I}_{0jh} + \mathbf{I}_{1jh} q_{jht} + \mathbf{I}_{2jh} nh_{jht} + \mathbf{I}_{3jh} q_{jht} nh_{jht} + \mathbf{I}_{4jh} q_{jht}^2 + \mathbf{I}_{5jh} nh_{jht}^2, \quad \forall j \in \mathcal{J}_h, \forall h \in \mathcal{H}, \forall t \in \mathcal{T} \tag{25k}$$

$$php_{ht} = \sum_{j=1}^{\mathbf{NJ}_h} phu_{jht}, \quad \forall h \in \mathcal{H}, \forall t \in \mathcal{T} \tag{25l}$$

$$Q_{ht} = \sum_{j=1}^{\mathbf{NJ}_h} q_{jht}, \quad \forall h \in \mathcal{H}, \forall t \in \mathcal{T} \tag{25m}$$

$$V_{ht} = V_{h,t-1} + \mathbf{K} \cdot \mathbf{Y}_{ht} - \mathbf{K} \cdot \left(Q_{ht} + S_{ht} - \sum_{\forall i \in \Omega_h} \left(Q_{i,t-\tau_{ih}} + S_{i,t-\tau_{ih}}\right) \right), \forall h \in \mathcal{H}, \forall t \in \mathcal{T} \tag{25n}$$

$$\alpha \geq \mathbf{M1}_i - \sum_{h \in \Psi} \mathbf{M0}_{hi} V_{h,\mathbf{NT}}, \quad i = 1, \ldots, \mathbf{NC} \tag{25o}$$

$$\sum_{\forall g \in \mathcal{U}_b} pt_{gt} + \sum_{\forall h \in \mathcal{U}_b} php_{ht} - \sum_{\forall l \in \mathcal{B}_b} pl_{lt} = \mathbf{P}_{bt}, \quad \forall b \in \mathcal{B}, \forall t \in \mathcal{T} \tag{25p}$$

$$pl_{lt} = (\theta_{at} - \theta_{bt})/\mathbf{x}_{ab}, \quad \forall l : (a,b) \in \mathcal{L}, \forall t \in \mathcal{T} \tag{25q}$$

$$\sum_{g=1}^{\mathbf{NG}} \left(\overline{\mathbf{pt}}_g x_{gt} - pt_{gt}\right) + \sum_{h=1}^{\mathbf{NH}} \sum_{j=1}^{\mathbf{NJ}_h} \left(\overline{\mathbf{phu}}_{jh} u_{jht} - phu_{jht}\right) \geq \mathbf{SR}_t, \quad \forall t \in \mathcal{T} \tag{25r}$$

$$\underline{\mathbf{q}}_{jh} u_{jht} \leq q_{jht} \leq \overline{\mathbf{q}}_{jh} u_{jht}, \quad \forall j \in \mathcal{J}_h, \forall h \in \mathcal{H}, \forall t \in \mathcal{T} \tag{25s}$$

$$0 \leq phu_{jht} \leq \overline{\mathbf{phu}}_{jht}, \quad \forall j \in \mathcal{J}_h, \forall h \in \mathcal{H}, \forall t \in \mathcal{T} \tag{25t}$$

$$\underline{\mathbf{pt}}_g x_{gt} \leq pt_{gt} \leq \overline{\mathbf{pt}}_g x_{gt}, \quad \forall g \in \mathcal{G}, \forall t \in \mathcal{T} \tag{25u}$$

$$\underline{\mathbf{V}}_h \leq V_{ht} \leq \overline{\mathbf{V}}_h;\ 0 \leq S_{ht} \leq \overline{\mathbf{S}}_h;\ 0 \leq php_{ht} \leq \overline{\mathbf{php}}_h, \forall h \in \mathcal{H}, \forall t \in \mathcal{T} \tag{25v}$$

$$\overline{\mathbf{pl}}_l \leq pl_{lt} \leq \overline{\mathbf{pl}}_l, \quad \forall\forall l : (a,b) \in \mathcal{L}, \forall t \in \mathcal{T} \tag{25w}$$

$$\underline{\theta}_b \leq \theta_{bt} \leq \overline{\theta}_b, \quad \forall b \in \mathcal{B}, \forall t \in \mathcal{T} \tag{25x}$$

$$u_{jht}, x_{gt}, z_{gt}, w_{gt} \in \{0,1\}, \quad \forall j \in \mathcal{J}_h, \forall h \in \mathcal{H}, \forall g \in \mathcal{G}, \forall t \in \mathcal{T} \tag{25y}$$

$$\theta_{ref,t} = 0, \quad \forall t \in \mathcal{T}. \tag{25z}$$

For this model, in the objective function, the term $\mathbf{C0}_g$ is the unit variable cost of thermoelectric g, i.e., the cost to produce 1 unit of power in a given instant time [$/p.u. of MWh]; $\mathbf{C1}_g$ is the fixed cost of g, i.e., the cost to keep the plant online independent of the amount of power that it produces [$]; $\mathbf{C2}_g$ is the cost to start g [$], and $\mathbf{C3}_g$ is the cost to shut down g [$]. $\mathcal{T}, \mathcal{G}, \mathcal{H}, \mathcal{J}_h$ are the set with the time periods, the set of thermal generators, the set of hydro plants, and the set of GUs of hydro plant h, respectively. $\mathbf{NC}$ is the number of cuts used to represent the FCF. To understand the characteristics of this optimization problem, the relation between the number of variables and constraints as a function of the size of the system are presented below, considering the following input data.

- $\mathbf{G}$ thermoelectric plants;
- $\mathbf{H}$ hydro plants, where each plant h contains $\mathbf{J}_h$ GUs;
- $\mathbf{B}$ buses and $\mathbf{L}$ transmission lines;
- $\mathbf{C}$ cuts for the FCF;
- $\mathbf{NT}$ time steps.

In this analysis, the constraints associated with limits on variables (including operational limits for thermoelectric plants) and the power limits of generators are ignored. Also, we ignore constraints $php = \sum_{j=1}^{\mathbf{J}_h} phu_i$, $Q = \sum_{j=1}^{\mathbf{J}_h} q_i$. In this case, the relation of variables and constraints is expressed in Table 2, where H, T, R, and N are, respectively, the hydro, thermoelectric, reservoirs (water balance and FCF), and network constraints. As can be seen, the number of time steps, combined with the number of hydros and thermoelectric plants, increases the STGS problem's complexity due to the increase in the the number of nonlinear constraints and binary variables.

Table 2 – Number of variables and constraints in STGS problem

	# continuous variables	# binary variables	# linear constraints	# nonlinear constraints
H	$(\sum_{i=1}^{\mathbf{H}} 5\mathbf{J}_i + 4\mathbf{H}) \cdot \mathbf{NT}$	$\sum_{i=1}^{\mathbf{H}} \mathbf{J}_i \cdot \mathbf{NT}$	0	$(\sum_{i=1}^{\mathbf{H}} 3\mathbf{J}_i + 2) \cdot \mathbf{NT}$
T	$2 \cdot \mathbf{G} \cdot \mathbf{NT}$	$3 \cdot \mathbf{G} \cdot \mathbf{NT}$	$5 \cdot \mathbf{G} \cdot \mathbf{NT}$	0
R	1	0	$\mathbf{H} \cdot \mathbf{NT} + \mathbf{C}$	0
N	$(\mathbf{B} + \mathbf{L}) \cdot \mathbf{NT}$	0	$(\mathbf{B} + \mathbf{L}) \cdot \mathbf{NT}$	0

Source: Author.

2.5 FINAL CONSIDERATIONS

In this chapter, the formulation of the STGS problem approached in this thesis was presented. Initially, the individual representation of the GUs of a hydroelectric plant was modeled as a nonlinear model. Then, the thermoelectric UC was presented using the 3-binary model, considering the minimum up and down times, ramp constraints, and power limits. In sequence, the DC formulation for the network was shown. Finally, the formulation of the STGS problem and the relation between the temporal discretization, number of generators, and the dimension of the STGS problem was presented, in which the number of nonlinear terms and binary variables stand out.

As seen, the STGS is formulated as a non-convex MINLP problem, and for large-scale systems, solving or finding a feasible solution is a hard task since the available optimization solvers do not perform well in problems with many variables and nonlinear non-convex constraints. Therefore, this model is approximated by a MILP problem in the Brazilian case. An approximation is to aggregate all the units of each hydroelectric plant and approximate the equivalent HPF by a PWL model based on CH techniques. Thus, two important features deteriorate, the non-linearities and discontinuities present in HPF. Another important aspect is the use of the DC formulation for the network, a simplified linear model that only holds under certain hypotheses.

The search for feasible and high-quality solutions for the STGS problem has motivated researchers in engineering, mathematics, and economics, in addition to being a special interest for power system operators, given the huge financial impacts caused by non-optimal decisions. For example, there is the case of the PJM system operator, which in 2005, changed its STGS model solved by LR for a MILP solved by a commercial solver, reporting an annual saving of between 60 and 100 million of dollars (O'NEILL, n.d.).

Another important factor in searching for a high-quality STGS problem solution is the computational time involved. Depending on the structure of the associated energy market, the system operator needs to deal with other issues not always described in the STGS problem, such as reactive power generation and transient and steady-state stability issues. In this way, the system operator, after executing the STGS model,

performs a post-processing step on the solution obtained, aiming to guarantee a viable real-time operation. If this post-processing is slow, fast execution of the STGS problem is necessary to guarantee the execution of the system operator framework in a timely way. In addition, the system operator can run the STGS model several times per day to include aspects that were not previously known (e.g., an offline generator due to a failure or an update in the renewable generation due to a massive solar or wind forecast).

Based on these issues, the next chapter details aspects related to the mathematical formulation of the STGS problem, aiming to analyze the approximations used in the DESSEM model. Notably, this thesis does not propose solving the STGS model formulated in this chapter, but rather a MILP-based approach that is more accurate in modeling than those used currently in DESSEM.

3 DETAILED FORMULATIONS FOR PLANT-BASED HPF

In this chapter, different formulations for the plant-based HPF are presented, aiming to be included in the STGS problem. As seen in Chapter 2, the STGS is formulated as an MINLP. For large instances, it becomes computationally intractable to produce an optimal or even a feasible solution. On the other hand, non-detailed formulations, particularly for HPF in a hydro-predominant power system, can lead to low-quality solutions. Therefore, this chapter presents formulations that compromise important aspects of HPF, including nonlinearities, discontinuities, and the computational complexity involved.

3.1 THE PLANT-BASED HPF MODEL

As commented in previous chapters, a common approach to overcome the computational complexity involved in representing the HPF of a plant considering all GUs is to represent the HPF by a plant-based model, which models the plant via a single equivalent GU. In this case, the equivalent unit possesses maximum power and turbined outflow given by the sum of individual GU capacity. However, even where only identical GUs exist, it is impossible to obtain a precise analytic expression for the HPF in the plant-based approach since the resulting nonlinear $\mathbf{php}_{ht}$ depends on the generation policy (i.e., 0-1 status and the respective power dispatch) for each unit. Therefore, the power generation in the operating point k $(\mathbf{V}^k_{ht},\mathbf{Q}^k_{ht},\mathbf{S}^k_{ht})$ can only be obtained by solving an auxiliary problem, typically an optimization model. For instance, considering null spillage, the output power of the plant, $\mathbf{php}_{ht}$ with $\mathbf{NJ}_h$ GUs, operating with fixed values of $\mathbf{Q}^k_{ht}$ and $\mathbf{V}^k_{ht}$ is found by solving the following MINLP problem:

$$\mathbf{php}_{ht}(\mathbf{V}^k_{ht},\mathbf{Q}^k_{ht}) = \max \quad \sum_{j=1}^{\mathbf{NJ}_h} phu_{jht} \tag{26a}$$

$$\text{s.t.} \quad \sum_{j=1}^{\mathbf{NJ}_h} q_{jht} = \mathbf{Q}^k_{ht} \tag{26b}$$

$$nh_{jht} = \sum_{i=0}^{4} \mathbf{F}_{ih} \cdot (\mathbf{V}^k_{ht})^i - \sum_{i=0}^{4} \mathbf{G}_{ih} \cdot (\mathbf{Q}_{ht})^i - \mathbf{D}_{jh} q^2_{jht} \tag{26c}$$

$$\eta_{jht} = \mathbf{I}_{0jh} + \mathbf{I}_{1jh} q_{jht} + \mathbf{I}_{2jh} nh_{jht} + \mathbf{I}_{3jh} q_{jht} nh_{jht} + \mathbf{I}_{4jh} q^2_{jht} + \mathbf{I}_{5jh} nh^2_{jht} \tag{26d}$$

$$phu_{jht} = 9.81 \times 10^{-3} \eta_{jht} nh_{jht} q_{jht} \tag{26e}$$

$$u_{jht} \cdot \underline{\mathbf{q}}_h \leq q_{jht} \leq u_{jht} \cdot \overline{\mathbf{q}}_h \tag{26f}$$

$$u_{jht} \in \{0,1\} \tag{26g}$$

$$j = \{1,2,\ldots,\mathbf{NJ}_h\} \tag{26)h}$$

As an illustrative example, the HPF of a 3-unit plant is presented in Figures 2-3. For both cases (considering the forbidden zones and ignoring these), each generation value is obtained by solving the MINLP optimization problem described in Equations (26)a-(26)h. The differences between these HPFs occur due to the consequences of considering the forbidden zones[1]. In the first case (Figure 2), Equation (26)f is replaced by the following equation:

$$0 \leq q_{jht} \leq \overline{\mathbf{q}}_h, \tag{27}$$

and Equation (26)g is removed from the model. In the second case (Figure 3), we consider the full model of Equations (26)a-(26)h.

Figure 2 – HPF of a 3-unit plant ignoring the forbidden zones.

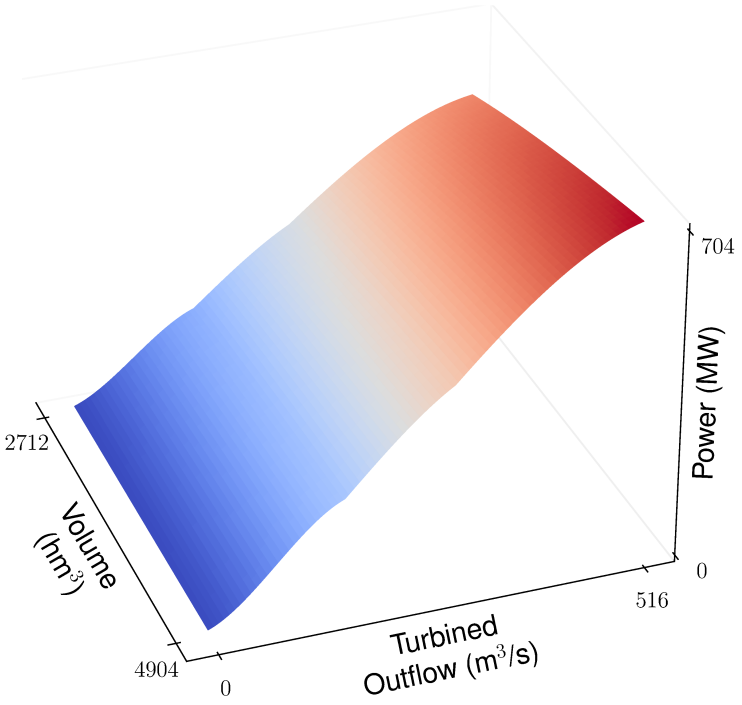

Source: Author

As observed in Figure 3, the HPF is quasiconcave in the NFZs and presents discontinuities. To model discontinuities in an optimization problem, a valid approach includes binary variables representing each feasible region of the independent variable. However, this approach can increase the computational complexity of the optimization problem.

[1] in the plant-based model, a forbidden zone is a value of plant's turbined outflow that can not be achieved due to the limits on GU's turbined outflow

Figure 3 – HPF of a 3-unit plant with forbidden zones.

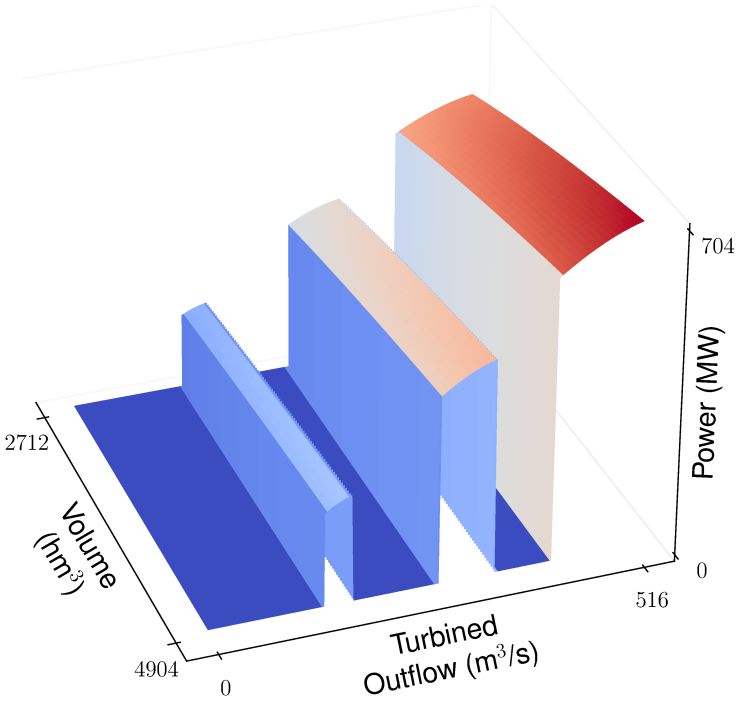

Source: Author

Thus, alternative models were proposed for this problem to reduce the computational complexity and represent the HPF with reasonable quality. Next, to simplify the notation, the subscripts *h* and *t* will be omitted in the rest of this chapter.

3.2 ENVELOPE MODELS

One of the main formulations used to approximate the nonlinear HPF is the Convex Hull (CH) model (DINIZ; MACEIRA, M. E. P., 2008), where the authors propose a PWL model as function of V, Q, with correction factors to reduce the average error in the approximation and a post-processing strategy to include S. In this model, there two main features: (i) it considers a continuous operation in Q using the plant-based model (ignoring the forbidden zones, as in Figure 2) and, (ii) the PWL approximations are evaluated through the CH, using only the upper planes of HPF obtained. Therefore, the CH model is modeled by Equations (28)-(29):

$$0 \leq php \leq \mathbf{a}_{0i} V + \mathbf{a}_{1i} Q + \mathbf{a}_{2i} S + \mathbf{a}_{3i}, i = 1, \ldots, \mathbf{N1}_{\text{CH}}, \tag{28}$$

$$0 \leq Q \leq \overline{\mathbf{q}} \cdot \mathbf{NJ}, \tag{29}$$

where $\mathbf{N1}_{\text{CH}}$ is the number of hyperplanes used to approximate the HPF and $\mathbf{NJ}$ is the number of generating units of the hydro plant. Experiments for this case present some numerical aspects, e.g., many of the hyperplanes obtained by the CH algorithm

are similar numerically, and the user does not control the number of hyperplanes obtained. Thus, in this thesis, we propose to find the hyperplanes through an optimization problem described as follows. First, consider a set $\mathcal{S}$ of points in the $V \times Q$ grid, where an element $k \in \mathcal{S}$ is the pair $(\mathbf{V}^k, \mathbf{Q}^k)$ and a subset $\mathcal{S}_1$ containing points of interest from the $V \times Q$ grid, such that the value of the approximated HPF model for each element of this subset is the same as the nonlinear HPF. With this, the following optimization problem is solved for each element $i \in \mathcal{S}_1$:

$$\min \quad \sum_{\forall k \in \mathcal{S}} \left[\mathbf{php}(\mathbf{V}^k, \mathbf{Q}^k) - (a_0 \mathbf{V}^k + a_1 \mathbf{Q}^k + a_2) \right]^2 \tag{30a}$$

$$\text{s.t.} \quad (a_0 \mathbf{V}^k + a_1 \mathbf{Q}^k + a_2) - \mathbf{php}(\mathbf{V}^k, \mathbf{Q}^k) \geq 0, \forall k \in \mathcal{S} \tag{30b}$$

$$(a_0 \mathbf{V}^i + a_1 \mathbf{Q}^i + a_2) - \mathbf{php}(\mathbf{V}^i, \mathbf{Q}^i) = 0. \tag{30c}$$

The resulting hyperplanes obtained (coefficients a_i, i = 0,1,2) for the CH model are shown in Figure 4. Since *php* is modeled by a set of inequalities that are upper limits, the value of *php* decided by the optimization model can be any value between 0 and the maximum value of *php* limited by the CH model. Also, *php* can be 0, even for a nonzero Q. To fix the null generation when $Q > 0$, a binary variable u that represents the on/off status of the hydro plant is included, and the resulting model, called Binary Convex Hull (BCH), is formulated by Equations (28), (31)-(32):

$$php \leq \overline{php} \cdot u \tag{31}$$

$$\underline{\mathbf{q}} \cdot u \leq Q \leq \overline{\mathbf{q}} \cdot \mathbf{NJ} \cdot u. \tag{32}$$

The hyperplanes of a 3-unit plant using the BCH model are presented in Figure 5. To improve the HPF model, hyperplanes that bound from below the HPF can be inserted in CH and BCH formulations. The following optimization problem, which obtains these hyperplanes, is solved for each element $i \in \mathcal{S}_1$, considering $\mathcal{S}, \mathcal{S}_1$ as the same used (although it is not required) in the optimization problem from Equations (30)a-(30)c.

$$\min \quad \sum_{\forall k \in \mathcal{S}} \left[\mathbf{php}(\mathbf{V}^k, \mathbf{Q}^k) - (b_0 \mathbf{V}^k + b_1 \mathbf{Q}^k + b_2) \right]^2 \tag{33a}$$

$$\text{s.t.} \quad \mathbf{php}(\mathbf{V}^k, \mathbf{Q}^k) - (b_0 \mathbf{V}^k + b_1 \mathbf{Q}^k + b_2) \geq 0, \forall k \in \mathcal{S} \tag{33b}$$

$$\mathbf{php}(\mathbf{V}^i, \mathbf{Q}^i) - (b_0 \mathbf{V}^i + b_1 \mathbf{Q}^i + b_2) = 0. \tag{33c}$$

Thus, the resulting HPF model using the CH formulation with $\mathbf{N2}_{\text{CH}}$ hyperplanes that are lower bounds of HPF, called CH-2, is modeled by Equations (28)-(29), together with Equation (34):

$$php \geq \mathbf{b}_{0i} V + \mathbf{b}_{1i} Q + \mathbf{b}_{2i} S + \mathbf{b}_{3i}, i = 1, \ldots, \mathbf{N2}_{\text{CH}}, \tag{34}$$

Figure 4 – Upper limits of a 3-unit plant using the CH model.

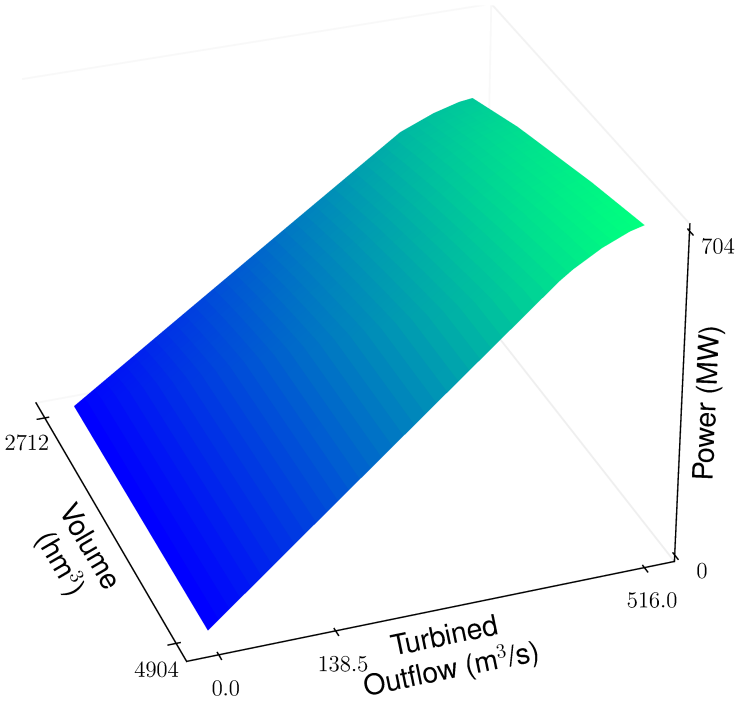

Source: Author

Figure 5 – Upper limits of a 3-unit plant using the BCH model.

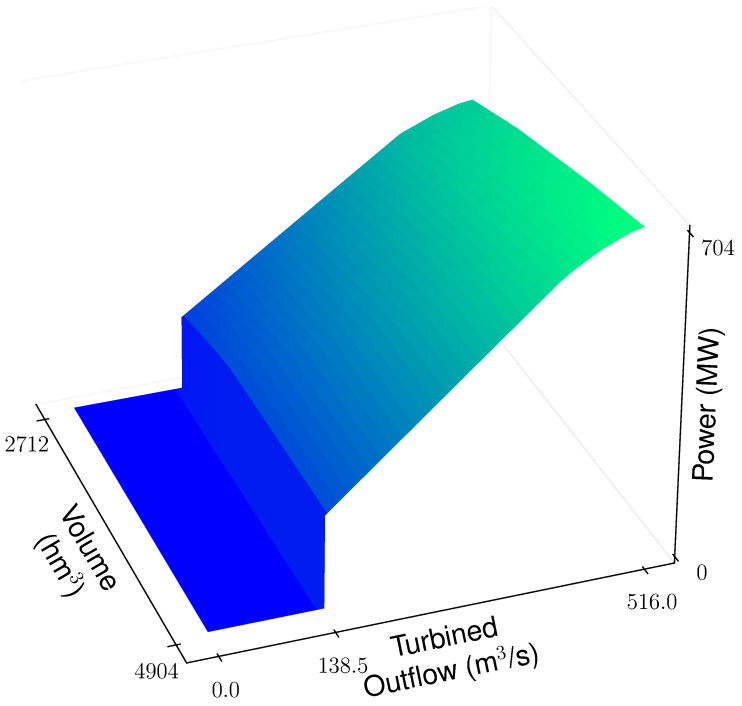

Source: Author

and the resulting HPF model using the BCH formulation with $\mathbf{N2}_{\mathrm{CH}}$ hyperplanes that are lower bounds of HPF, called BCH-2, is modeled by Equations (28), (31)-(32), and (35):

$$php \geq \mathbf{b}_{0i} V \cdot u + \mathbf{b}_{1i} Q + \mathbf{b}_{2i} S \cdot u + \mathbf{b}_{3i} u, i = 1, \ldots, \mathbf{N2}_{\mathrm{CH}}. \tag{35}$$

In this case, a product between a continuous and a binary variable can be converted into a MILP formulation (Appendix B). For example, the hyperplanes that are upper and lower limits for HPF of a 3-unit plant using the CH-2 model are presented in Figure 6.

Figure 6 – Upper and lower limits for HPF of a 3-unit plant using the CH-2 model.

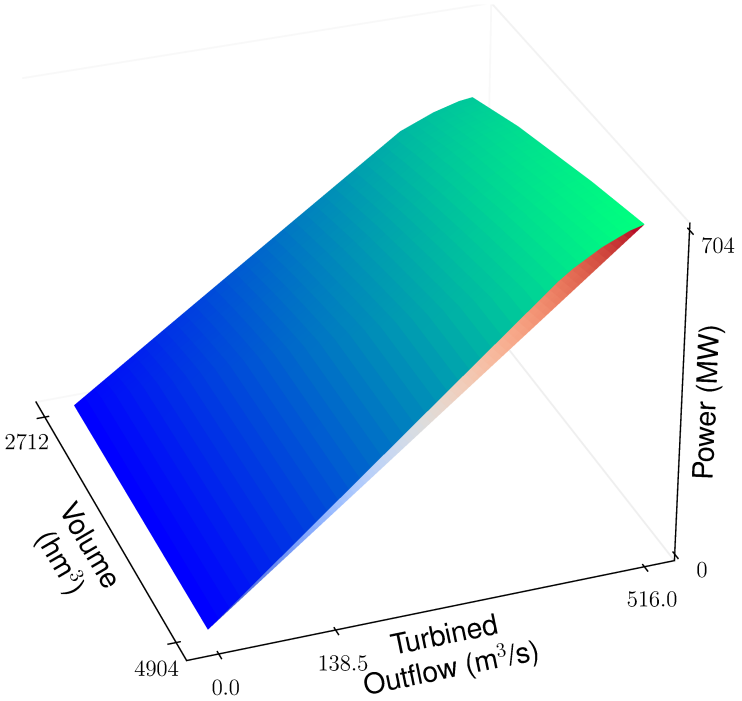

Source: Author

Thus, inserting these lower limits can reduce the error between the nonlinear HPF and *php*. Despite that, in all models of this section, the forbidden zones are ignored, which can lead to significant differences between the original and approximate HPF models. Forbidden zones are an important aspect, especially for plants with few GUs. For example, in SIN, according to ONS (ONS, 2021), from 158 hydro plants analyzed, 145 possess at most 6 GUs (representing approximately 50% of total hydro capacity), and from these, 122 have at most 4 GUs. Considering that usually a plant operates with null spillage, in the rest of this chapter, all proposed HPFs models are formulated considering the forbidden zones and ignoring the spillage.

Considering that the HPF with forbidden zones can have a concave behavior in the NFZs, we propose a model where each NFZ is modeled through the CH tech-

niques, and binary variable addresses each NFZ. This resulting model, called Piecewise Convex-Hull (PCH) model, is formulated by Equations (36)-(41):

$$php \leq \mathbf{a}_{0ki} V \cdot u_i + \mathbf{a}_{1ki} \widehat{Q}_i + \mathbf{a}_{2ki} y_i, k = 1, \ldots, \mathbf{N1}_{\text{PCH}_i}, \forall i \in \mathcal{I} \quad (36)$$

$$php \geq \mathbf{b}_{0ki} V \cdot u_i + \mathbf{b}_{1ki} \widehat{Q}_i + \mathbf{b}_{2ki} y_i, k = 1, \ldots, \mathbf{N2}_{\text{PCH}_i}, \forall i \in \mathcal{I} \quad (37)$$

$$Q = \sum_{\forall i \in \mathcal{I}} \widehat{Q}_i \quad (38)$$

$$Q_{i1} \cdot u_i \leq \widehat{Q}_i \leq Q_{i2} \cdot u_i, \forall i \in \mathcal{I} \quad (39)$$

$$\sum_{\forall i \in \mathcal{I}} u_i \leq 1 \quad (40)$$

$$u_i \in \{0,1\}, \forall i \in \mathcal{I}, \quad (41)$$

where $\mathcal{I}$ is the set of NFZs, and $i \in \mathcal{I}$ has the form $i = [Q_{i1}, Q_{i2}]$, $Q_{i1} < Q_{i2}$ and represents an NFZ on Q, $\mathbf{N1}_{\text{PCH}_i}, \mathbf{N2}_{\text{PCH}_i}$ are the number of hyperplanes used to limit *php* from above and below for each NFZ i, respectively, Q_{i1} and Q_{i2} are the extreme points in Q for the NFZ i, and u_i is a binary variable that represents the NFZ i. The hyperplanes that are lower and upper limits of HPF used in Equations (36)-(37) are evaluated in the same way presented in Section 3.2, but for each NFZ i, i.e., the grid of points used to generate sets S, S_1 in the Q-axis are restricted to $[Q_{i1}, Q_{i2}]$ interval.

In the PCH model, constraints (36)-(37) are upper and lower envelopes for *php*, and Equations (38)-(41) enforce that Q has to be 0 or a value between one of the NFZs. In terms of computational complexity, the number of binary variables used in this formulation is equal to the number of NFZs (at least ≥ 1), i.e., in the best case, this model will insert the same number of binary variables as the BCH model. The same approach is valid for the number of constraints, considering that in the PCH model, there are lower and upper limits for each NFZ. Finally, as an example, the hyperplanes of a 3-unit plant using the PCH model are shown in Figure 7.

3.3 PWL MODELS

This section presents mixed-integer formulations that approximate the nonlinear HPF by PWL models on each NFZ. The focus is on two types: a one-dimensional model as a function of Q and a two-dimensional model as a function of Q and V. The one-dimensional model is appropriate if the volume variations are negligible in the planning horizon (plants with large reservoirs). For example, consider the 3-unit plant where the maximum plant turbined outflow is 516 m^3/s, and the limits on volume are $\underline{V}$ = 2,711.49 [hm^3] and $\overline{V}$ = 4,904.45 [hm^3]. Also, let $V_{\text{med}} = 0.5(\underline{V} + \overline{V})$ = 3,807.97 [hm^3]. The HPF for the 3-unit plants as a function of Q with fixed volumes is presented in Figure 8.

However, considering the STGS problem, given a fixed initial volume V_0, the variations in volume for this plant in a one-day or 1-week are relatively small. For

Figure 7 – Hyperplanes for HPF of a 3-unit plant using the PCH model.

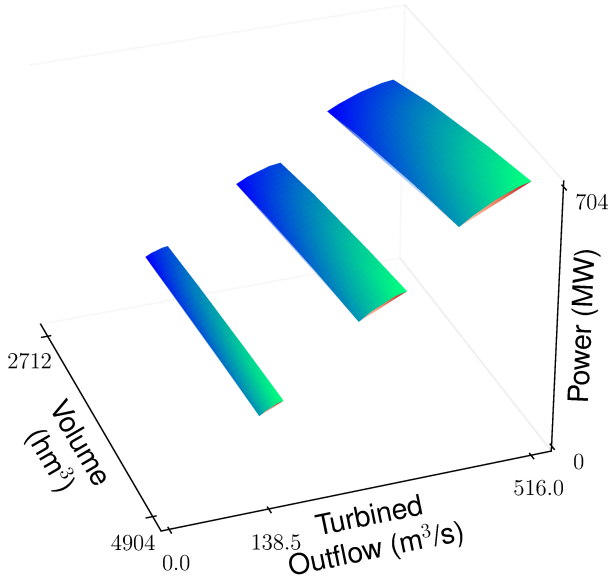

Source: Author

Figure 8 – HPF for the 3-unit plants as function of Q for fixed volumes.

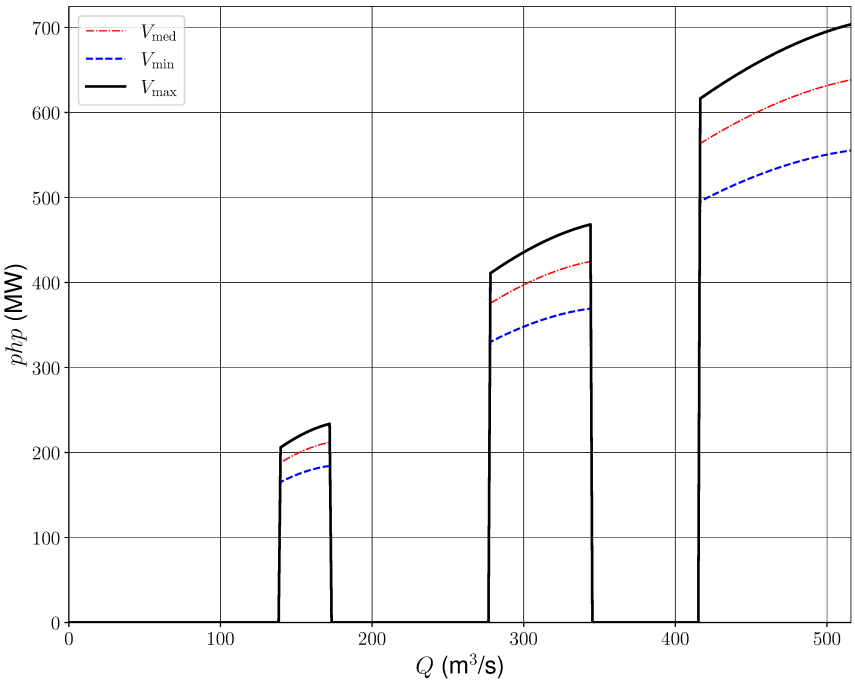

Source: Author

example, if V_0 = 50% of the useful volume, i.e., $V_0 = 0.5(\overline{V} - \underline{V}) + \underline{V}$, considering that for each hour the plant turbines the maximum plant outflow $\overline{Q}$ = 516 m^3/s and the inflow is constant, i.e., $\mathbf{Y}$ = 1000 m^3/s, for this planning horizon[2], the minimum volume is $V_1 = V_0 - \mathbf{K} \cdot \mathbf{NT} \cdot \overline{Q}$ = 3,763.38 m^3/s and the maximum volume is $V_2 = V_0 + \mathbf{K} \cdot \mathbf{NT} \cdot \mathbf{Y}$ = 3,894.37 m^3/s. The resulting HPF for these three fixed volumes is presented in Figures 9-10.

Figure 9 – HPF considering fixed volumes V_0, V_1, V_2.

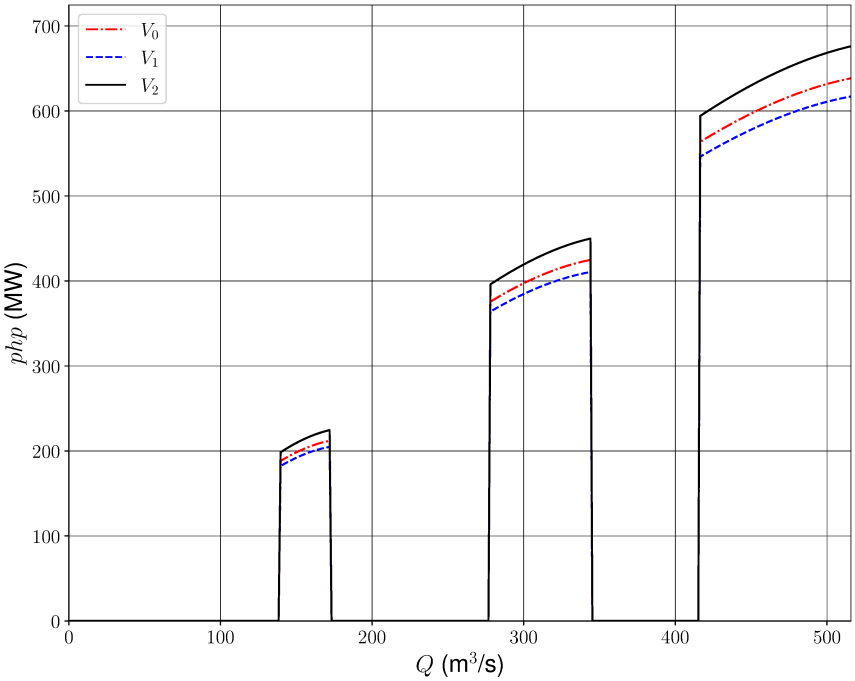

Source: Author

In Figure 10, the maximum difference between the HPFs is less than 5.0%, which is the maximum expected error for a model that ignores the volume. Although this error could be significant, it is important to note that this maximum difference only occurs when the plant achieves volume V_2. This fact only happens if the turbined outflow is 0 until the last period of the planning horizon. In practice, it is expected that the plant generates power on each period of the planning horizon, and the volume at each period is near to V_0; therefore, the volume variations have minimal impact on *php*.

For representing the HPF through a mixed-integer PWL model as (VIELMA; AHMED; NEMHAUSER, 2010; HUCHETTE; VIELMA, 2019), defining the polytopes used on the linear approximations is first necessary. Then, let $\mathcal{P}$ be the set of polytopes used in the mixed-integer PWL approximation of HPF and $p \in \mathcal{P}$ on the form $p = [Q_{p1}, Q_{p2}]$, $Q_{p1} < Q_{p2}$. This formulation must be imposed to represent the

[2] The planning horizon for simulations presented in this chapter is one week, or 24 hours, i.e., $\mathbf{NT}$ = 24, and $\mathbf{K} = 3600 \cdot 10^{-6}$.

Figure 10 – Detail of HPF in the turbined outflow range [415.5, 516] m^3/s.

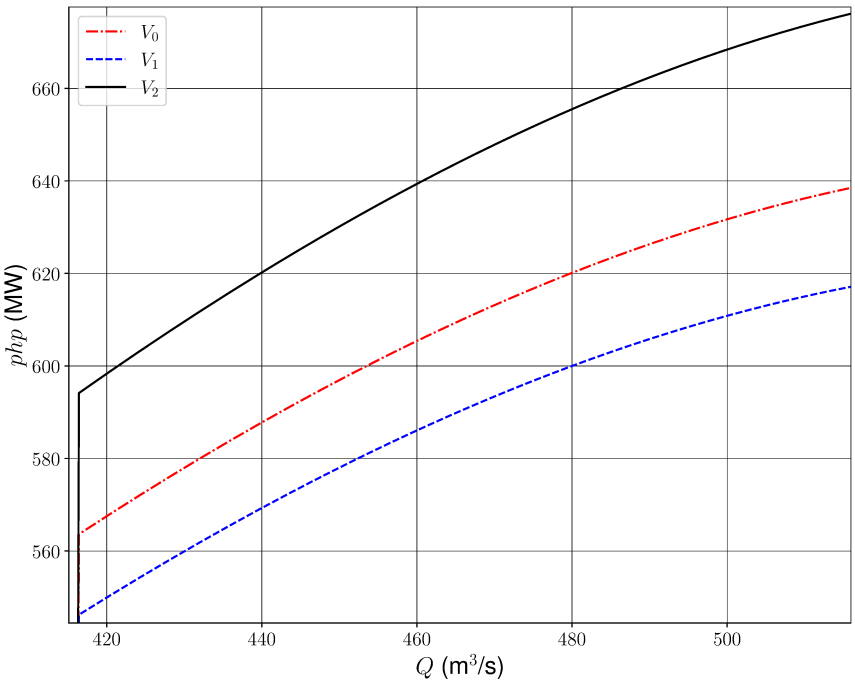

Source: Author

HPF in all NFZs, where each polytope is contained in one of the NFZs. Thus, the one-dimensional PWL model (PWL-1) for HPF considering a reference volume $\mathbf{V}_{\text{ref}}$ is given by:

$$Q = \sum_{\forall p \in \mathcal{P}} \widehat{Q}_p \tag{42}$$

$$php = \sum_{\forall p \in \mathcal{P}} \widehat{php}_p \tag{43}$$

$$Q_{p1} \cdot u_p \leq \widehat{Q}_p \leq Q_{p2} \cdot u_p, \forall p \in \mathcal{P} \tag{44}$$

$$\widehat{php}_p = \mathbf{php}(\mathbf{V}_{\text{ref}}, Q_{p1}) \cdot u_p + \frac{\mathbf{php}(\mathbf{V}_{\text{ref}}, Q_{p2}) - \mathbf{php}(\mathbf{V}_{\text{ref}}, Q_{p1})}{Q_{p2} - Q_{p1}} (\widehat{Q}_p - Q_{p1} \cdot u_p), \forall p \in \mathcal{P} \tag{45}$$

$$\sum_{\forall p \in \mathcal{P}} u_p \leq 1 \tag{46}$$

$$u_p \in \{0,1\}, \forall p \in \mathcal{P}, \tag{47}$$

where $\mathbf{V}_{\text{ref}}$ is a value between V_1 and V_2 (usually, the mean value is chosen). Note that the number of intervals is related to the quality of the linear approximation. Thus, more intervals lead to better representations at the price of an increase in the computational effort.

The second formulation for HPF considers the effects of volume. First, it can

represent the HPF from Figure 9 as a piecewise bidimensional model using formulations (VIELMA; AHMED; NEMHAUSER, 2010). However, the high number of binary variables needed to represent the functions and the approximation precision does not make the approach attractive for a large-scale. So instead, we are proposing an alternative formulation.

Analyzing Figure 10, the three HPFs have similar graphics, differentiating by a factor $\beta_p(Q) \cdot V$. Considering $\beta_p(Q)$ as constant, we can derive a two-dimensional PWL formulation for HPF (PWL-2). In this work, the equation used to define $\beta_p(Q)$ is:

$$\beta_p = \beta_p(Q) = \frac{\mathbf{php}(V_2, Q_{p1}) - \mathbf{php}(\mathbf{V}_{\text{ref}}, Q_{p1})}{V_2 - \mathbf{V}_{\text{ref}}}, \tag{48}$$

and the PWL-2 model is formulated by Equations (42)-(47), where Equation (45) is replaced by:

$$\widehat{php}_p = \mathbf{php}(\mathbf{V}_{\text{ref}}, Q_{p1}) \cdot u_p + \frac{\mathbf{php}(\mathbf{V}_{\text{ref}}, Q_{p2}) - \mathbf{php}(\mathbf{V}_{\text{ref}}, Q_{p1})}{Q_{p2} - Q_{p1}} (\widehat{Q}_p - Q_{p1} \cdot u_p)$$
$$+ \beta_p(V - \mathbf{V}_{\text{ref}}) \cdot u_p, \forall p \in \mathcal{P}. \tag{49}$$

3.4 ASSESSING HPF MODELS

Given the formulations presented in this chapter, an important aspect to be considered when choosing a specific model type for HPF is to assess the approximation in terms of errors and computational complexity. In this section, these aspects will be analyzed for a better understanding of how to compare the HPF models proposed.

To assess the approximation errors for HPF models presented in this thesis, consider the 3-unit plant presented, where the following data are used: V_1 = 3,982.8 m^3/s, V_2 = 4,113.7 m^3/s, $\mathbf{V}_{\text{ref}} = 0.6(V_2 - V_1) + V_1$. The validation points are obtained through the cartesian product between 200 equally spaced points in Q, where each point belongs to an NFZ $i \in \mathcal{I}$, with $\mathcal{I}$ = [(138.5,172), (277,344), (415.5, 516)], and ten equally spaced points in V on the range $[V_1, V_2]$. The approximation errors are calculated based on the following definitions.

Definition 3.4.1 (Relative Error) *The relative error (R_{err}) between a function $f(x)$ and an approximation $\widetilde{f}(x)$ at point x_0 is the absolute error divided by the absolute value of the function $f(x)$ at x_0:*

$$R_{err}(x_0) = \left| \frac{f(x_0) - \widetilde{f}(x_0)}{f(x_0)} \right|, f(x_0) \neq 0. \tag{50}$$

Definition 3.4.2 (Normalized Accumulated Error) *Given an interval $[x_0, x_1]$, the normalized accumulated error (NA_{err}) is the sum of errors at all valid points of function $f(x)$ in this range divided by the number of interval elements.*

Each type of model used on HPF must be considered to evaluate the NA_{err}. For example, in the envelope models, we use two types of error: the first, which measures the difference between the value of the approximation on the upper bound and the value of the nonlinear HPF, called ub_{err}, and the second error, related to the difference between the nonlinear HPF and the approximation on the lower limit, called lb_{err}.

Considering a set $\mathcal{Q}$ with N points in the interval $[Q_1, Q_2]$, the ub_{err} is obtained as:

$$\frac{1}{N}\sum_{\forall k\in\mathcal{Q}} \max\left\{\left|\frac{php(\mathbf{V},k)-php^{*}(\mathbf{V},k)}{php(\mathbf{V},k)}\right|,0\right\}, \tag{51}$$

where k is an element of set $\mathcal{Q}$, $\mathbf{V}$ is a fixed volume, and php^{*} is the value of php in the upper limit of Equation (28) for CH and BCH models, Equation (34) for CH-2 model, Equation (35) for BCH-2 model and Equation (36) for PCH model. The lb_{err}, which is associated with the CH-2, BCH-2 and PCH models, is given by:

$$\frac{1}{N}\sum_{\forall k\in\mathcal{Q}} \max\left\{\left|\frac{php(\mathbf{V},k)-php^{**}(\mathbf{V},k)}{php(\mathbf{V},k)}\right|,0\right\}, \tag{52}$$

where php^{**} is the value of php in the lower limit of Equation (34) for the CH-2 model, Equation (35) for BCH-2 model, and Equation (37) for the PCH model. Note there is no measure of lb_{err} for CH and BCH models once these models do not have a lower limit (the lower bound is equal to 0). Finally, for PWL models, considering the interval $[Q_1, Q_2]$ divided into M segments, where $\mathcal{Q}_m$ is the subinterval related to segment m and each element k belonging to one of the segments, an expression for the NA_{err} is given by:

$$\frac{1}{N}\sum_{m=0}^{M-1}\sum_{\forall k\in\mathcal{Q}_m}\left|\frac{php(\mathbf{V},k)-php(\mathbf{V},k)}{php(\mathbf{V},k)}\right|. \tag{53}$$

Now, it is possible to assess each HPF approximation presented in this chapter, using the following parameters for each model[3]:

- CH-based models: elements of set $\mathcal{S}_1$ obtained as the result of the cartesian product between $[0, 172, 344, 516]$ on Q and $[V_1, 0.5(V_1 + V_2), V_2]$ on V. Type of Error: ub_{err} for CH;
- PCH: $\mathcal{I} = [(138.5, 172), (277, 344), (415.5, 516)]$. Each subset $\mathcal{S}_{1i}$ contains elements obtained through the cartesian product between $i \in \mathcal{I}$ and $[V_1, 0.5(V_1 + V_2), V_2]$. Type of Error: ub_{err} and lb_{err};
- PWL: $\mathcal{P} = [(138.5, 172), (277, 344), (415.5, 466), (466, 516)]$. Type of Error: NA_{err} from Equation (53).

[3] since we are considering only the NFZs, the BCH model will result in the same errors as CH model. For CH-2, and BCH-2 model, the ub_{err} is the same as CH model, and lb_{err} is the same as PCH model, therefore, they are excluded from this analysis

The graphics of HPFs of this example are shown in Figures 11-12. The approximation errors are summarized in Table 3, where Nlin is the number of linear equations used to represent *php*, Nbv is the number of binary variables used in the model, and Npcv is the number of products between a continuous and a binary variable of the model. From these results, it is possible to observe that PCH and PWL models are superior for representing the HPF, at the price of increasing the number of equations and variables used to represent *php* in the optimization problem.

Table 3 – HPF models and their characteristics.

Type	Nlin	Nbv	Npcv	Error in NFZ #		
				1	2	3
CH	6	0	0	5.60%	5.19%	1.27%
PCH	30	3	30	0.46-1.01%	0.46-0.25%	0.46-0.25%
PWL-1	5	5	0	1.04%	1.03%	1.03%
PWL-2	5	5	5	1.04%	0.39%	0.39%

Figure 11 – Different HPFs for 3-unit plant considering fixed volume.

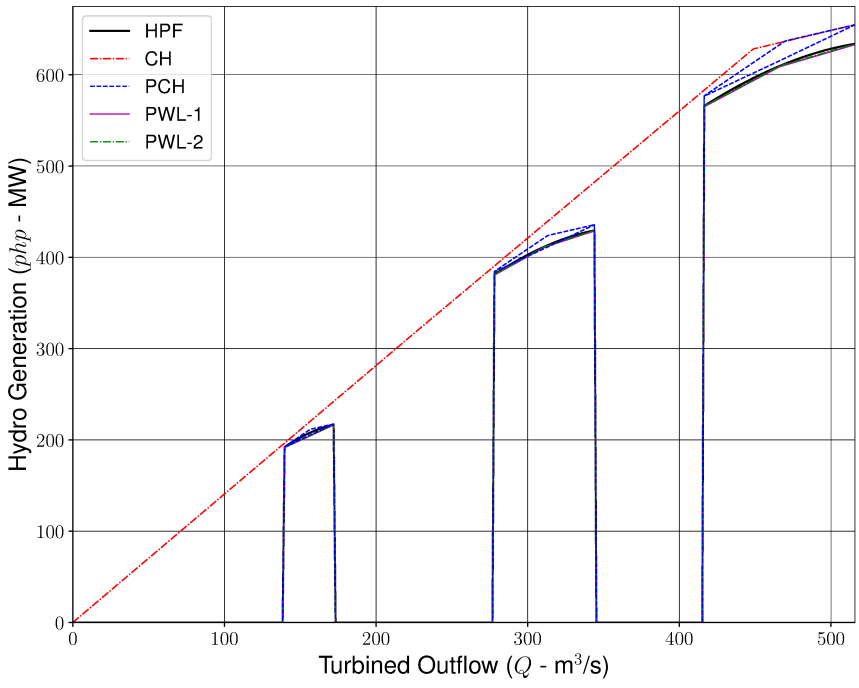

Source: Author

Figure 12 – Detail on the turbined outflow range $[415.5, 516]$ m^3/s.

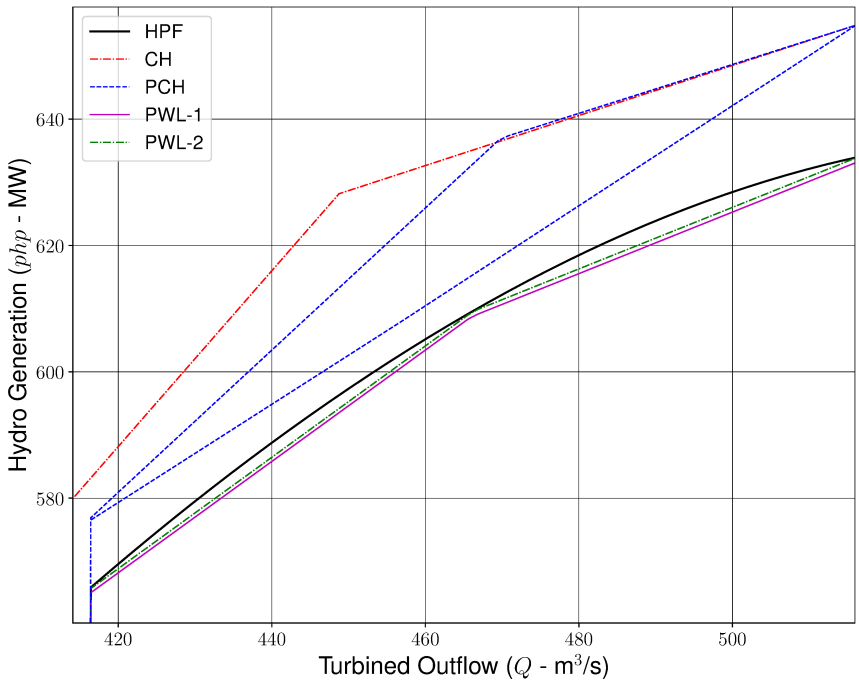

Source: Author

3.5 COMPUTATIONAL EXPERIMENTS

In this thesis, the different formulations for the HPF on the STGS problem are assessed in a modified version of the IEEE 118-bus system, where 15 hydro plants replace a subset of 14 thermal plants. The optimization model has been developed and implemented in Julia and solved using the optimization solver GUROBI (GUROBI, 2022), performed on a computer with a Ryzen 9 3900X 12-core processor with 16 GB of RAM. Each simulation has a 10-minute limit, and an optimality gap of 0.1% is imposed. The modifications and hydro data can be found in Appendix A; the planning horizon considered is 24 hours discretized in hourly steps, the STGS model is formulated by Equations (25), and the following simulations are realized:

- Case 1: CH-2 formulation for all hydro plants, i.e., Equations (25)g-(25)m, (25)s-(25)t, will be replaced by Equations (28)-(29) and (34).
- Case 2: BCH-2 formulation for all hydro plants, i.e., Equations (25)g-(25)m, (25)s-(25)t, will be replaced by Equations (28), (31)-(32), and (35).
- Case 3: PCH formulation for all hydro plants, i.e., Equations (25)g-(25)m, (25)s-(25)t, will be replaced by Equations (36)-(41).
- Case 4: PWL formulation for all hydro plants, i.e., Equations (25)g-(25)m, (25)s-(25)t, will be replaced by Equations (42)-(47) for the PWL-1 model and Equations

(42)-(44), (46)-(49) for PWL-2 model. The choice between PWL-1 and PWL-2 formulations for each plant will be presented in this section.

All the experiments are performed considering three initial volumes on the reservoirs (30, 60, and 90% of volume) and two inflows ($\mathbf{Y}_0$ and $\mathbf{Y}_1$), totalizing 24 different experiments[4]. Regarding the use of binary variables in HPF, Case 1 does not use binary variables; Case 2 includes one binary variable for each hydro plant; Case 3 includes one binary variable for each NFZ; and Case 4 is a model in which it is possible to set the precision of the HPF, at the price of using a large number (possibly more than used in Case 3) of binary variables. To choose the number of polytopes in Case 4, we developed a methodology that evaluates each hydro capacity concerning the hydro system; a minimal error is imposed depending on this participation. Also, a variation of the Douglas-Peucker algorithm (DOUGLAS; PEUCKER, 1973) is used to determine the partitions of the polytopes for each hydro. These details are described in the next subsection.

3.5.1 Generation of the Set of Polytopes

As mentioned before, the precision of HPF on PWL formulations depends on the set of polytopes $\mathcal{P}$. Therefore, a pre-processing step to generate this set is performed considering the specific characteristics of the hydro plants. Specifically, the dependency of volume and the total participation on the installed hydro generation capacity are analyzed, and after, the polytopes are generated. For the system used in this paper, Table 4 shows this information for the hydro plants, where the hydro generation capacity is 64% of the total system capacity.

In Table 4, PHH is the participation of the hydro plant concerning the capacity of all hydro plants, and $\Delta php(Q)$ is a factor that measures the influence of volume on the HPF, given by the following equation:

$$\Delta php(Q) = \frac{php(Q,V_2) - php(Q,V_1)}{php(Q,V_0)}, \tag{54}$$

where V_0 is the initial volume used in the experiment, $V_1 = \max(\underline{V}, V_0 - \mathbf{K}\cdot\mathbf{NT}\cdot\overline{Q})$ is the minimum volume available in the reservoir, and $V_2 = \min(\overline{V}, V_0 + \mathbf{K}\cdot\mathbf{NT}(\mathbf{Y} + \overline{Q}_{\text{ups}}))$ is the maximum volume available of the reservoir, $\overline{Q}_{\text{ups}}$ is the maximum outflow of the reservoirs on the upstream and γ is a parameter used to set the initial volume, i.e., $V_0 = \gamma \times (\overline{V} - \underline{V}) + \underline{V}$. To evaluate $\Delta php(Q)$, we use $Q = \overline{Q}$, because it is expected that the maximum difference occurs in $\overline{Q}$ due to the HPF being directly proportional to Q.

We use the parameter PHH as a reference to generate the partitions on Q for each hydro. N. Avanhandava, Jupiá, and Foz do Chapecó plants account for approximately 50% of the hydro installed capacity. The number of partitions chosen for these

[4] Cases CH and BCH are not included since cases CH-2 and BCH-2 has the same formulations, with an addition of lower bounds

Table 4 – Characteristics of hydro plants

Plant	PHH (%)	$\Delta php(\overline{Q})$ (%)		
		$\gamma = 30$	$\gamma = 60$	$\gamma = 90$
PROMISSÃO	7.37	2.57	2.34	2.28
BARRA BONITA	3.91	5.26	3.49	3.12
N. AVANHANDAVA	9.70	0	0	0
JUPIÁ	15.47	0	0	0
BARIRI	4.02	0	0	0
MONJOLINHO	2.06	3.41	3.38	3.34
QUEBRA QUEIXO	3.35	3.44	3.30	1.95
SÃO JOSÉ	1.42	0	0	0
PASSO SÃO JOÃO	2.15	4.43	4.37	4.32
PASSO FUNDO	6.31	0.10	0.08	0.66
PEDRA DO CAVALO	4.47	0.17	0.15	0.14
BALBINA	6.98	0.61	0.49	0.42
GARIBALDI	5.19	6.10	5.99	4.57
FOZ DO CHAPECÓ	23.88	2.02	2.01	2.00
IBITINGA	3.67	0	0	0

Source: Author.

plants results in an average approximation error of less than 3%; for the other plants, we use $\mathcal{P} = \mathcal{I}$. The partitions are defined for each NFZ, and the points on Q are defined based on a modification of the Douglas-Peucker algorithm (JILIN et al., n.d.) stated as follows:

Algorithm 1: modified Douglas-Peucker

Input: number of points ($\mathbf{NP}$), minimum average error ($\mathbf{MAE}$), set of NFZs ($\mathcal{I}$) and $\mathcal{P} = \emptyset$

Output: set $\mathcal{P}$

1 **for** $i \in \mathcal{I}$ **do**
2 set $p = i$, i.e., $p = [Q_{i1}, Q_{i2}]$
3 discretize $[Q_{i1}, Q_{i2}]$ into $\mathbf{NP} = M + 1$ points obtaining the set $[Q_{i1}, \ldots, Q_k, \ldots, Q_{i2}]$
4 compute the NA_{err} from Equation (53)
5 **if** $NA_{err} \leq \mathbf{MAE}$ **then**
6 go to Step 10
7 **else**
8 find $k \in [Q_{i1}, \ldots, Q_k, \ldots, Q_{i2}]$ that generates the highest approximation error; insert k in p; Go to Step 4
9 **end**
10 let the resulting set $p = [Q_1, Q_2, \ldots, Q_K]$, in which $Q_1 = Q_{i1}$, $Q_K = Q_{i2}$ and $Q_1 < Q_2 < \cdots < Q_K$. For $k = 1, \ldots, K-1$, take the interval $[Q_k, Q_{k+1}]$ and insert into $\mathcal{P}$
11 **end**

Algorithm 1 can be executed *a priori* and has no impact on the computational time of the STGS problem. To decide which PWL type must be used for each hydro, PHH and $\Delta php(\overline{Q})$ are analyzed. If PHH > 5% and $\Delta php(\overline{Q}) > 2\%$, the model chosen for the HPF is the PWL-2; otherwise, the option is PWL-1. With all these considerations, Table 5 contains the number of partitions (NoP) used in each NFZ and highlights the PWL model chosen.

Finally, the system reserve is equal to 5% of the demand. To evaluate the effects of the HPF models and to avoid numerical issues due to the FCF, the simulations presented in this chapter will be performed without the FCF. Still, instead, we impose volume targets at the end of the planning horizon, i.e., Equation (55) is imposed in the STGS problem.

$$V_{h,\mathbf{NT}} \geq \mathbf{V}^*_h, \tag{55}$$

where $\mathbf{V}^*_h = 98\% V_{h,0}$, i.e., the volume target admitted is equal to 2% of variation on the initial volume of hydro h. It is important to note that this equation is only imposed for hydros with large reservoirs.

3.5.2 Results

The main results obtained from all experiments are presented in this section. Table 6 shows information about the size of optimization problems, the relaxed objective

Table 5 – Number of partitions for each NFZ and PWL model chosen

Plant	NoP for NFZ #			PWL-1	PWL-2
	1	2	3		
PROMISSÃO	1	1	1		X
BARRA BONITA	1	1		X	
N. AVANHANDAVA	1	1	1	X	
JUPIÁ	2			X	
BARIRI	1	1	1	X	
MONJOLINHO	1	1	1	X	
QUEBRA QUEIXO	1	1	1	X	
SÃO JOSÉ	1	1		X	
PASSO SÃO JOÃO	1	1		X	
PASSO FUNDO	1	1	1	X	
PEDRA DO CAVALO	1	1		X	
BALBINA	1	1		X	
GARIBALDI	1	1	1		X
FOZ DO CHAPECÓ	1	1	2		X
IBITINGA	1	1	1	X	

Source: Author.

function, and runtime for different optimality gaps, where Ncons is the number of constraints of the optimization model, Ncvar is the number of continuous variables of the problem, (R)Fobj is the (relaxed) objective function value obtained with 1% gap (for the MILP). Since variations on the initial volume impact the runtime, we present information with 60% initial volume and inflow equal to $\mathbf{Y}_1$. We observe that problem with PCH formulations is three times slower than with the PWL model. Also, the computational effort for problems with the BCH-2 model is relatively small compared to those with the CH-2 model. On the other hand, simulation with the PWL model has significant computational effort compared with the BCH-2 model. Moreover, the gap between the RFobj and Fobj with a 1% gap is around 6% for all simulations.

Table 6 – Information about the optimization problems

Simulation Type	Ncons	Nbvar	Ncvar	RFobj	Fobj 1%	Runtime (s)	
						Gap 1%	Gap 0.1 %
CH-2	35,936	2,880	12,529	454,583	482,986	6.10	27.79
BCH-2	37,376	3,240	12,529	454,583	483,160	8.70	31.34
PCH	35,096	3,744	14,257	454,986	482,253	103.37	233.88
PWL	35,864	3,792	14,593	455,729	484,516	33.00	71.15

Source: Author.

For the rest of this section, all results are obtained considering an optimality gap of 1%. Regarding the formulation and the impact on the computational burden, the

results are presented in Figures 13-14. Optimization problems with CH-2 and BCH-2 models are solved in a few seconds. On the other hand, experiments using the PWL model consume an average of seven times more computational time than the CH experiments. And for the PCH model, this average increases to 23.4. The optimal cost increases for the same γ and $\mathbf{Y}$ in the following order: CH-2 (less expensive), BCH-2, PCH, and PWL. Although this does not happen in all simulations, due to the gap used, the objective function is expected to increase as the HPF formulation gets more details.

Figure 13 – Values of objective functions obtained from simulations.

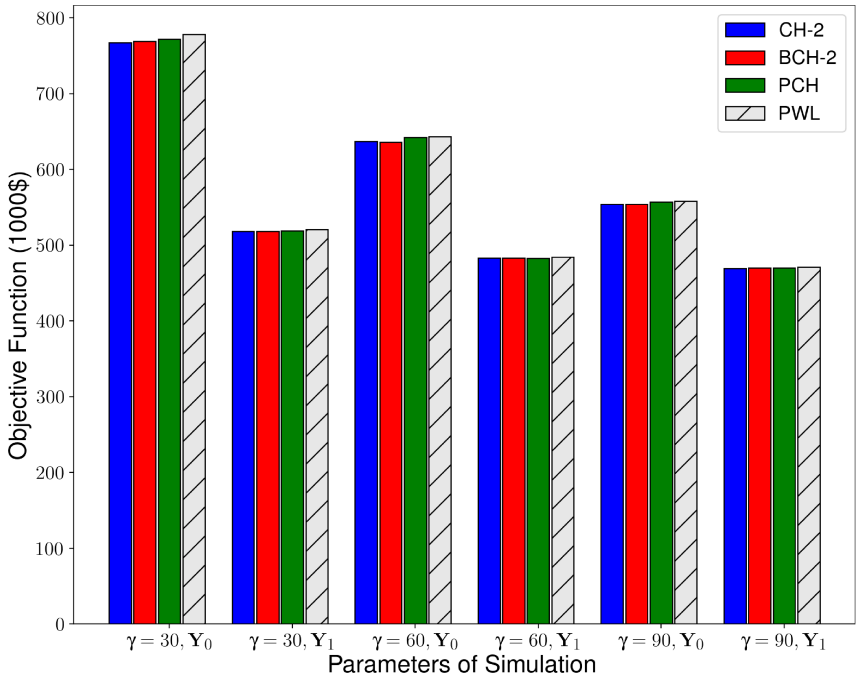

Source: Author

Figure 14 – Computational time spent of simulations.

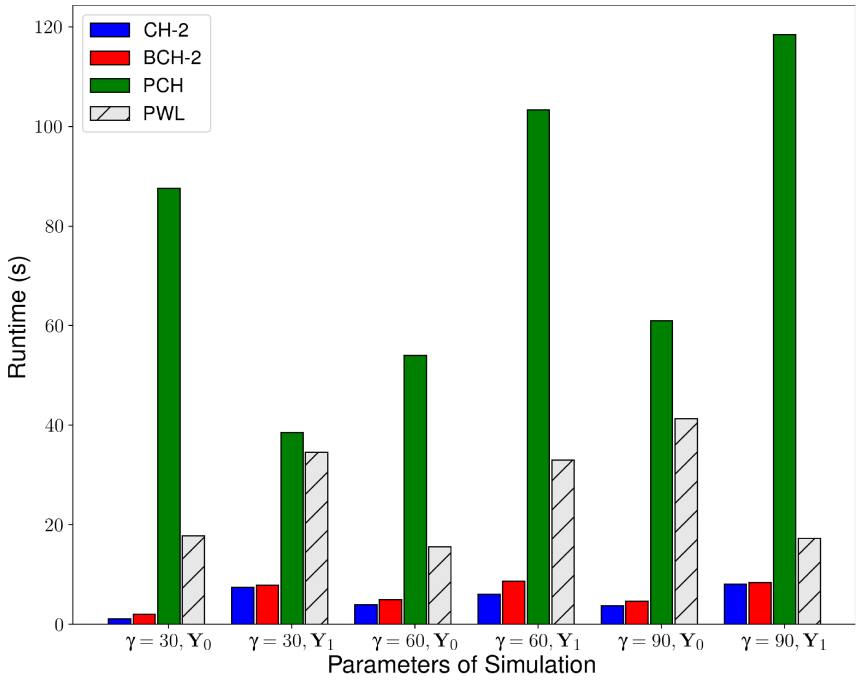

Source: Author

The impact on dispatch is directly noticeable when using models with more detailed HPF. For example, in experiments with $\gamma = 30$ and inflow $\mathbf{Y}_0$, when analyzing the total thermoelectrical generation of subsystem 2 (IEEE, 2022) presented in Figure 15, we notice an increase in the generation for the PCH and PWL models of, respectively, 4.32 and 3.01%, when compared with the dispatch obtained from CH model.

The results in Tables 7-8 present the violations of forbidden zones. Note that this only occurs on the CH-2 and BCH-2 models. The results can be interpreted in the following way. First, consider $\gamma = 30$ and $\mathbf{Y}_0$. In Table 7, for the Garibaldi plant, considering the power scheduled for each hour of the planning horizon obtained through the optimization problem, 63.79% occur in forbidden zones. For the BCH-2 model, on the other hand, the generation in forbidden zones is 14.79%. This number, combined with the PHH and the total scheduled for this plant, can help the ISO to assess the feasibility of the generation scheduled.

For illustrative purposes, consider Figure 16, which presents the Foz do Chapecó plant generating scheduling over the planning horizon. The shadow rectangles highlight the forbidden zones. This plant possesses PHH = 23.88%. Note that almost 25% of the generation for the CH-2 and BCH-2 operate in the forbidden zones. Figure 16 shows that the CH-2 model operation occurs in forbidden zones within several hours of the planning horizon. On the other hand, in the BCH-2 model, this aspect occurs less frequently.

Figure 15 – Thermoelectrical generation in Subsystem 2 for $\gamma = 30$ and $\mathbf{Y}_0$.

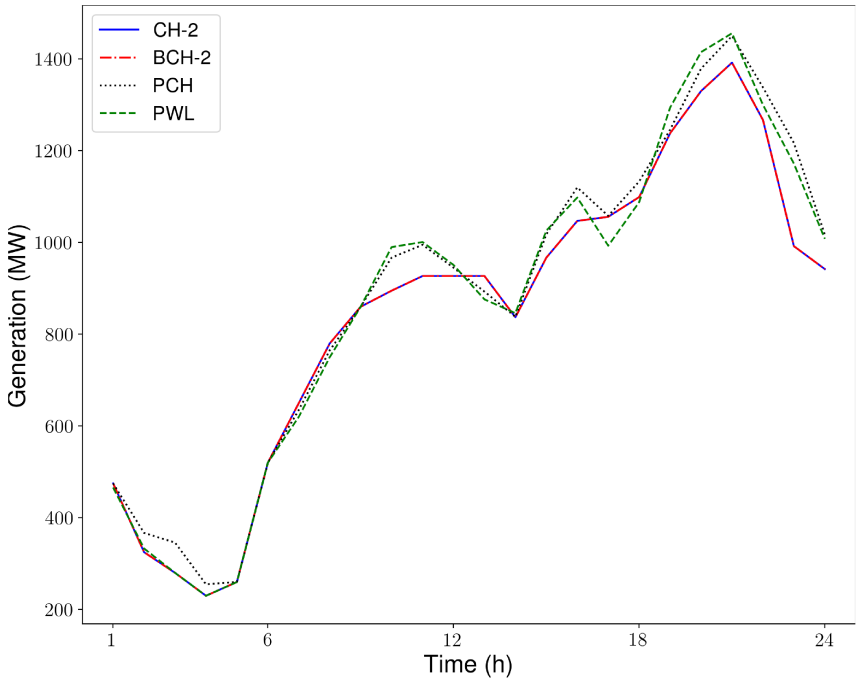

Source: Author

Table 7 – Violations due to the operation on forbidden zones for simulations with CH-2 model.

Plant	$\gamma = 30$		$\gamma = 60$		$\gamma = 90$	
	$\mathbf{Y}_0$	$\mathbf{Y}_1$	$\mathbf{Y}_0$	$\mathbf{Y}_1$	$\mathbf{Y}_0$	$\mathbf{Y}_1$
PROMISSÃO	0	3.29	0	0	6.05	0.09
BARRA BONITA	0	0	4.36	0	0	0
N. AVANHANDAVA	0	8.78	0	7.32	0	7.67
JUPIÁ	0	0	0	0	0	0
BARIRI	30.72	0	0	0	0	0
MONJOLINHO	0	0	0	0	0	0
QUEBRA QUEIXO	63.43	0	5.17	0	38.39	0
SÃO JOSÉ	10.72	0	0.75	0	3.50	0
PASSO SÃO JOÃO	92.68	0	0	0	0	0
PASSO FUNDO	0	0	0	0	0	0
PEDRA DO CAVALO	0	0	0	0	0	0
BALBINA	0	0	0	0	0	0
GARIBALDI	63.79	0	79.12	21.69	45.71	10.50
FOZ DO CHAPECÓ	23.64	0	7.27	1.72	0	1.74
IBITINGA	0	0	0	0	0	0

Source: Author.

We present in Table 9 the impact of the volume effects in the hydro plants. Also,

Table 8 – Violations due to the operation on forbidden zones for simulations with BCH-2 model.

Plant	$\gamma = 30$		$\gamma = 60$		$\gamma = 90$	
	$\mathbf{Y}_0$	$\mathbf{Y}_1$	$\mathbf{Y}_0$	$\mathbf{Y}_1$	$\mathbf{Y}_0$	$\mathbf{Y}_1$
PROMISSÃO	1.96	0	0	3.20	3.68	5.48
BARRA BONITA	0	0	1.67	0	0	0
N. AVANHANDAVA	0	4.26	0	2.41	0	2.44
JUPIÁ	0	0	0	0	0	0
BARIRI	34.80	0	0	0	0	0
MONJOLINHO	0	0	0	0	0	0
QUEBRA QUEIXO	18.09	0	13.70	0	12.13	0
SÃO JOSÉ	0	0	4.23	0	3.34	0
PASSO SÃO JOÃO	41.05	0	0	0	0	0
PASSO FUNDO	0	0	0	0	0	0
PEDRA DO CAVALO	0	0	0	0	0	0
BALBINA	0	0	0	0	0	0
GARIBALDI	14.79	0	51.35	10.46	29.17	3.54
FOZ DO CHAPECÓ	25.74	0	10.59	1.53	0	0
IBITINGA	0	0	0	0	0	0

Source: Author.

Figure 16 – Scheduled generation of Foz do Chapecó plant.

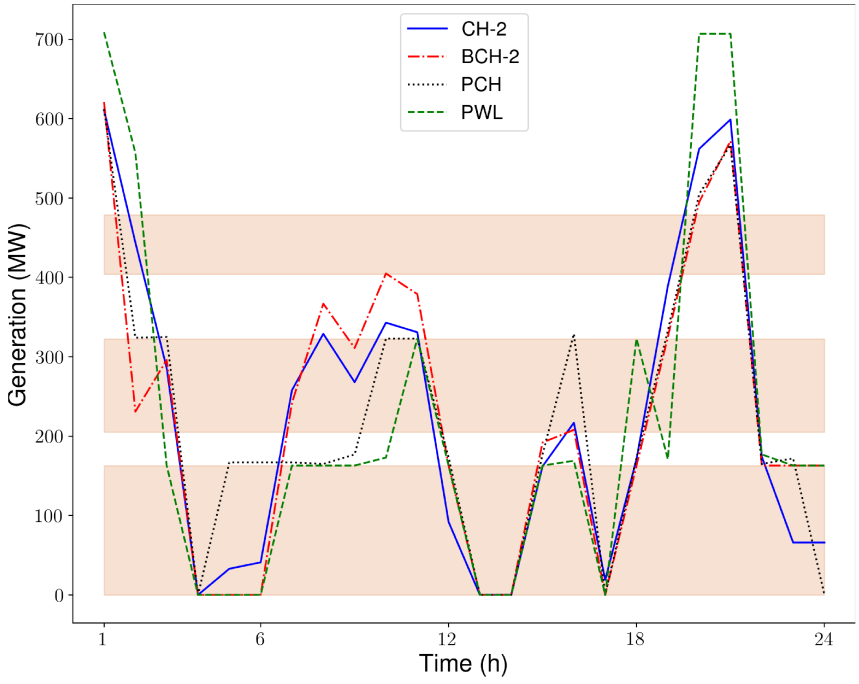

Source: Author

we have increased the number of partitions for each NFZ (equally spaced) to have an

HPF model closer to the nonlinear function. For comparison, we include the overall HPF error (OHPFe) measure, which is the relative error over the planning horizon for all hydro plants related to the total hydro generation, and the results obtained for the reference (Ref) simulation. In contrast, for the PWL model, we use the mixed strategy presented in Table 5. All simulations are performed considering a 1% optimality gap, $\gamma = 60$, $\mathbf{Y}_1$, and a time limit of 600 seconds (achieved only in simulation 6).

Table 9 – Results for different parameters of PWL formulation.

Simulation #	PWL-#		NoP for each NFZ	Fobj ($)	Runtime (s)	OHPFe (%)
	1	2				
1	X		3	483,138	47.70	5.41
2		X	3	484,024	126.92	5.19
3	X		5	484,515	43.28	5.24
4		X	5	482,368	325.70	4.79
5	X		8	483,122	75.31	4.74
6		X	8	483,744	600	4.62
Ref	-	-	-	484,516	33.00	5.64

Source: Author.

Notice that the PWL formulation can achieve reasonable OHPFe values, although the increase of NoP is the price to pay for better precision. Also, the inclusion of the volume effects on HPF significantly impacts the computational effort. As can be seen, the different formulations on the HPF can directly impact the STGS problem. For these experiments, a relative number of hydro plants showed violations on the CH and BCH model scheduling. Of course, if the total amount of violations is relatively high, the PCH and PWL models can fix this problem.

On the other hand, the BCH formulation can be interesting in cases where the violations are minor. The PWL formulation is attractive if a high level of accuracy is required for the HPF. Still, many binary variables are required depending on the precision, and a higher computational effort is required. Also, it is possible to impose a particular formulation for each hydro plant of the system, but this is out of this work scope.

3.6 FINAL CONSIDERATIONS

This chapter presented different formulations to approximate the nonlinear HPF using the plant-based approach. Initially, the nonlinear formulation was detailed, and the differences when considering the NFZs were shown. Then, envelope models were proposed, where the CH model from (DINIZ; MACEIRA, M. E. P., 2008) was improved with the addition of a binary variable to represent the on/off status of the plant, and the addition of lower limits for plants where the spillage does not have influence on *php*.

Also, the PCH model was formulated, being an extension of the CH model for each NFZ. In sequence, PWL models were proposed to improve the HPF as the price to add fewer binary variables and constraints. In this sense, two formulations were formulated, where one only considers the effects of Q, and the second imposes a correction factor to take into account the effects of V, in a linear way. In the end, a discussion about assessing the HPF formulations, considering the different models proposed, was presented.

From the simulations performed, it was possible to observe that the PCH and PWL models are attractive alternatives to represent the HPF since both models can handle precisely the operation in forbidden zones. The increase in computational time is an issue that needs more investigation in large-size systems, although decomposition techniques and parallel processing are natural options in this context. Also, depending on the accuracy required, a particular HPF model can be chosen, enabling an STGS problem where each hydro has a specific type of formulation presented in this work. This analysis can be performed *a priori*, using a pre-processing algorithm, and has no impact on the computational time required to solve the STGS problem.

Despite such aspects, it is possible to find formulations in which the approximation error of HPF is relatively small. Still, the computational effort can turn the problem impossible to be solved, even in high-performance computers. It is important to measure the computational effort involved to evaluate the impacts of all formulations proposed in this chapter in the STGS problem. Considering the importance of solving the STGS problem quickly and using detailed formulations in particular for the HPF, considering systems with a dominance of hydro generation (as in Brazil), the next chapter is focused on a decomposition strategy that can be applied to the STGS problem with a large horizon (168 hours), aiming to turn viable the improvements on HPF presented in this chapter.

4 DUAL DYNAMIC INTEGER PROGRAMMING APPLIED TO STGS PROBLEM

In this chapter, a temporal decomposition scheme for the STGS problem is proposed. Considering the STGS problem is modeled as a MILP, the BD is a natural scheme to decompose the problem. However, the vanilla BD can only have a convex subproblem, i.e., binary variables are not allowed. Due to the complexity of the STGS problem, a major challenge is how to break the problem in a way allowing to obtain subproblems that contain only information about a specific part of the temporal resolution of the original problem. In this sense, Dual Dynamic Integer Programming (DDiP) can be applied to STGS to solve this problem efficiently. Therefore, in this chapter, the DDiP and improvements to accelerate the algorithm's convergence are presented and applied to the STGS problem.

For the remaining of this chapter, the following definitions will be used. A multi-period MILP problem with $t = \{1, \ldots, T\}$ periods is called full-space MILP. This problem can be viewed as a multistage problem, where each stage is related to one or more periods. A multi-period stage p contains more than one period; for example, $p = 1$ contains periods $t = \{1,2,3,4\}$ represented by all single-periods of this stage without any simplification. An aggregated stage $q = 1$ containing periods $t = \{1,2,3,4\}$ is an aggregation of this four time-periods into an one equivalent stage q. These definitions can be visualized in Figure 17.

4.1 DECOMPOSITION METHODS AND BENDERS DECOMPOSITION

A decomposition method applied to an optimization problem is one of the fundamental techniques that can be used to attempt to solve the problem. For large-scale problems, fully solving the problem without any technique can be impossible, even for modern computers and the recent advances in optimization solvers. Recognizing some structure and using a decomposition technique to break the original problem into several subproblems that are easier to solve is a valid approach and has been used over the years by the mathematical optimization community. As mentioned in Chapter 1, decomposition strategies can be classified according to their structure, resulting in the primal and dual methods.

A particular decomposition scheme can be applied according to the problem structure. For example, if the problem has complicating variables[1], the Benders Decomposition (BD) can be applied if the subproblem obtained has a particular structure. On the other hand, a Lagrangian Relaxation (LR) can be applied if the problem has complicating constraints. A decomposition called Nested BD (NBD) can be applied for a particular structure of optimization problems, where each subproblem is coupled only

[1] complicating variables are variables where if we remove them, the resulting optimization problem becomes more easy to be solved

Figure 17 – Example of single, multi-period and aggregated stages.

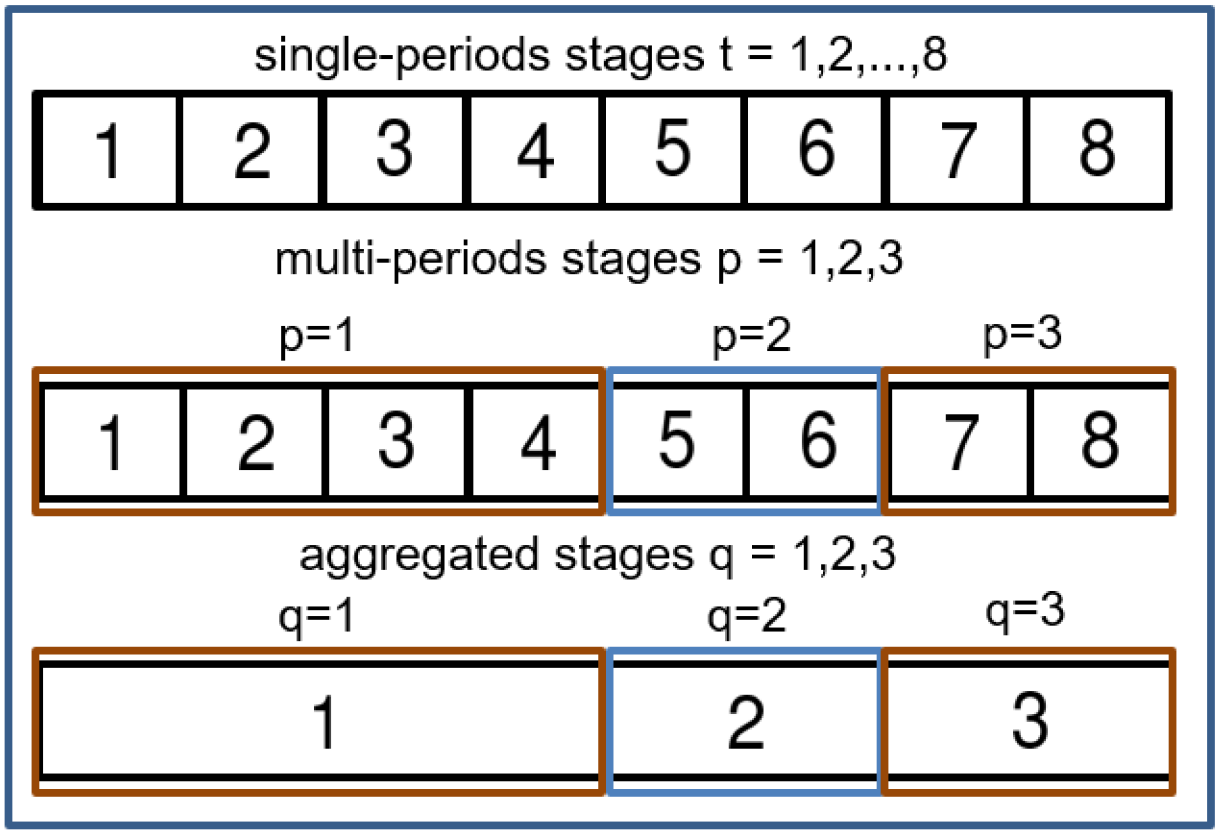

Source: Author

with the adjacent subproblem. To summarize, Figure 18 presents each type of structure found in optimization problems that can be applied to one of the decomposition schemes mentioned, where lines represent constraints and each column represent a variable, highlighted with different colors. As this thesis focuses on partially-coupled problems with complicating variables, the remainder of this section gives an overview of BD.

The BD was originally proposed by Benders (BENDERS, 1962) and generalized by Geoffrion (GEOFFRION, 1972), where the objective is to break an optimization problem into a sequence of two problems, one called master problem (MP) and the other called subproblem (SP). The idea of this decomposition is to deal with problems that contain complicating variables, which, when assumed fixed values, yield a problem that is easier to solve. Although BD can be applied in several classes of optimization problems, including NLP and MINLP, this section will focus on the BD applied to the

Figure 18 – Schematic of optimization problems with a particular structure, where (a) contain complicating constraints, (b) complicating variables, and (c) is partially coupled.

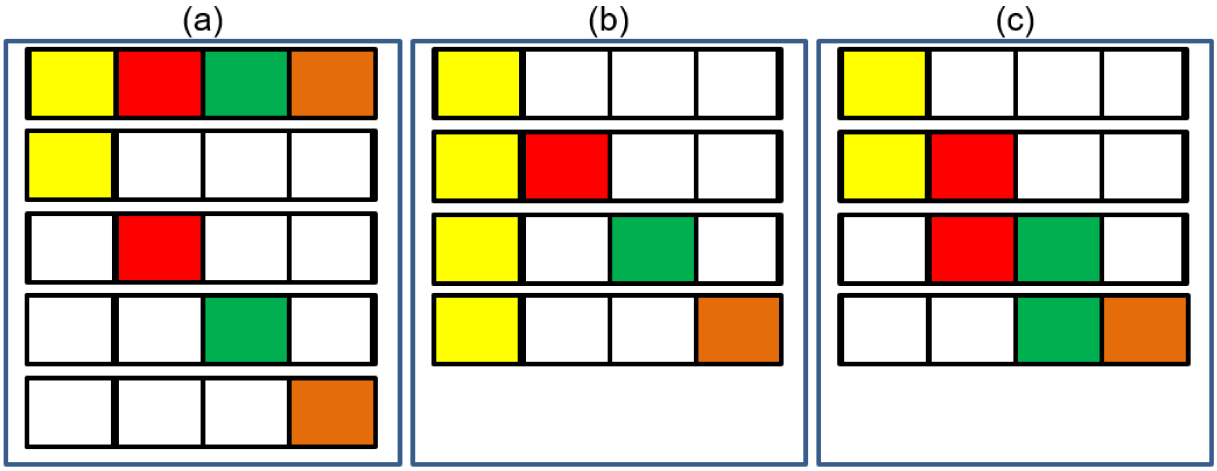

Source: Author

MILP problem. Therefore, let the following MILP problem:

$$\begin{aligned} \min \quad & d^T y + c^T x \\ \text{s.t.:} \quad & Ay = b \\ & Fy + Ex = h \\ & y \in \mathbb{Z}_+^{n_1}, x \in \mathbb{R}_+^{n_2}, \end{aligned} \tag{56}$$

with $d \in \mathbb{R}^{n_1}, c \in \mathbb{R}^{n_2}, A \in \mathbb{R}^{m_1 \times n_1}, E \in \mathbb{R}^{m_2 \times n_2}, F \in \mathbb{R}^{m_2 \times n_1}, b \in \mathbb{R}^{m_1}$ and $h \in \mathbb{R}^{m_2}$. In this problem, y is the complicating variable and, for a fixed value $\widehat{y}$, the MILP problem described in Equation (56) is linear in x. Therefore, problem (56) can be written as:

$$\min_{\widehat{y} \in \mathcal{Y}} d^T \widehat{y} + \min \left\{ c^T x : Ex = h - F\widehat{y} \right\}, \tag{57}$$

where $\widehat{y}$ is an element belonging to the set $\mathcal{Y} = \left\{ y | Ay = b, y \in \mathbb{Z}_+^{n_1} \right\}$. The inner minimization, which is an LP, can be dualized using dual variables λ associated with the constraints $Ex = h - F\widehat{y}$:

$$\max_{\lambda \in \mathcal{R}^{m_2}} \left\{ \lambda^T (h - F\widehat{y}) : \lambda^T E \leq c \right\}, \tag{58}$$

and since the primal and dual formulations can be interchanged, due to the duality theory (RAHMANIANI et al., 2016), an equivalent formulation for problem (56) is obtained:

$$\min_{\widehat{y} \in \mathcal{Y}} d^T \widehat{y} + \max_{\lambda \in \mathcal{R}^{m_2}} \left\{ \lambda^T (h - F\widehat{y}) : \lambda^T E \leq c \right\}. \tag{59}$$

Analyzing problem (59), it is possible to conclude that the feasible space of the inner maximization, $\mathcal{S} = \left\{ \lambda | \lambda^T E \leq c \right\}$ is independent of $\widehat{y}$ chosen. If $\mathcal{S}$ is not empty,

the inner problem can be unbounded or feasible for any choice of $\widehat{y}$. To avoid the inner problem be unbounded, which means the $\widehat{y}$ chosen is infeasible, a feasibility constraint of type $r_f^T(h - F\widehat{y})$ (where r_f^T is obtained through a feasibility problem) is added to the problem to avoid movements in the directions of unboundedness r_f. And for the case when the inner problem is feasible given a $\widehat{y}$ chosen, the solution of the inner maximization is an extreme point $\lambda_o, o \in \mathcal{O}$, where $\mathcal{O}$ is the set of extreme points of $\mathcal{S}$. If all feasibility cuts belonging to the set of extreme rays $\mathcal{F}$ of $\mathcal{S}$ are added to the outer minimization problem, the decision of the inner problem is an extreme point. Consequently, problem (59) is rewritten as the master problem (MP), formulated as:

$$\min \quad d^T y + \alpha \tag{60a}$$

$$\text{s.t.} \quad Ay = b \tag{60b}$$

$$\alpha \geq \lambda_o^T(h - Fy), \quad \forall o \in \mathcal{O} \tag{60c}$$

$$0 \geq r_f^T(h - Fy), \quad \forall f \in \mathcal{F} \tag{60d}$$

$$y \in \mathbb{Z}_+^{n_1}. \tag{60e}$$

The Benders SP is formulated by Equation (58). Because it is practically impossible to enumerate all elements of $\mathcal{F}$ and $\mathcal{O}$, the BD algorithm is formulated as an iterative scheme of solving the MP to obtain a trial solution $\widehat{y}$ and SP to generate a feasibility or optimality cut to MP. The iterative process repeats until a stop criterion is achieved, which is normally the optimality gap. The BD algorithm is illustrated in Figure 19 and presented as follows.

Figure 19 – Schematic of Benders decomposition.

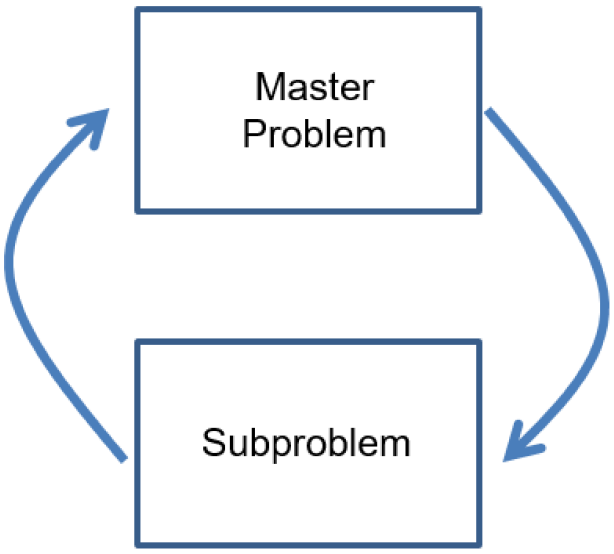

Source: Author

Algorithm 2: Benders Decomposition

Input: A MILP problem of type (56)

Output: Solution of MILP, y^*, x^* and the value of $f^* = d^T y^* + c^T x^*$

initialize $\mathcal{O}$,$\mathcal{F} = \emptyset$, and a tolerance ε. Solve MP (60). If it is obtained an infeasible solution, **stop** (the original problem is infeasible). Else, $\widehat{y}^1 \leftarrow y, z^{\text{LB}} \leftarrow \min d^T y^1 + \alpha^1$ (if MP is unbounded, set an arbitrary $\widehat{y}$ and $z^{\text{LB}} \leftarrow -\infty$) ;

for $k = 1,2,\ldots$ **do**

  solve SP (58) for $\widehat{y}^k$;

  if SP (58) *is infeasible* **then**

    the original problem is either infeasible or unbounded. **Stop**.

  end

  if SP (58) *for* $\widehat{y}^k$ *is unbounded* **then**

    generate a feasibility cut of type $r_f^T(h - F\widehat{y}^k)$, **update** $\mathcal{F} \leftarrow \mathcal{F} \cup \{r_f^T(h - F\widehat{y}^k)\}$ and go to Step 16

  end

  SP is feasible. Set $\widehat{\lambda}_o^k \leftarrow \lambda$, $z^{\text{UB}} = d^T\widehat{y}^k + \lambda^T(h - F\widehat{y}^k)$;

  if $z^{UP} - z^{LB} < \varepsilon$ **then**

    Get x^* as the dual variables of SP (58). Set $y^* \leftarrow \widehat{y}^k$ and $f^* \leftarrow d^T y^* + c^T x^*$. **Stop** ;

  else

    generate an optimality cut $\alpha \geq \lambda_o^k(h - \widehat{y}^k)$, **update** $\mathcal{O} \leftarrow \mathcal{O} \cup \{\lambda_o^k(h - \widehat{y}^k)\}$ and go to Step 16 ;

  end

  solve MP (60) and $\widehat{y}^{k+1} \leftarrow y, z^{\text{LB}} \leftarrow \min d^T y^{k+1} + \alpha^{k+1}$;

end

return y^*, x^*, f^* if converged.

4.2 NESTED BENDERS DECOMPOSITION AND DUAL DYNAMIC INTEGER PROGRAMMING

Certain optimization problems have a particular structure, such as Figure 18(c), which allows applying the BD in different nested schemes. This particular approach is the Nested BD (NBD) and was first proposed to solve a multistage stochastic linear problem in (BIRGE, 1985). Each pair of adjacent stages is considered a particular SP. As an example, Figure 20 presents a case of the NBD applied to the problem represented in Figure 18(c). The original problem is decomposed into an MP and an SP, where the decisions variables of the MP are sent to the SP (represented by the variable with an over hat symbol).

Figure 20 – Example of Nested Benders Decomposition, applied in problem of Figure 18. For this case, three SPs are obtained, where (a) is the SP-1, (b) is the SP-2 and (c) is the SP-3.

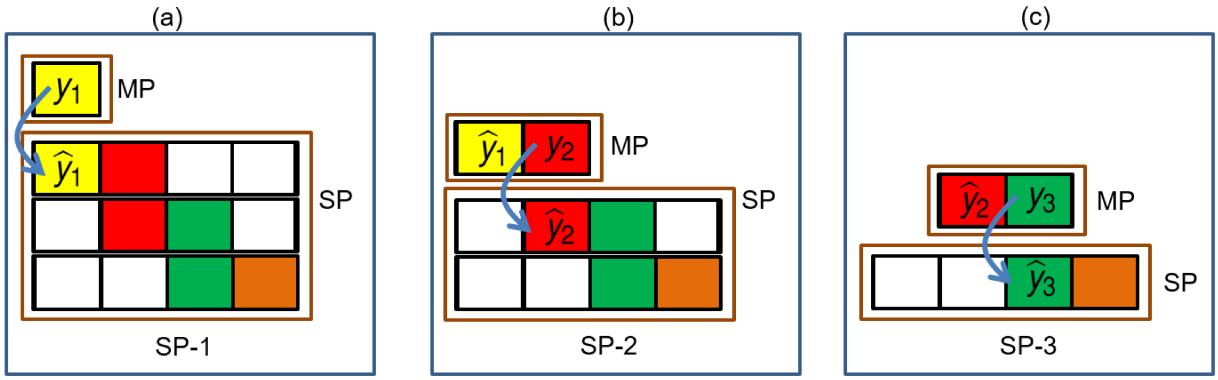

Source: Author

BD and NBD require convex SPs to generate valid cuts; therefore, these approaches do not allow sets of integer variables. To overcome this issue in MILP problems, DDiP generalizes the NBD with these particular sets. To illustrate the DDiP approach, consider the following MILP problem in a compact representation.

$$\min \quad \sum_{t=1}^{T} \left(d_t^T y_t + c_t^T x_t \right) \tag{61a}$$

$$\text{s.t.} \quad A_t y_t = b_t, \quad \forall t \in \{1, \ldots, T\} \tag{61b}$$

$$D_t y_t + B_t x_t = g_t, \quad \forall t \in \{1, \ldots, T\} \tag{61c}$$

$$F_t y_t + E_t y_{t-1} = h_t, \quad \forall t \in \{2, \ldots, T\} \tag{61d}$$

$$y_t \in \mathbb{Z}^{n_1} \times \mathbb{R}^{n_2}, \quad \forall t \in \{1, \ldots, T\} \tag{61e}$$

$$x_t \in \mathbb{Z}^{m_1} \times \mathbb{R}^{m_2}, \quad \forall t \in \{1, \ldots, T\}, \tag{61f}$$

where $n = n_1 + n_2, m = m_1 + m_2$ are the dimensions of vectors y_t and x_t, respectively, $\forall t$ belonging to the set of stages $\{1,2,\ldots,T\}$ (the dimensions of x_t, y_t are the same just for simplicity). In this problem, x_t are local variables (non-linking), and y_t are linking variables, and both can contain continuous and discrete components, A_t, D_t, B_t, F_t, E_t are matrices and d_t, c_t, b_t, g_t, h_t are vectors on the compatible dimensions. Problem (61) can be cast as dynamic programming (KUMAR et al., 2021). In this case, for each stage t, there is an optimization problem that minimizes the sum of the current stage cost and a cost-to-go function, which contains the cost of the future stages. Thus, introducing auxiliary variables $z_t \in \mathbb{R}^n$ to represent the previous stage variable y_{t-1}, the cost-to-go function for stage t, $Q_t(x_t,y_t,y_{t-1})$, is given by:

$$Q_t(x_t,y_t,y_{t-1}) = \min \quad d_t^T y_t + c_t^T x_t + Q_{t+1}(y_t) \tag{62a}$$

$$\text{s.t.} \quad A_t y_t = b_t \tag{62b}$$
$$D_t y_t + B_t x_t = g_t \tag{62c}$$
$$F_t y_t + E_t z_t = h_t \tag{62d}$$
$$z_t = y_{t-1} \tag{62e}$$
$$y_t \in \mathbb{Z}^{n_1} \times \mathbb{R}^{n_2} \tag{62f}$$
$$x_t \in \mathbb{Z}^{m_1} \times \mathbb{R}^{m_2} \tag{62g}$$
$$z_t \in \mathbb{R}^{n}, \tag{62h}$$

with $Q_{T+1} = 0$. The DDiP scheme can now be applied to the problem (62). The proposed scheme approximates the cost-to-function Q_t by a function φ_t modeled by PWL equations obtained in each iteration. Thus, to obtain these equations, the cost-to-go functions must be convex; therefore, an LP relaxation of stage SPs is imposed. Using an iterative scheme based on the forward and backward passes, the DDiP aims to improve φ_t iteratively. At iteration k, the forward pass solves a sequence of SPs formulated by Equations (63)a-(63)i for each stage t, following the order $t = 1,2,\ldots,T$, as presented in Figure 21 (highlighted by the black arrow).

$$\Phi_{tk}(x_t, y_t, \widehat{y}_{t-1,k}) = \min \quad d_t^T y_t + c_t^T x_t + \varphi_{t+1} \tag{63a}$$
$$\text{s.t.} \quad A_t y_t = b_t \tag{63b}$$
$$D_t y_t + B_t x_t = g_t \tag{63c}$$
$$F_t y_t + E_t z_t = h_t \tag{63d}$$
$$z_t = \widehat{y}_{t-1,k} : (\mu_{tk}) \tag{63e}$$
$$\varphi_{t+1} \geq \Phi_{t+1,l} + (\mu_{t+1,l})^T (y_t - \widehat{y}_{tl}),$$
$$l = 0,\ldots,k-1 \tag{63f}$$
$$y_t \in \mathbb{Z}^{n_1} \times \mathbb{R}^{n_2} \tag{63g}$$
$$x_t \in \mathbb{Z}^{m_1} \times \mathbb{R}^{m_2} \tag{63h}$$
$$z_t \in \mathbb{R}^{n}, \tag{63i}$$

where φ_{t+1} is a PWL approximation of Φ_{t+1}, μ is a dual variable (only valid for the continuous relaxation of the problem) associated with constraint (63)e, $\widehat{y}_{t-1,k}$ is the decision obtained for y in the previous stage $t-1$ at iteration k, and Equation (63)f contains the collection of Benders cuts obtained from previous iterations, used to approximate Φ_{t+1}. The forward pass yields an upper bound and a feasible solution to the original problem. After finishing the forward, the backward pass is performed. In the backward, a sequence of relaxed versions of the problem (63) for each t is solved, aiming to update the cost-to-go function Φ_t, and obtain the dual variables μ_t. The order in which the SPs are solved is the reverse of the forward pass, i.e., $t = \{T,\ldots,2,1\}$, as shown in Figure 21 (red arrows). The backward pass yields a lower bound to the optimal value of the original problem.

Figure 21 – An overview of the DDiP scheme at iteration k.

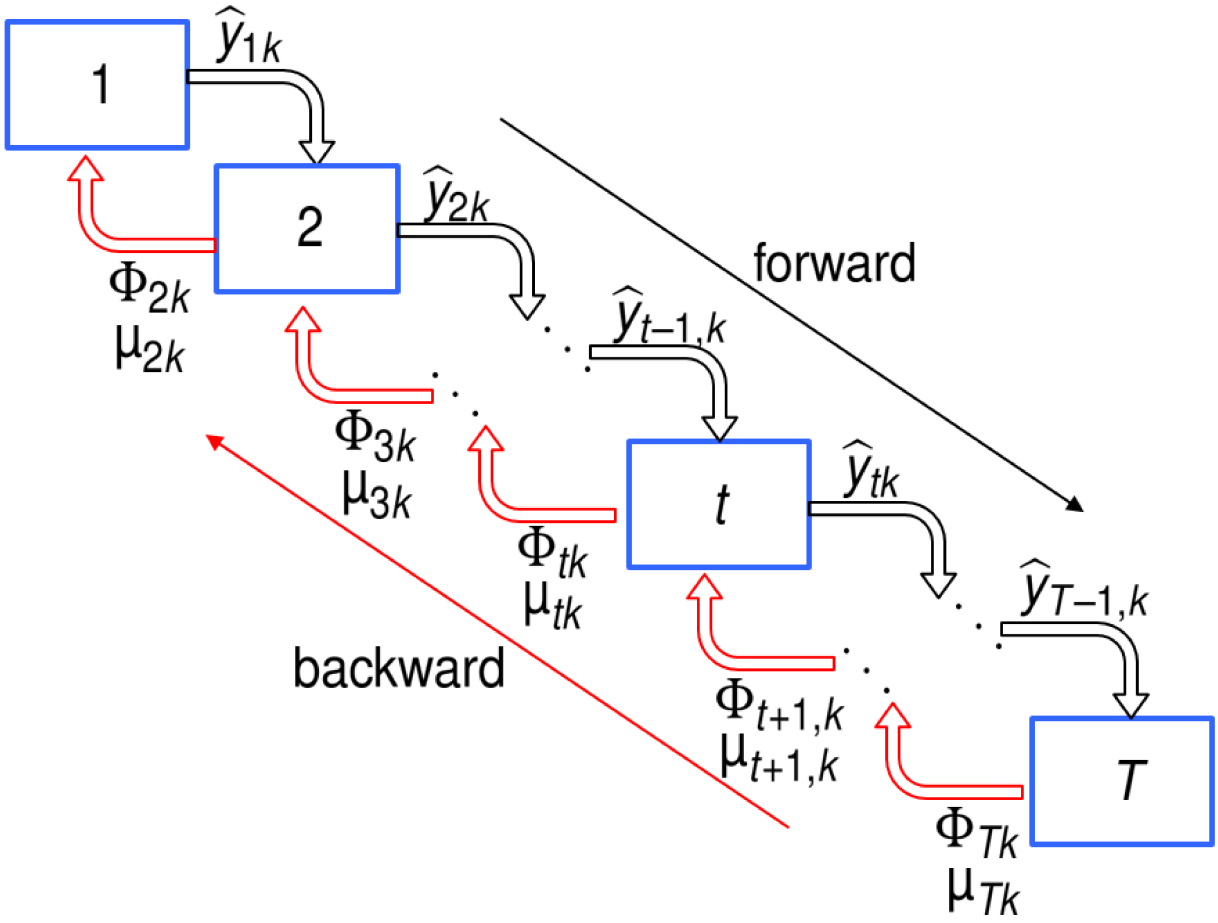

Source: Author

To summarize, the standard DDiP scheme is given by:

Algorithm 3: The standard DDiP scheme

Input: A MILP problem of type (61)

Output: Solution of MILP, y^*, x^* and $f^* = d^T y^* + c^T x^*$

Initial Setup: start with $\Phi_{T+1,0} = \mu_{T+1,0} = 0$. Set the iteration counter $k = 0$, a tolerance ε and an initial upper bound UB

for $k = 0,1,\ldots$ **do**

  The Forward Pass: for $t = 1,\ldots,T$, solve the MILP problem (63), obtaining y_t, x_t. Compute the current upper bound (ub_k), using:

$$ub_k = \sum_{t=1}^{T} d^T y_{t,k} + c^T x_{t,k} \tag{64}$$

  if $UB < ub_k$ **then**

    $UB = ub_k$

  end

  The Backward Pass: for $t = T,\ldots,1$, solve a relaxation of problem (63), obtaining $\Phi_{t,k}, \mu_{t,k}$. For each stage t, a Benders cut is constructed from the dual variables $\mu_{t,k}$ and inserted in the subsequent backward problem referring to $t-1$ period in the form of Equation (63)f. At the $t = 1$ period, we evaluate the current lower bound (lb_k), using Equation (65):

$$lb_k = \Phi_{1k} \tag{65}$$

  if $gap = (UB - lb_k)/UB \leq \varepsilon$ **then**

    Stop (converged)

  end

end

return y^*, x^*, f^* if converged.

A key advantage of DDiP is that it decomposes the original problem into more easier SPs. A disadvantage is that DDiP does not have guaranteed finite convergence (due to the presence of integer state variables). However, experimental results show that the optimality gap can be relatively small, and the solution is mostly near-optimal. Also, the BD requires that all decisions obtained in the MP must be valid in the SP; otherwise, the SP will be infeasible. Thus, to avoid that, usually, feasibility cuts are created. However, since the use of feasibility cuts can increase the computational effort drastically, in this thesis, slack variables are added in constraints (63)b-(63)d with a high penalty value in the objective function. Adding slack variables makes every solution in the MP feasible, as the price to obtain a positive value for some of these variables.

4.3 IMPROVEMENTS ON DDIP

Different approaches have been developed to improve the performance of BD algorithms when applied to MILP problems. However, in the context of DDiP, only a few works have been reported. Seminal works that explore BD algorithms with integer state variables are (ZOU; AHMED; SUN, 2019a; LARA; SIIROLA; GROSSMAN, 2020; SHAHIDEHPOUR et al., 2021). In (ZOU; AHMED; SUN, 2019b), different classes of cuts, e.g., Benders, Lagrangian, strengthened Benders, and integer optimality cuts, are explored. In (LARA et al., 2018), a comparison of the first three types of cuts in a power system planning problem is explored. The authors show that, in general, although Benders cuts are less tight than others, the convergence of the DDiP with Benders cuts has superior performance due to the less computational effort required.

To improve the DDiP, we use an acceleration scheme to initialize the DDiP with a warm-start cost-to-go function since this has been proven to work efficiently in large-scale problems (LARA et al., 2018). In addition, a multi-period stage scheme is proposed, with aggregation of multiple sequential single-periods in one SP. This strategy allows for solving fewer SPs and obtaining high-quality cuts in each stage; however, the computational effort to solve each SP increases. Finally, a particular overlap strategy is performed to find better solutions in each stage of the forward step. Details of these improvements are presented in the remainder of this section.

4.3.1 Pre-solve Strategy for DDIP

The proposed DDiP algorithm has interesting properties, particularly temporal decomposition, suitable for STGS problems. However, since it is an NBD strategy, the DDiP has the same issues as the BD, such as oscillating in the upper bound and poor-quality cuts, especially in early iterations (RAHMANIANI et al., 2016). To improve the DDiP, (LARA et al., 2018) proposed an acceleration strategy that aims to initiate the algorithm with a warm-start, using an initial cost-to-go function obtained by solving an auxiliary problem. This work will perform a similar acceleration technique denominated pre-solve step, as presented below.

The first step is to solve an auxiliary problem related to the original MILP problem (called full-space MILP, using the same notation as (LARA et al., 2018)) and use its solution to generate cuts, as long as the cuts are valid before applying the DDiP scheme. This auxiliary problem can be an aggregated version (LARA et al., 2018), a version of the original MILP problem where sequential periods are aggregated into one equivalent period, or a relaxed version of the full-space MILP. The aggregation level must be chosen carefully to generate valid cuts in the first option. Likewise, a lower level of aggregation can lead to a problem that can take almost the same time to solve as the original problem. On the other hand, a high level of aggregation can lead to a problem

that can be solved quickly, at the price to obtain weaker cuts.

As an alternative for aggregation, we can solve a relaxed problem that has to be chosen in a way that can not take much computational effort. In particular, the LP relaxation of the original problem can be applied, or a MILP without a subset of hard constraints. The solution $\widehat{y}_{t,0}$ obtained in this step is used to generate cuts in a pre-backward pass, obtaining initial cuts related to variables $\varphi_{t,0}, \mu_{t,0}$. In this work, we used the LP relaxation of the original problem in the presolve step. An overview of the DDiP with this pre-solve step is presented in Figure 22.

Figure 22 – DDIP with a pre-solve step (adapted from (LARA et al., 2018)).

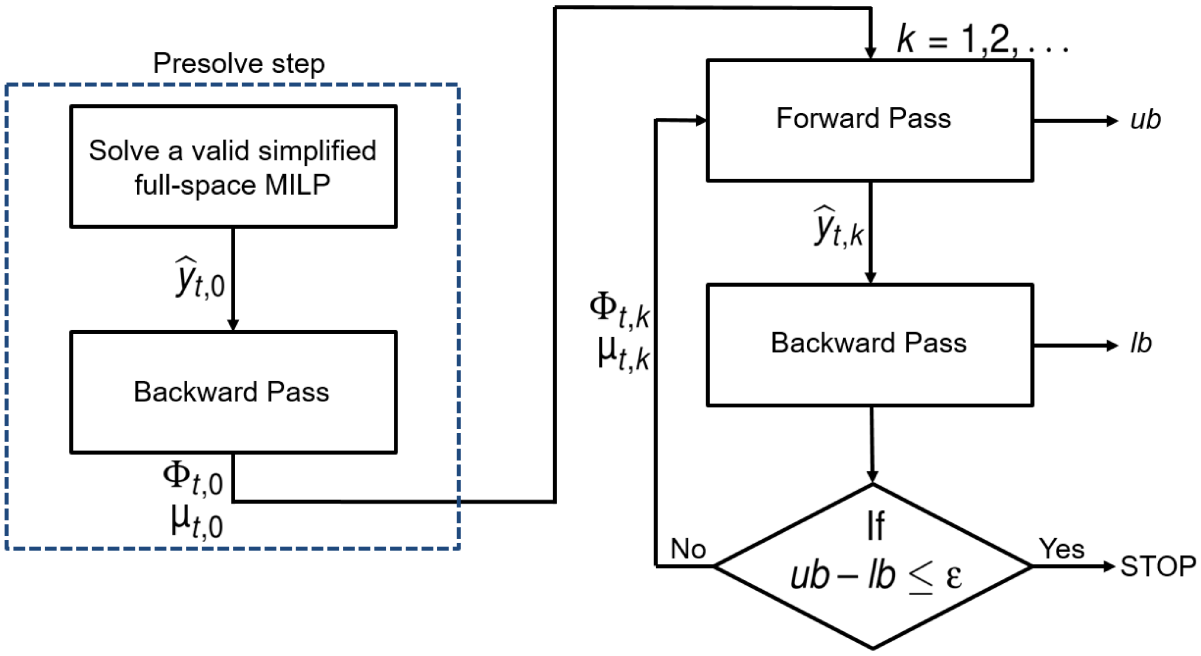

Source: Author

4.3.2 Multi-period Strategy and Overlap

Based on the main ideas presented in (SANTOS; DINIZ, 2009), we propose a multi-period aggregation scheme by aggregating sequential single-periods as one single SP. The main objective is to speed up the DDiP convergence by reducing the number of SPs. However, since the size of SPs will increase in this approach, the number of periods that compound the stage must be chosen carefully. Ideally, this number should not significantly impact the SP's computational performance. Since the definition of aggregation only implies that multiple adjacent periods must be used to create a multi-period stage p, different multi-period stages for the same problem can be generated, as shown in Figure 23.

Figure 23 – Some multi-periods stages for a MILP: (a) stages with one period, (b) stages with two periods, and (c) stages with non-uniform size.

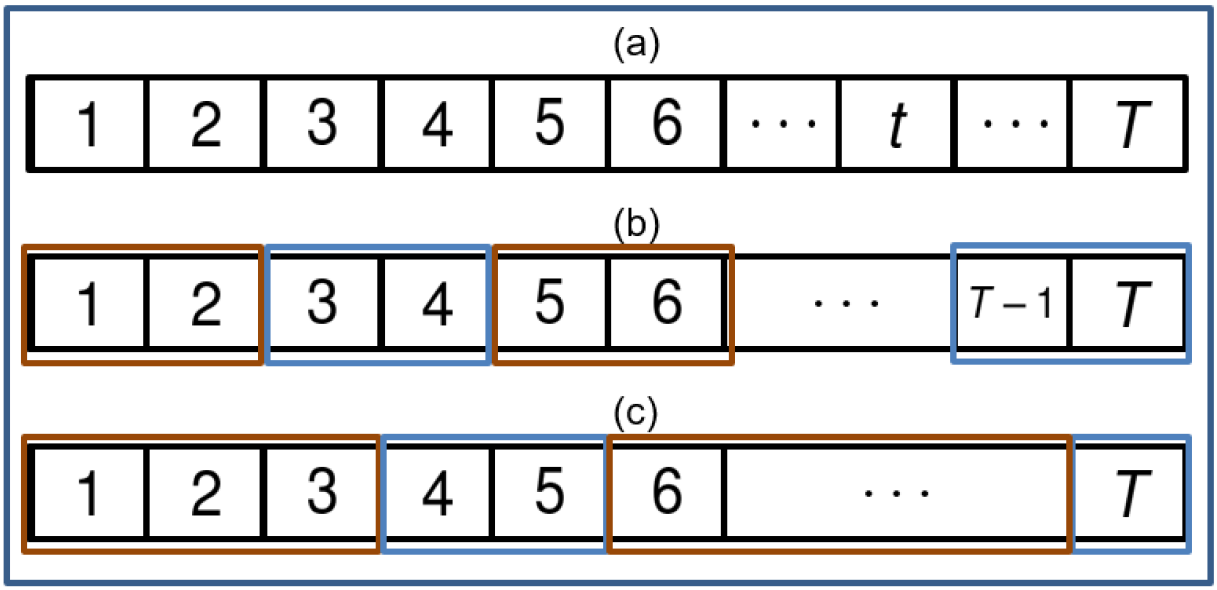

Source: Author

In Figure 23, case (a) is the most frequent decomposition scheme used in standard DDiP (i.e., each SP refers to one period). Without loss of generality, we can consider that each stage contains two periods, i.e., the first block includes the first two periods and so on, resulting in the multi-period stage presented in (b). Since the stages do not need to be uniform, we can decompose the problem like (c). The multi-period stages performed will directly impact the performance of the DDiP in terms of computational effort and duality gap. In cases with uniform sizes aggregation, a factor K is defined as the number of periods in stage p. For instance, $K = 1$ for case (a), $K = 2$ is the case (b), and $K = T$ means the original problem without decomposition, i.e., one unique stage containing all periods.

Considering that in the forward step, the current stage's decisions do not precisely consider the constraints and costs associated with the future stages, the solutions obtained in the initial iterations of the DDiP are usually of low quality or even infeasible. The infeasibility issue can be avoided by using feasibility cuts or slack variables with high penalty costs, where the last strategy is used in this work. On the other hand, an additional strategy must be employed to avoid low-quality solutions. In this work, we employ a strategy based on the overlap Schwarz decomposition (NA et al., 2021), aiming to improve the overall convergence of the DDiP scheme.

The overlapping strategy includes some variables and constraints of subsequent SPs in the current SP. The aim is to avoid potential nonzero slack variables obtained in the current SP due to the lack of precise information about the next SPs. Choosing

which variables and constraints to be included must be carefully performed because the overlapping strategy increases the size of the optimization problem of each SP. An example of a DDiP case with no aggregation of periods and overlap can be visualized in Figure 24. For this example, each SP contains constraints and variables of the current period and the next two SPs, except the two last SPs. The last SP does not contain overlap, and the last but one SP contains overlap constraints of the next SP, which is the last SP. A second example, presented in Figure 25, is a case where each stage contains two periods, and the overlap contains constraints and variables of all subsequent SPs. This case demonstrates that combining the overlapping and multi-period strategies in the DDiP strategy is possible.

Figure 24 – Illustration of overlap decomposition scheme with no multi-period strategy.

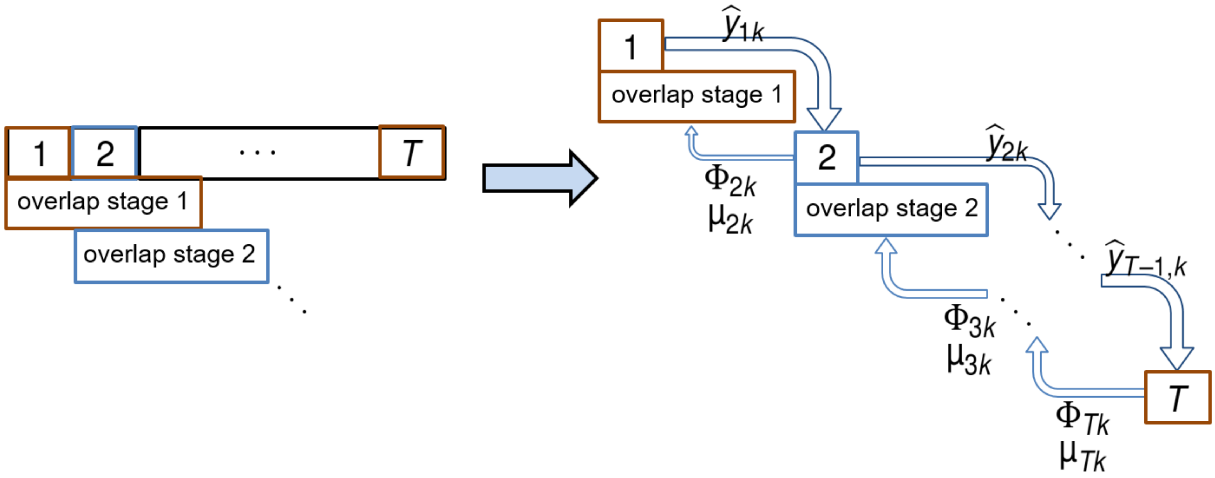

Source: Author

Figure 25 – Illustration of overlap decomposition scheme with multi-period strategy.

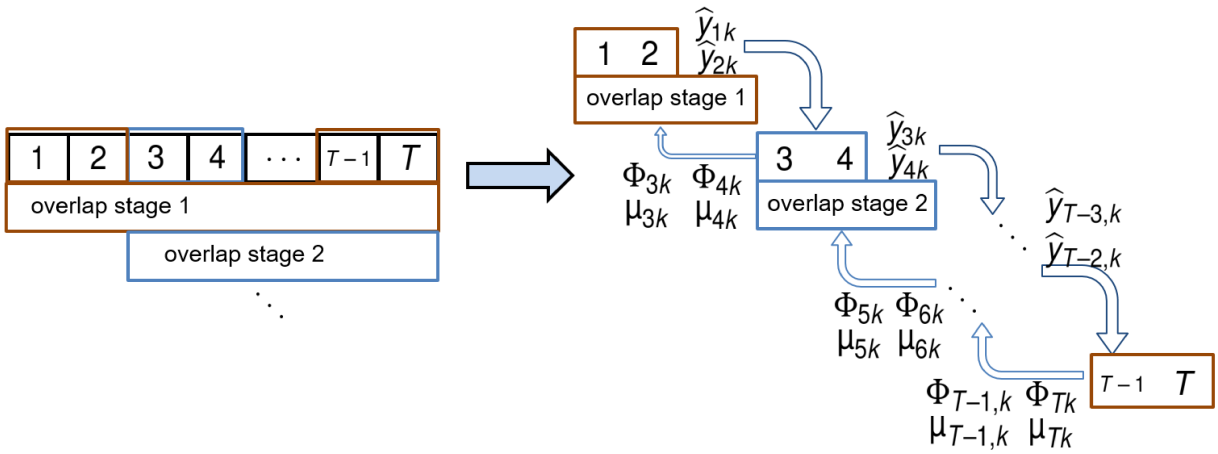

Source: Author

4.4 COMPUTATIONAL EXPERIMENTS

This section presents computational experiments performed on the STGS problem using the DDiP scheme framework proposed in this thesis.

4.4.1 Data and Initial Setup

The STGS problem is performed in the modified IEEE-118 system. All experiments are performed on a machine with a Ryzen 9 3900X 12-core processor, 16 GB RAM, and Windows 10. The DDiP is implemented in Julia with the algebraic language JuMP (DUNNING; HUCHETTE; LUBIN, 2017). Gurobi (GUROBI, 2022) is used to solve the MILP problems. The DDiP is performed considering a planning horizon of 168 hours (periods). For comparison, the STGS without any decomposition strategy is also solved and compared the performance in terms of computational effort and solution with several schemes of the DDiP approach. All SPs in DDiP have a limit runtime of 900s and a 0.1% optimality gap. The DDiP presents a limit of 25 iterations and $\varepsilon = 0.5\%$. For illustrative purposes, Table 10 gives an overview of the size of the STGS problem when represented as a single MILP.

Table 10 – Number of variables and constraints in STGS problem

Variables	**Binary Variables**	**Constraints**
196,297	23,010	366,985

Source: Author.

In the results, the DDiP implementation is called s-DDiP. In turn, DDiP with the pre-solve step is termed as a-DDIP, where the pre-solve strategy is performed by solving the LP relaxation of the original problem. The original MILP without any decomposition strategy is labeled f-MILP. Concerning the multi-period strategy, different values for parameter K were tested (we consider only strategies with uniform sizes), aiming to find the value that gives the best overall performance. Additionally, to implement the overlapping strategy (o-DDiP), it is necessary to analyze the STGS problem to find which constraints are more interesting to insert.

Some subsets of constraints are interesting to include in the overlap because they contain key information about the problem. In experiments, the water balance (25)n, network (25)p-(25)q, HPF (25)l, and TUC constraints (25)b-(25)u are included in the overlapping strategy, while the FCF is not included. To support this assumption, consider the water balance equation, which gives stored water value on the reservoirs at the end of the planning horizon for a specific hydro h, and supposes that the s-DDiP is used to solve the STGS problem. In the first stage (and in the subsequent others until the final stage T), the current decision on the volume of hydro h does not contain precise information about the value of water stored. Therefore, any feasible decision is valid,

usually forcing the reservoir to a low-level volume. Since this is not an optimal decision due to water use in the next stages, it is important to include this information in some way in the current stage. Thus, the water balance equation concerning the p subsequent stages, denominated p_{WB}, is included in the current stage in the overlapping strategy.

Similarly, the inclusion of network constraints of the subsequent SPs can increase the quality of the solution in the current stage. For example, consider the case without overlapping. Since the current problem does not have information about the demand profile for the next stages, the solutions obtained in this stage could be to turn off some thermal plant units that must be online in the next stages due to an increase in demand. The inclusion of the network constraints is expected to minimize this issue. Considering that the network constraints can increase the computational effort dramatically, and taking into account that we are using the DC network model, we represent a hydrothermal economic dispatch (ED) model of the p subsequent stages (denominated p_{DC}) for the overlapping constraints:

$$\sum_{\forall g \in \mathcal{G}} pt_{gt} + \sum_{\forall h \in \mathcal{H}} ph_{ht} = \mathbf{P}_{bt}. \tag{66}$$

Considering the network constraints are included for p_{DC} subsequent stages, it is also interesting to insert the HPF and TUC constraints for the same subsequent stages. First, consider p_{TUC} (p_{HPF}) the p subsequent stages related to the TUC (HPF) constraints. It is important to note that each subset of constraints does not need to include the same subsequent stages, e.g., $p_{WB} \neq p_{DC}$. However, for simplification, in all simulations the overlapping constraints will be applied to the same subsequent stages, i.e., $p_{WB} = p_{DC} = p_{TUC} = p_{HPF} = P$. Also, the HPF constraints included in the overlap are inserted in the full version, i.e., without simplification or relaxation. The set of TUC constraints is included in the overlapping strategy via linear relaxation of (25)y, which means that we are removing the integrality constraint of each binary variable. The choice of insert the full version of HPF constraints and the linearized version of TUC is due to computational aspects observed in simulations.

4.4.2 Influence of the size of stages

A comparison of different values for the K parameter used in the DDiP applied to the STGS problem is presented in this section. The values of K (number of periods for stage) chosen are 1, 4, 8, 12, 14, 21, 24 and 168 ($K = 168$ is the original MILP problem solved without decomposition, so-called f-MILP), and experiments for s-DDiP and a-DDiP (with linear relaxation in the pre-solve step) are performed. The results for the s-DDiP are presented in Figure 26 and summarized in Table 11.

Figure 26 – Optimality gap and CPU time for s-DDiP.

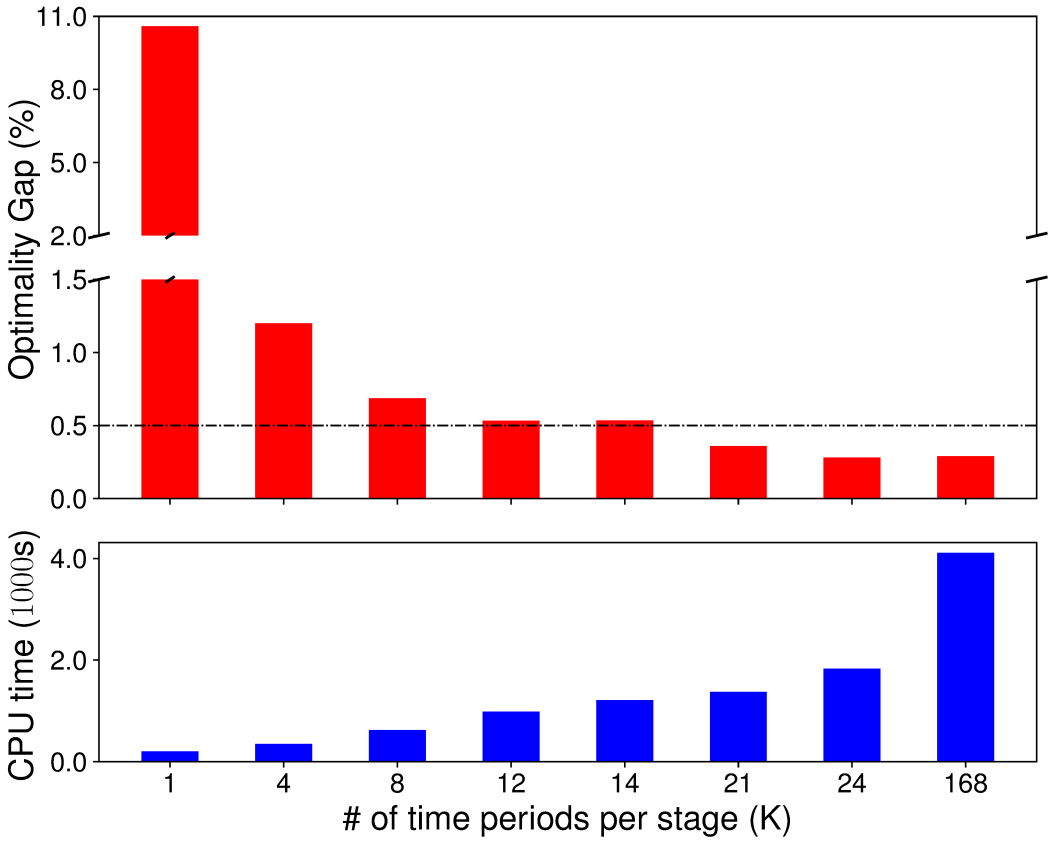

Table 11 – Summary of results obtained for s-DDiP.

K	**Optimality gap (%)**		**Final result**		
	2 minutes	10 minutes	CPU time (sec.)	Optimality gap (%)	Iterations
1	12.67	–	197.96	10.59	25
4	3.31	–	347.57	1.20	25
8	29.03	0.68	619.62	0.68	25
12	22.00	1.88	985.23	0.53	25
14	100	9.30	1211.35	0.53	25
21	100	3.86	1338.93	0.38	15
24	100	11.24	1831.94	0.28	13
168	–	–	4110.00	0.29	–

As can be seen, there is a trade-off between a small optimality gap and the CPU time required. For small values of K, the DDiP runs relatively fast if compared with simulations for large values of K, but the optimality gap does not reach the tolerance $\varepsilon = 0.5\%$. On the other hand, as the value of K increases, the optimality gap reaches

the tolerance; however, with the increase in the CPU time. With 25 iterations, cases with $K = 1, 4, 8, 12$, and 14 do not reach the optimality gap. In particular, cases $K = 12$ and 14 almost reach the 0.5% tolerance. For the remaining cases, the optimality gap was reached with less CPU when compared to f-MILP. For the a-DDiP case, the results are presented in Figure 27 and summarized in Table 12.

Figure 27 – Optimality gap and CPU time for a-DDiP.

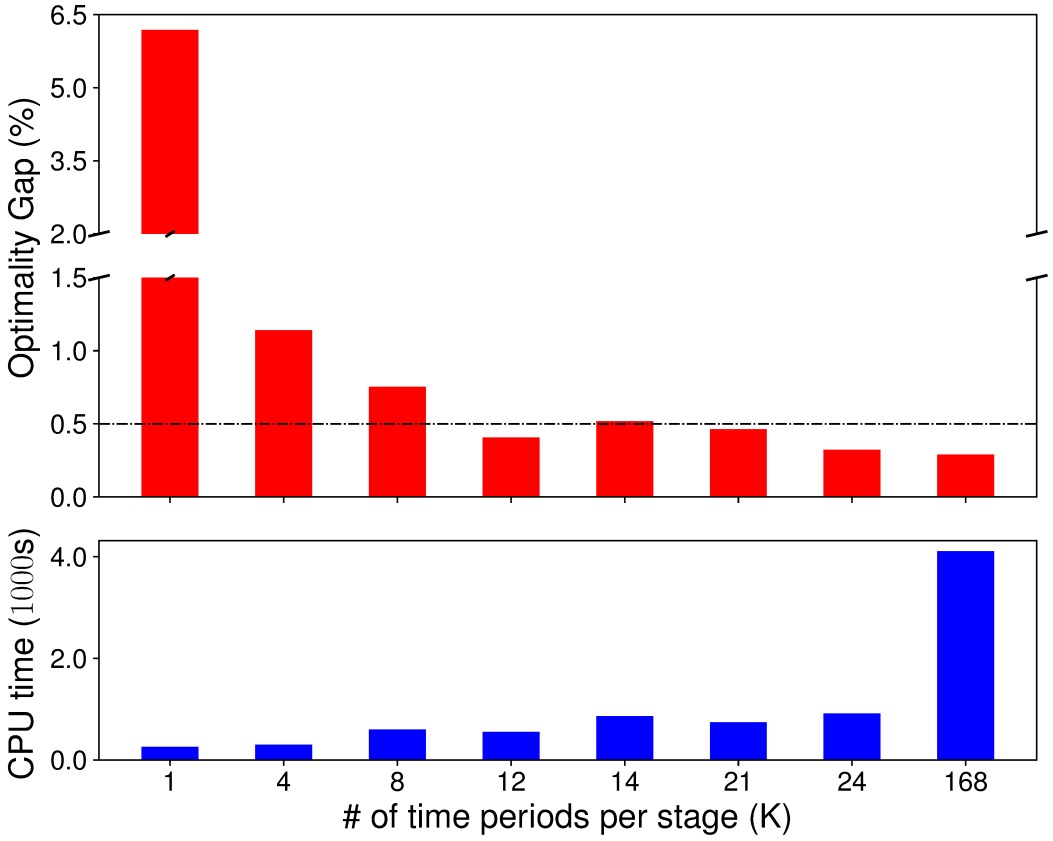

Table 12 – Summary of results obtained for a-DDiP.

K	**Optimality gap (%)**		**Final result**		
	2 minutes	10 minutes	CPU time (sec.)	Optimality gap (%)	Iterations
1	7.85	–	256.45	6.18	25
4	1.41	–	299.91	1.14	25
8	6.85	0.75	601.72	0.75	25
12	100	0.76	703.45	0.40	19
14	100	0.62	863.50	0.51	25
21	100	0.95	739.66	0.46	9
24	100	0.93	913.05	0.28	9
168	–	–	4110.00	0.29	–

The case $K = 12$ presents the best trade-off between the optimality gap and CPU time. Also, except for $K = 8$, in the final result, all simulations presented improvements in the CPU time or optimality gap compared with s-DDiP cases. Since case a-DDiP executes a pre-solve step, it is expected to increase the computational time at the beginning of the DDiP iterations. As seen for $K = 12$, the DDiP did not complete the first iteration in two minutes. On the other hand, the improvements are significant compared to Tables 11 and 12. The performance of the DDiP can be visualized in Figure 28, where we observe that the DDiP can achieve solutions with a 1% optimality gap faster than the problem solved without a decomposition strategy. Analyzing these experiments, case $K = 12$ reaches good performances in general, being this case used for the rest of the computational experiments of this chapter.

Figure 28 – DDiP performance for cases with different values of K.

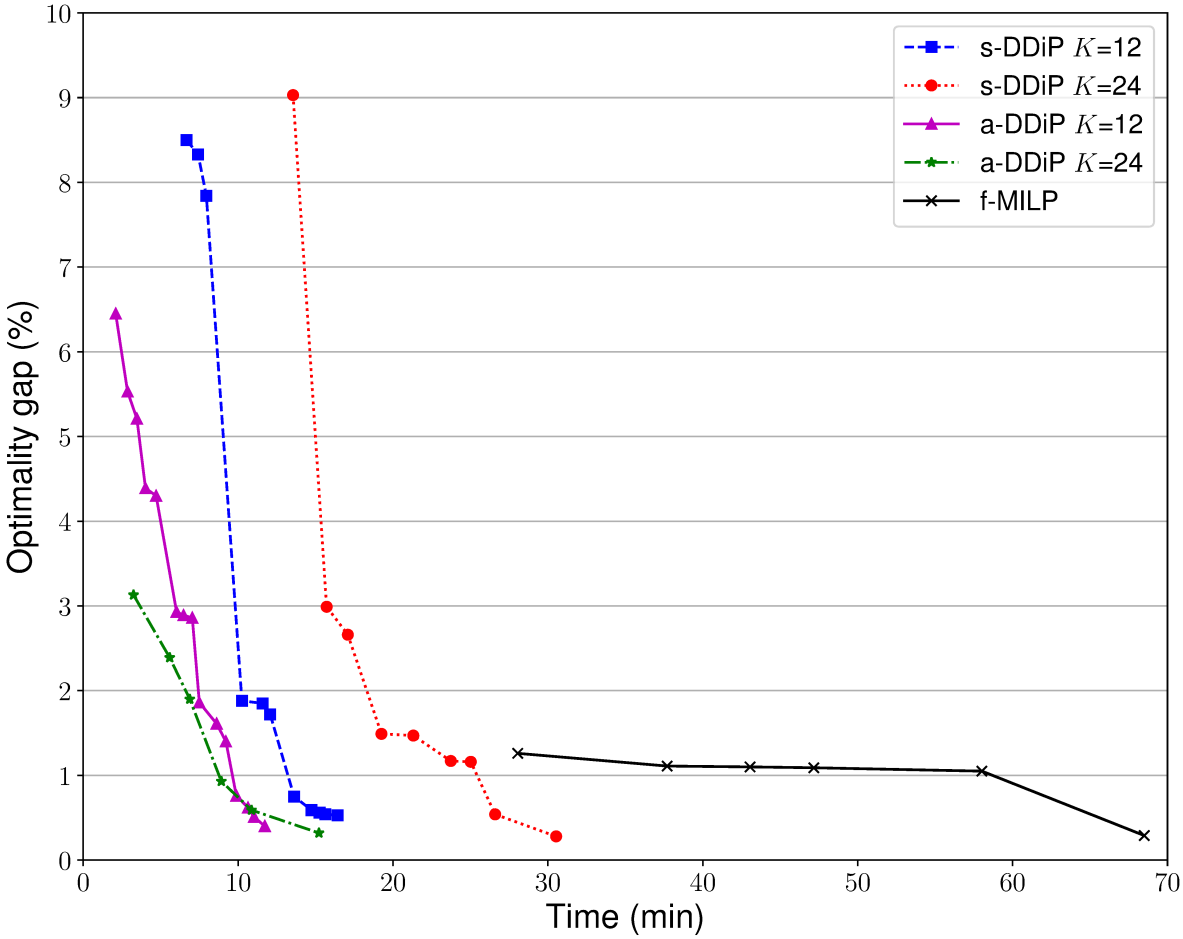

4.4.3 Impact of overlapping constraints

The overlapping strategy offers new options to improve the DDiP framework, although there are many possibilities for using it. In this work, only the size of overlapping constraints is analyzed, and the set of constraints will be the same as in Section 4.4.1. Due to the number of combinations between the size of stages and the size of overlap constraints (K, P, respectively), and chosen based on the results from the previous section, only cases $K = 1, 12$ and 24 are used to assess the impact of the strategy. The values of P chosen are 1, 2, 3, 4, and 6. The initial experiments will consider case $K = 1$ since it presents the worst results in the optimality gap. The results for cases s-DDiP and a-DDiP are presented in figures 29-30 and tables 13-14.

Figure 29 – Optimality gap and CPU time for s-DDiP.

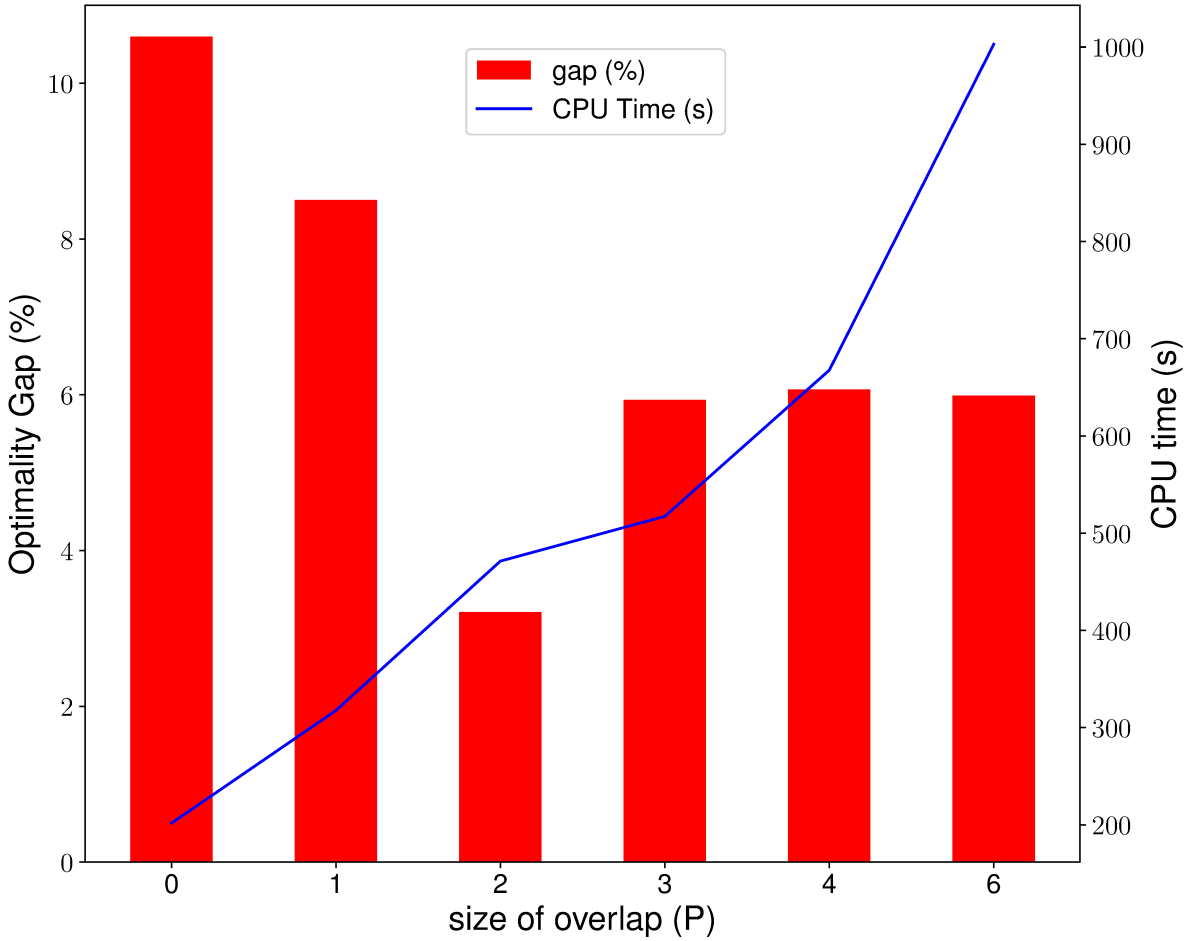

Figure 30 – Optimality gap and CPU time for a-DDiP.

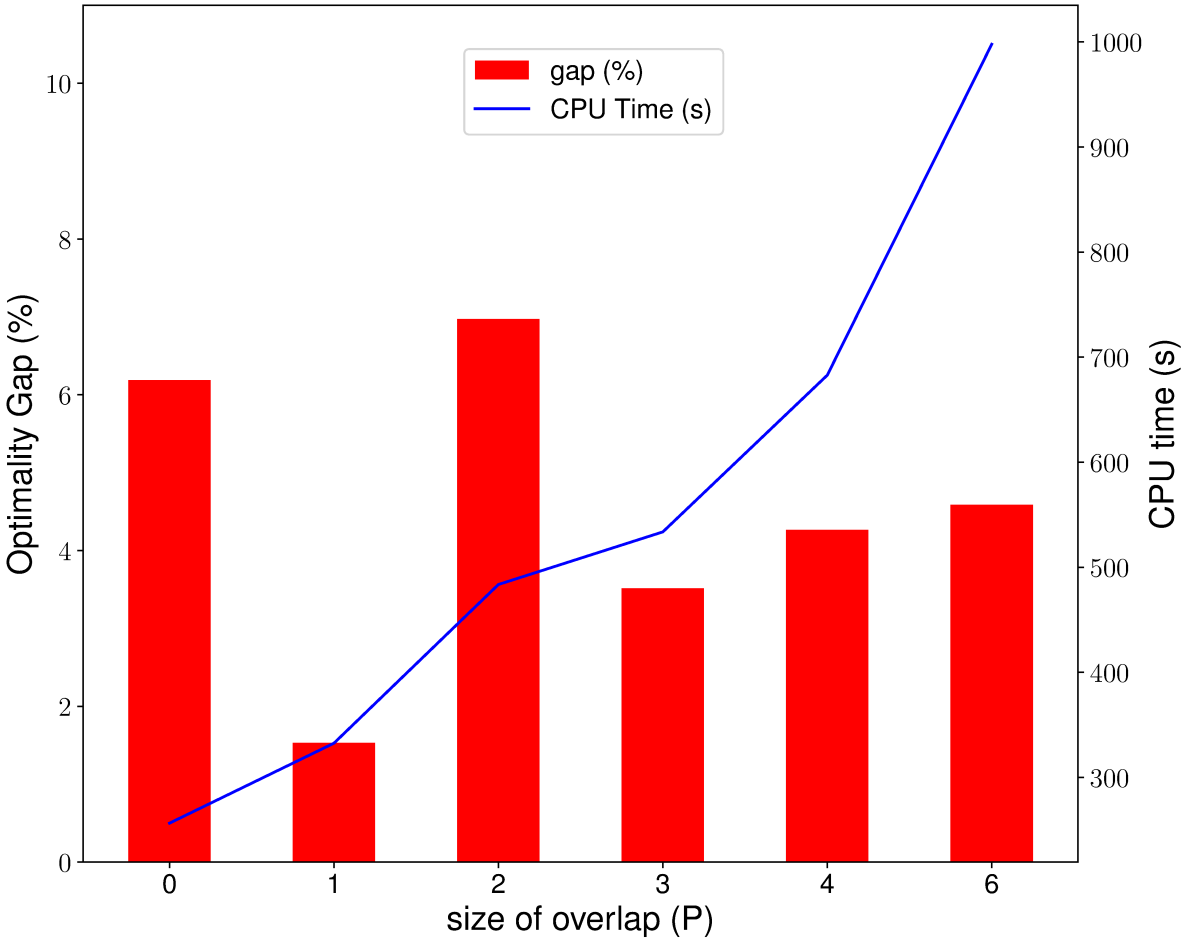

Table 13 – Summary of results obtained for s-DDiP with $K = 1$.

P	**Optimality gap (%)**		**Final result**		
	2 minutes	10 minutes	CPU time (sec.)	Optimality gap (%)	Iterations
0	12.67	–	197.96	10.59	25
1	16.91	–	317.69	8.50	25
2	18.42	–	471.28	3.21	25
3	13.23	–	517.31	5.93	25
4	19.95	8.08	667.62	6.06	25
6	67.91	10.67	1002.81	5.98	25

Table 14 – Summary of results obtained for a-DDiP with $K = 1$.

P	**Optimality gap (%)**		**Final result**		
	2 minutes	10 minutes	CPU time (sec.)	Optimality gap (%)	Iterations
0	7.85	–	256.45	6.18	25
1	11.91	–	332.58	1.52	25
2	9.58	–	483.60	6.97	25
3	11.27	–	533.66	3.51	25
4	11.44	5.16	682.82	4.26	25
6	23.35	11.97	997.70	4.58	25

In Tables 13-tab:PaDDiPK1, the results are presented as follows. For case $P = 4$, the optimality gap in minute 2 is 19.95%, and in minute 10 is 8.08%. For case 3, the optimality gap of minute 10 is not presented since the DDiP converged in less than 10 minutes. As can be seen, the inclusion of overlapping constraints improves the optimality gap at the price of increasing the computational effort, which is expected since there is an increase in each SP involved in the DDiP. For the case s-DDiP, $P = 2$ achieved the lowest optimality gap, and for case a-DDiP, $P = 1$ returns the best optimality gap, due to the limit of iterations. For the remaining experiments concerning the overlap, the results are presented only in the computational effort once the tolerance of the optimality gap is always achieved. The results for s-DDiP and a-DDiP considering cases $K = 12$ and 24 are presented in figures 31-33 and summarized in Table 15.

Figure 31 – Impact of overlap constraints in the DDiP for cases K = 12 and K = 24

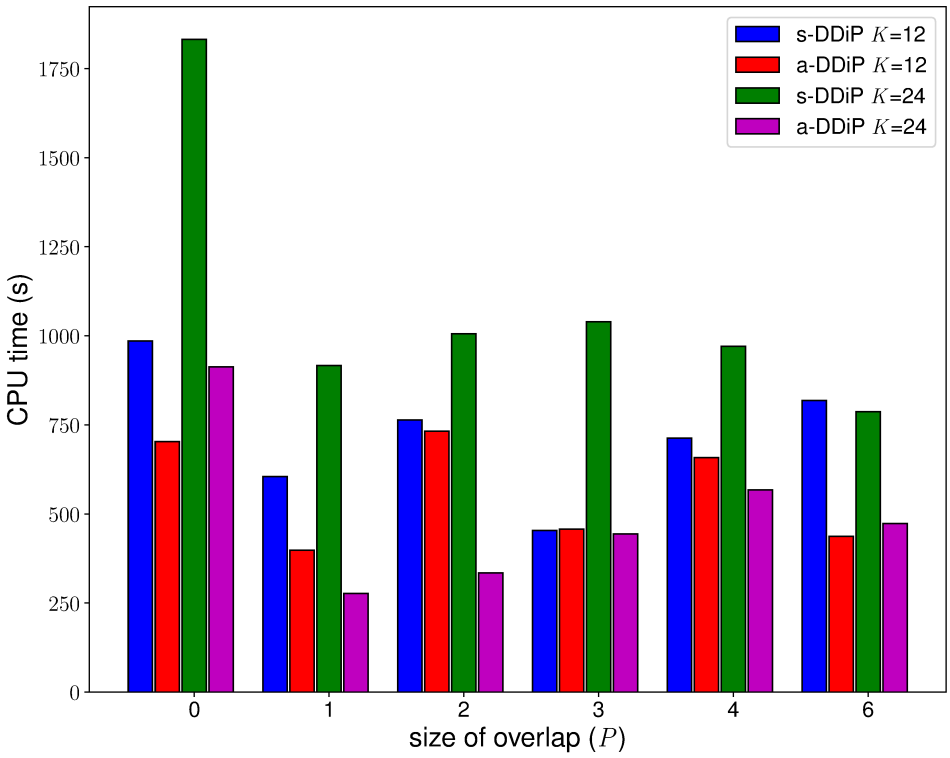

Figure 32 – DDiP performance for cases with different values of P and K = 12.

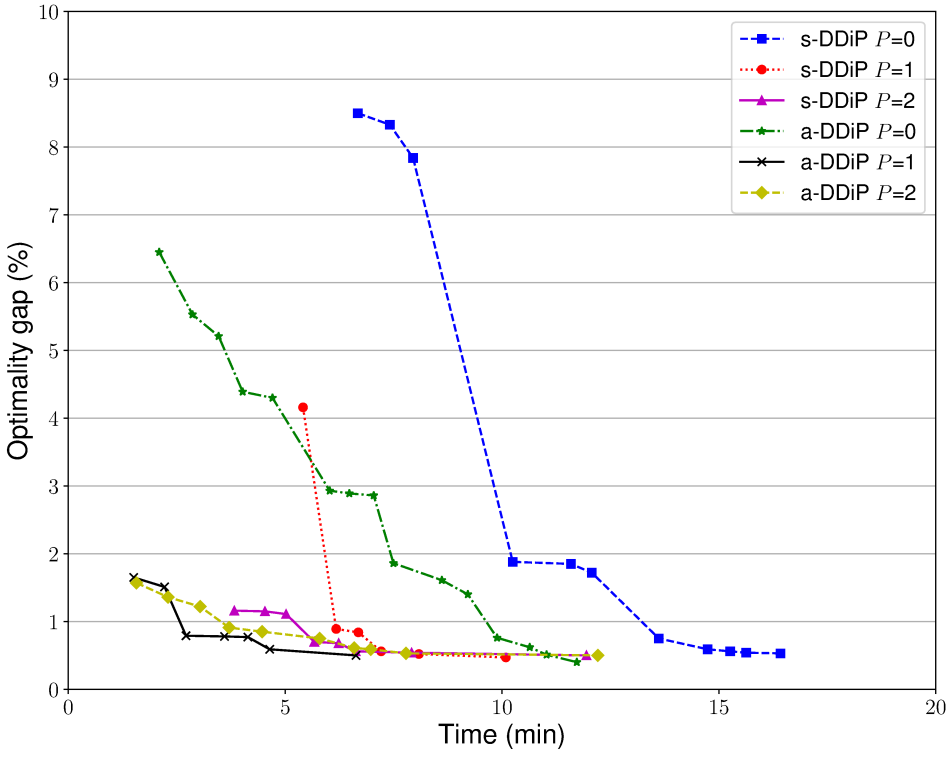

Figure 33 – DDiP performance for cases with different values of P and $K = 24$.

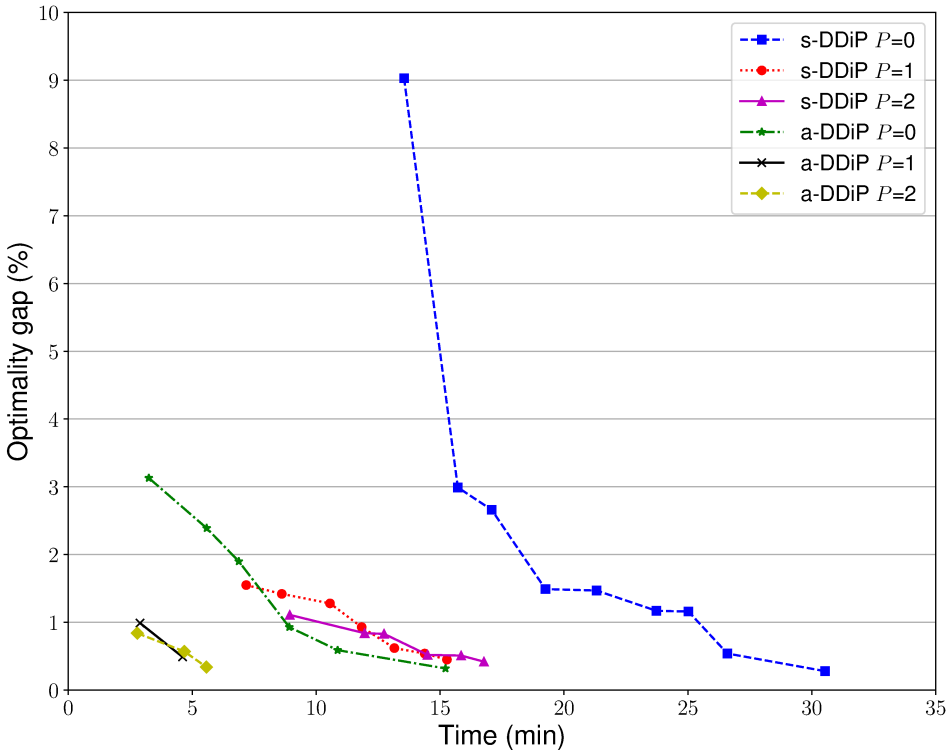

Table 15 – Summary of results obtained of DDiP for different P values with $K = 12$ and $K = 24$.

Case	K	P	Optimality gap (%)	CPU time (s)	K	P	Optimality gap (%)	CPU time (s)
s-DDiP	12	0	0.53	985.23	24	0	0.28	1831.94
		1	0.47	605.28		1	0.45	916.62
		2	0.50	764.07		2	0.42	1006.11
		3	0.47	453.67		3	0.40	1039.53
		4	0.49	712.82		4	0.49	970.46
		6	0.50	818.41		6	0.46	786.88
a-DDiP	12	0	0.40	703.45	24	0	0.28	913.05
		1	0.50	397.94		1	0.49	276.58
		2	0.49	732.55		2	0.34	334.34
		3	0.40	457.23		3	0.32	444.09
		4	0.49	658.00		4	0.46	567.32
		6	0.48	437.30		6	0.48	472.85

In general, the overlapping constraints significantly impact the overall performance of DDiP. Particularly, for case $K = 24$ with $P = 1$ reduces the computational effort by approximately 70%, showing the potential of this approach.

Finally, to consolidate the results presented, we performed other experiments by changing the original inflows $\mathbf{Y}$. Specifically, we created two other computational instances, where the first is referred as $\mathbf{Y}^{+}$, and the inflows used are 1.6 $\times$ $\mathbf{Y}$. The second one is referred to as $\mathbf{Y}^{-}$ = 0.4 $\times$ $\mathbf{Y}$. For these new cases, we performed the s-DDiP and a-DDiP with K = {12, 24}, and P = {0,1,2}. The results obtained are presented in tables 16-17.

Table 16 – Summary of results obtained of DDiP for case with $\mathbf{Y}^{+}$.

Case	*K*	*P*	Optimality gap (%)	Time (s)	*K*	*P*	Optimality gap (%)	Time (s)
s-DDiP	12	0	0.55	819.02	24	0	0.47	1586.49
		1	0.47	353.37		1	0.45	885.38
		2	0.51	751.97		2	0.41	983.44
a-DDiP	12	0	0.53	616.63	24	0	0.49	464.70
		1	0.47	332.72		1	0.43	378.14
		2	0.38	518.71		2	0.45	375.11
f-MILP	–						1.07	1800
							0.92	3600
							0.36	5079

Table 17 – Summary of results obtained of DDiP for case with $\mathbf{Y}^{-}$.

Case	*K*	*P*	Optimality gap (%)	Time (s)	*K*	*P*	Optimality gap (%)	CPU time (s)
s-DDiP	12	0	0.52	698.45	24	0	0.40	1341.42
		1	0.50	498.89		1	0.43	1012.26
		2	0.49	765.99		2	0.36	1026.43
a-DDiP	12	0	0.38	694.72	24	0	0.31	485.39
		1	0.49	341.71		1	0.38	299.16
		2	0.46	417.88		2	0.44	424.82
f-MILP	–						0.92	1800
							0.65	3600
							0.26	5849

Although the DDiP did not reach the 0.5% tolerance in some cases, the CPU time is significantly lower when compared with the f-MILP. Therefore, these results show the potential of the strategies presented in this thesis when applied to STGS problems.

4.4.4 Assessment of primal solutions

This section compares the primal solutions obtained for the different experiments involving the DDiP strategy for simulations with inflows equal to $\mathbf{Y}$. Only the first 24 hours are used for this analysis since a rolling horizon strategy in the Brazilian STGS

problem is performed. In other words, despite running a 168 hours STGS problem, the independent system operator is interested only in the decisions obtained for the first 24 hours (day-ahead dispatch). The number of active thermal plants for the first 24 hours with $K = 24$, $P = 0$, and $K = 168$ is presented in Figure 34. As can be seen, there are differences between the number of online thermal plants, especially in the last hours.

Figure 34 – Number of active thermal plants for the first 24 hours of the planning horizon, considering cases $K = 168$, s-DDIP, a-DDIP with $K = 24$, $P = 0$.

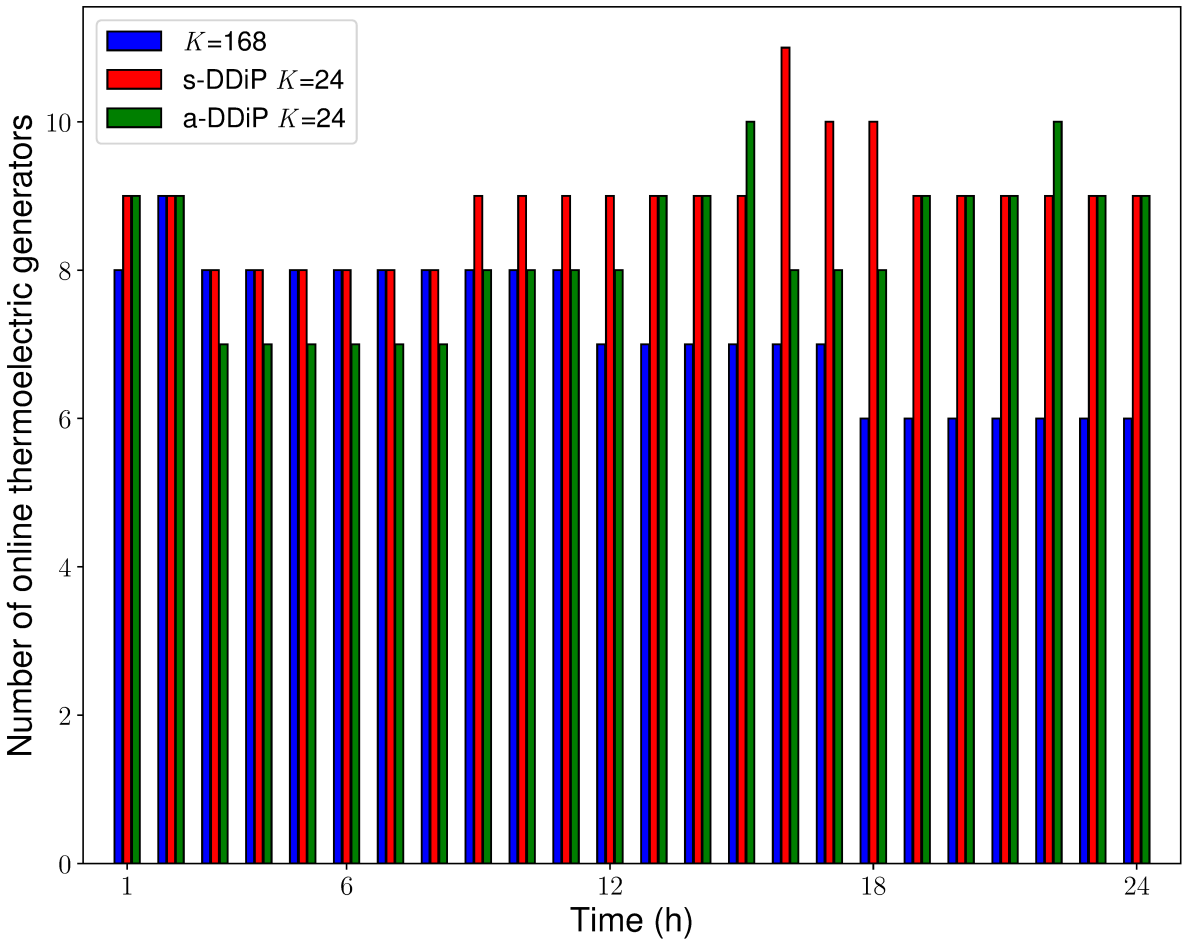

The total thermal plant generation for simulations with $K = 24$, $P = 0$, and $K = 168$ is presented in Figure 35. Despite the differences in the total amount of thermal generation between each case, it is possible to observe the same generation patterns (generation curves) in all simulations.

Figure 35 – Thermal plant generation for cases $K = 168$, s-DDIP, a-DDIP with $K = 24$, $P = 0$.

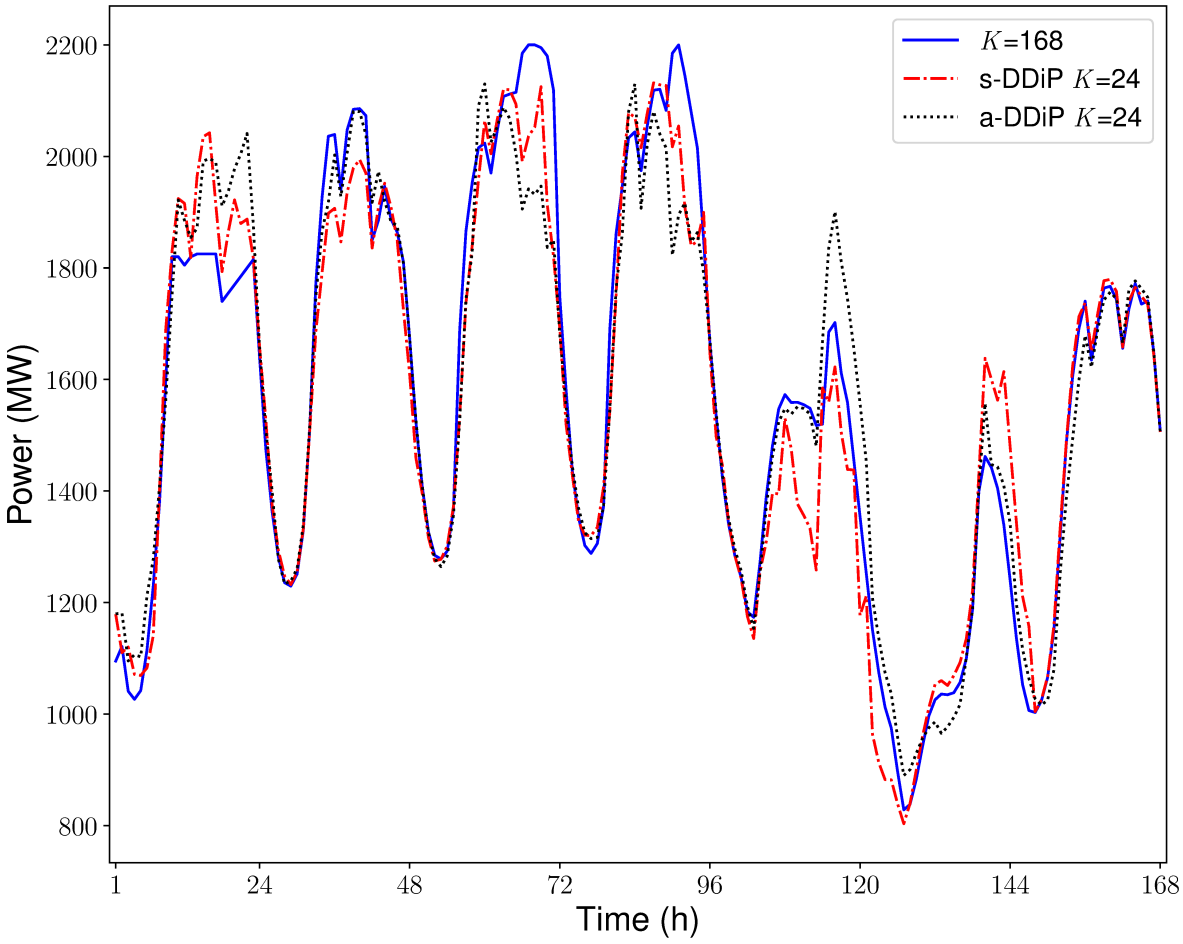

Concerning the total hydro generation, the results from simulations with $K = 24$, $P = 0$, and $K = 168$ is presented in Figure 36. Like the thermal generation, the hydro generation presents some differences between each simulation, but the generation patterns are similar.

Figure 36 – Hydro generation for cases K = 168, s-DDIP, a-DDIP with K = 24, P = 0.

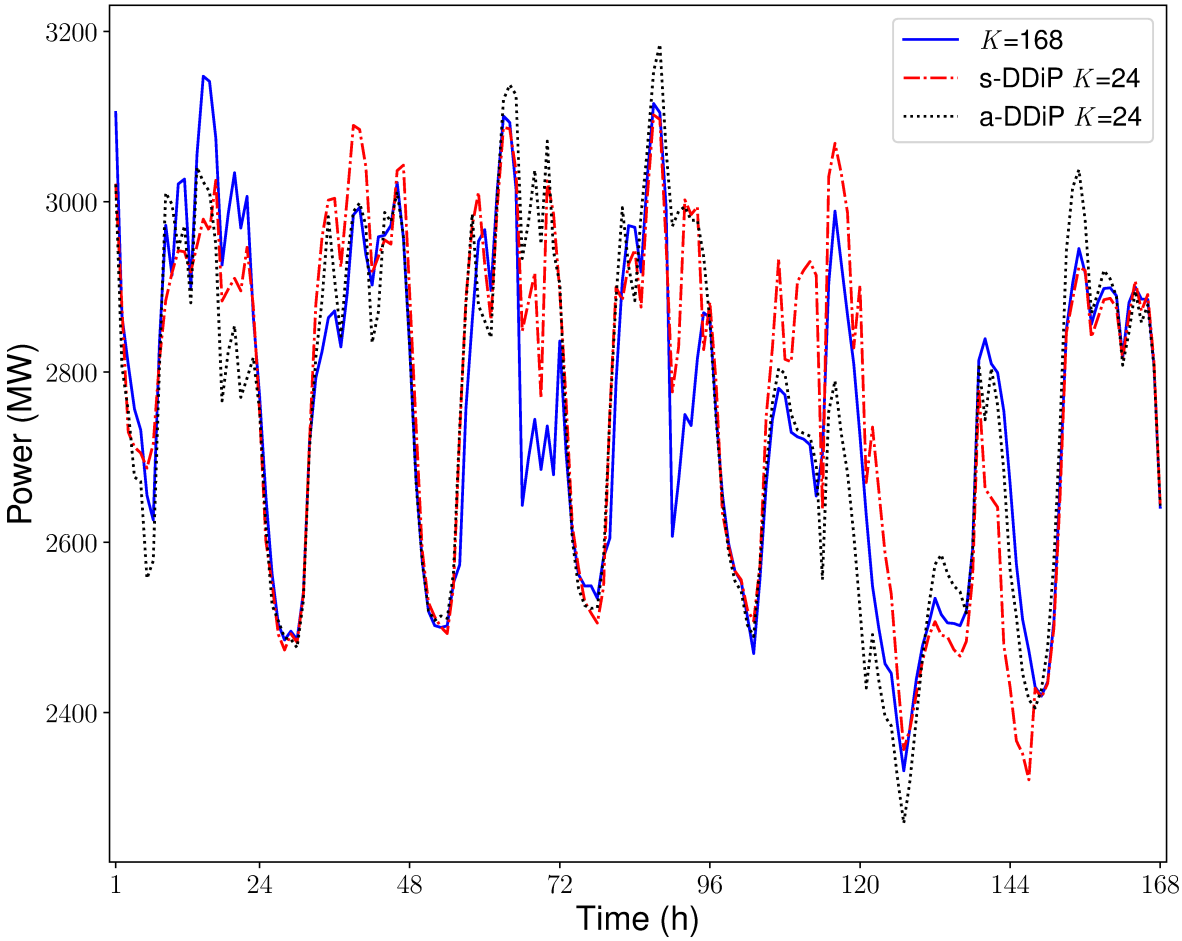

These results make it possible to observe differences in the generation obtained from these experiments and the thermal plant's on/off status. Although this is expected, due to the optimality gap imposed, the power dispatches generally follow the same pattern, and the differences are not significantly high. As mentioned, we use slack variables instead of feasibility cuts. Tables 18-19 present the summation of all slack variables (SV) obtained from each simulation to clarify the effects of the slack variables. These variables are included in TUC, WB, and power balance (PB) constraints. The penalty term (P_0) associated with slack variables in TUC and PB constraints is ten times greater than the most expensive unitary variable cost. In contrast, the penalty term in WB constraints is $P_0 \times 10^6$.

Table 18 – Summation of all slack variables for simulations with different sizes of stages.

Case	***K***	***SV***
s-DDiP	1	**1.50**
	4	**0.91**
	8	**1.07**
	12	**0.92**
	14	**0.90**
	21	**1.96**
	24	**1.83**
a-DDiP	1	**1.82**
	4	**1.19**
	8	**1.77**
	12	**2.00**
	14	**0.69**
	21	**2.24**
	24	**0.92**
f-MILP	-	**0.78**

Table 19 – Summation of all slack variables for simulations with different overlap sizes.

Case	***K***	***P***	***SV***	**Case**	***K***	***P***	***SV***	**Case**	***K***	***P***	***SV***
s-DDiP	1	0	1.50	**s-DDiP**	12	0	0.92	**s-DDiP**	24	0	1.83
		1	0.78			1	0.83			1	0.82
		2	0.82			2	0.82			2	0.43
		3	1.58			3	1.39			3	0.40
		4	0.38			4	0.22			4	0.22
		6	0.36			6	0.25			6	0.21
a-DDiP	1	0	1.82	**a-DDiP**	12	0	2.00	**a-DDiP**	24	0	0.92
		1	0.77			1	1.58			1	1.43
		2	1.61			2	1.56			2	1.48
		3	1.28			3	1.01			3	1.40
		4	0.61			4	0.88			4	0.32
		6	0.56			6	0.71			6	0.17

Although the values of the slack variables are not zero for all simulations (including the original problem solved without a decomposition strategy), the values of the slack variables are low enough and have a negligible impact on the solution quality. Therefore, we conclude that DDiP is a promising strategy that can be used to solve STGS problems.

4.5 FINAL CONSIDERATIONS

This chapter presented a stage decomposition strategy denominated Dual Dynamic Integer Programming (DDiP). Initially, the BD was presented, and the concepts of MP and SP, feasibility, and optimality cuts were introduced. Then, the NBD was introduced, aiming to propose the standard DDiP algorithm. In sequence, improvements on

DDiP were proposed to accelerate the overall convergence of the method. In particular, the pre-solve strategy was presented based in (LARA et al., 2018). Next is the multi-period strategy, where stages with more than one period were introduced. In advance, the overlapping strategy based on the overlap Schwarz decomposition is proposed to DDiP.

The experiments were performed on a modified version of the IEEE-118 bus system to validate the different types of DDiP strategies. The results show that the DDiP can obtain solutions with an optimality gap of less than 0.5% way faster than solving the STGS without decomposition, showing the potential of the DDiP, especially on large-size problems.

The impact of period aggregation is significant and shows the potential approach in other optimization problems with a similar mathematical structure. For the problem under analysis, there is an optimal value of the aggregation parameter that leads to the minimal computational effort. Regarding the overlap constraints, our results show that this approach is promising and can be applied to several other problems employing the BD strategy.

Also, the improvements presented in this thesis can be extended in several ways. For example, a natural extension of this study is to evaluate different types of presolve strategies, specifically how to use the decomposition scheme of the DDiP to generate initial cuts. Another extension is to use this strategy with off-the-shelf solvers, including free mixed-integer optimization solvers.

Considering the objective of this work is to solve the STGS problem, the next chapter will introduce an overview of the structure of the STGS problem, and how to deal with the planning horizon efficiently. In particular, we introduce a recent strategy called diffusing-horizon (SHIN; ZAVALA, 2021) that has been proved to work efficiently in a multi-period OCP problem .

5 ASSESSING TEMPORAL AGGREGATIONS AND MODEL SIMPLIFICATIONS IN THE STGS PROBLEM

In this chapter, we propose strategies to reduce the computational complexity of the STGS problem by using model simplifications and temporal aggregations via a so-called diffusing-horizon (DH) strategy. We consider the recent results of DH strategy applied in model predictive control (MPC) problems, where the exponential decay of sensitivity (EDS) property holds and, therefore, impacts of parametric perturbations at future periods exponentially decay as one moves backward in time. Inherent challenges of using DH strategy in the STGS concern the lack of dual variables since the concept of sensibility analysis in MILP problems is not unique, and the condition to EDS holds in MPC problems takes into account the dual variables of an LP and their properties. Thus, this chapter will present some analysis of this DH strategy to find a strategic approach that can be applied to the STGS problem.

5.1 AGGREGATION METHODS

The GS problem is tipically decomposed into several simpler problems with different planning horizons. Each decomposed problem (LTGS, MTGS and STGS) has particular characteristics to reduce the computational effort in GS problems. For example, the LTGS problem normally deals with the stochastic aspects (inflows, demand, wind generation) and long-year planning horizon, with simplified formulations of physical components. In contrast, in the STGS problem, the physical components have a very detailed formulation.

One common strategy to increase the computational tractability of GS problems is to use simplified formulations to model the physical components. In this case, linearization-based formulations are a natural alternative, but in practice, this type of simplification can be far away from the behavior of the system components. On the other hand, some strategies deal with the temporal resolution of the GS problem. A temporal decomposition occurs when the GS problem is decomposed in the LTGS, MTGS and STGS problems. Also, since one of the main targets of the system operator is to find the GS over the planning horizon, a common approach is to solve the STGS problem to find the day-ahead decisions on a rolling horizon strategy, i.e., solving this problem in a daily basis. Specifically for the Brazilian case, an overview of the planning horizon and the GS problems can be viewed in Figure 37.

As mentioned in Chapter 1, an FCF is used in the STGS problem to keep the operation coordinated. Even for the LTGS problem, if renewable energy generation has a considerable impact, it is noteworthy to include information on an hourly level to evaluate scenarios taking into account the variability of this source (PINA; SILVA, C. A.; FERRÃO, 2013). For the STGS problem, the hourly or sub-hourly level is nor-

Figure 37 – Overview of the different planning horizons in the GS problems of Brazilian case, where t_m, t_w, t_d concerns each period belong to LTGS, MTGS, and STGS, respectively.

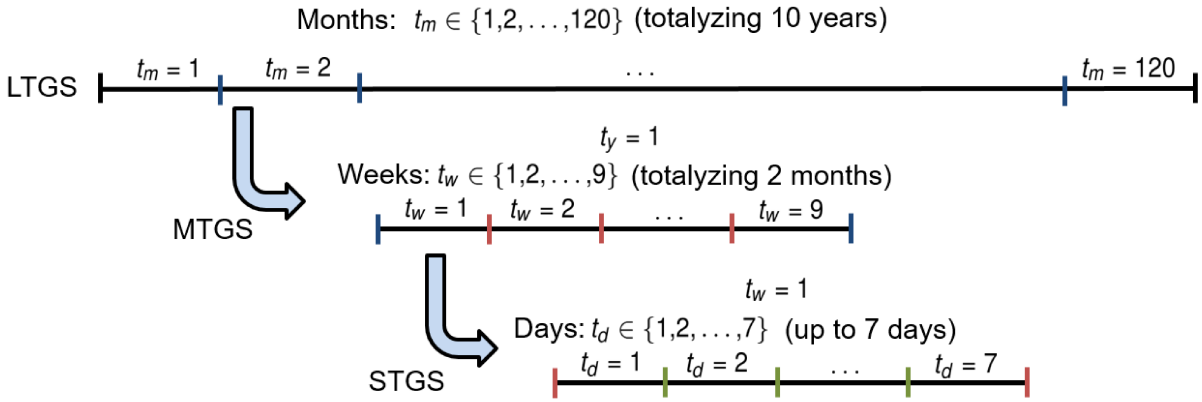

mally the common approach, especially for the day-ahead, since practical solutions to the real-time operation are required,. As a result, it requires a high level of detail in the mathematical model of the STGS problem. In fact, with a detailed time resolution, the decisions obtained for the GS problem will be more accurate. However, the computational effort can be high enough to make it impossible to obtain a solution under the usual running time limit. Therefore, normally strategies to reduce the number of intervals used in the planning horizon are applied.

In (NAHMMACHER et al., 2016), a novel approach for selecting representative days in the LTGS problem is presented, including a clustering algorithm, choosing one representative day per cluster, and weighting and scaling the time series. The approach has some potential when the LTGS problem contains high penetration of renewable generation. The replication of the proposed algorithm for other power systems is easy to be implemented. From simulations, the authors have shown that with 48-time slices (six representative days per year), they obtain equivalent results to simulations with 800-time slices. As mentioned before, in MTGS and LTGS problems, temporal aggregation is a common approach for handling computational tractability (WOGRIN; GALBALLY; RENESES, 2016; TEJADA-ARANGO; WOGRIN; CENTENO, 2018; PINA; SILVA, C. A.; FERRÃO, 2011). Concerning other optimization problems, temporal aggregations are also employed to reduce the computational effort (MAVROTAS et al., 2008; BAHL et al., 2017; PINEDA; MORALES, 2018; FAZLOLLAHI et al., 2014; FAZLOLLAHI; MARÉCHAL, 2013; BENÍTEZ et al., 2014).

The work (WOGRIN et al., 2014) proposed an alternative approach to handle the computational effort in which, instead of approximating the demand curve by load levels, the concept of system states was introduced, allowing to incorporate of chronological information of the system in models. They argue that the load levels only consider

one feature, the demand or net demand. Using the system states allows incorporating more information such as non-dispatchable renewable energy. In the simulations, they execute an STGS problem in a system composed of 13 thermal plants and wind generation, with a 168-hours planning horizon discretized in hourly steps. For comparison, they use an aggregated demand assuming six load levels, providing an alternative that better capture the electricity prices. The methodology to obtain the system states and transition matrix is the major bottleneck of the approach. Despite using the *k*-means clustering (LLOYD, 1982), it is unclear how to reproduce other large-scale systems with different time scales.

In (LARA et al., 2018), an approach based on *k*-means clustering to select representative days from historical data is performed. The authors deal with electric power with high renewable penetration, where the horizon is composed of 30 years. Each year is represented by up to 12 days to simplify the optimization problem. Even with this reduction, the resulting optimization problem is a large-size MILP, and the DDiP is applied to solve it. The *k*-means approach described in Algorithm 4 below aims to find several clusters in which each observed data belongs to the nearest cluster. Since the demand plays an important role in the GS problem, the *k*-means method can be applied to identify a number *k* of clusters and their respective centroids based on load levels in the first step. After that, an approximated load curve quantized by the load levels obtained in the first step can be generated, and as a consequence, temporal aggregation can be performed. In Figure 38, a load curve of 24 hours discretized in hourly steps is approximated using the *k*-means algorithm with 3 clusters.

Algorithm 4: *k*-means clustering algorithm

Input: number of clusters *k* to assign and a collection of points (data)
Output: *k* clusters with known centroids
1 initialize *k* centroids chosen randomically
2 **while** *the centroids position do not change* **do**
3 assign each point of data to its closest centroid
4 evaluate the new centroid of each cluster, computing the mean of all points belonging to the cluster and set the new centroid
5 **end**

In general, there is no rule in the procedure to choose the number of load levels and the periods where the approximated load curve should be used. Another possibility is combining multiple periods into one equivalent aggregated stage, as shown in Figure 17. As illustrated in Figure 38, each sequential period where the load level does not change can be aggregated. As a result, four aggregated stages are obtained, recuding the optimization problem dimension six times. Naturally, this approximation will lead to different solutions once the optimization problem is changed; some consequences of

Figure 38 – Original and Quantized Load Curve with 3 Levels.

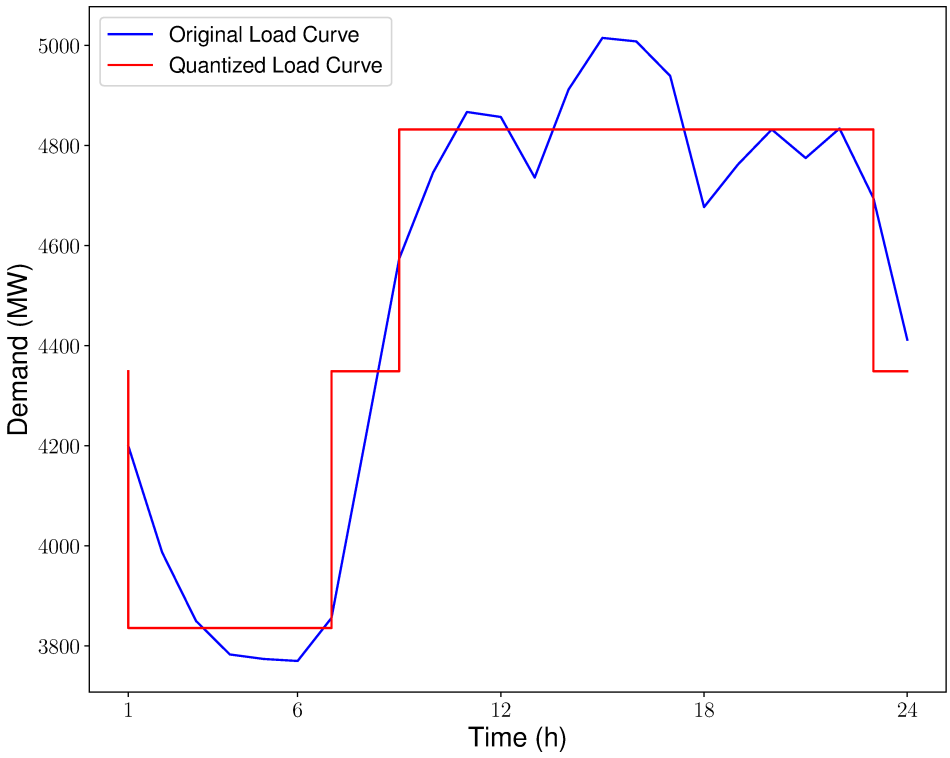

using this approach will be presented in this Chapter.

Also, since this work aims to solve the STGS problem to find the day-ahead scheduled decisions, some questions can be pointed out. First, what are the implications in day-ahead decisions of not using a full resolution in the temporal horizon (168 hours discretized in hourly steps)? And second, how do the day-ahead scheduled decisions change if we employ model simplifications in some periods? Figure 39 represents the time horizon of the STGS problem solved in this work, where each black circle represents a period of one hour. In an attempt to answer these questions, we explore a recent result presented in (SHIN; ZAVALA, 2021), where authors show that for a continuous MPC problem, the impacts of parametric perturbations at a future time decay exponentially as one moves back in time, allowing a strategy called diffusing-horizon, which is explained in Section 5.2.

5.2 MODEL SIMPLIFICATIONS AND TEMPORAL AGGREGATIONS FOR THE STGS PROBLEM

Recent technologies such as renewable energy have increased their participation in power generation. Due to the stochastic behavior of these energy sources, the system operator has to deal with the risk of intermittency, which can lead to a mismatch between energy supply and demand in the system. One consequence of this

Figure 39 – Temporal Resolution of STGS problem.

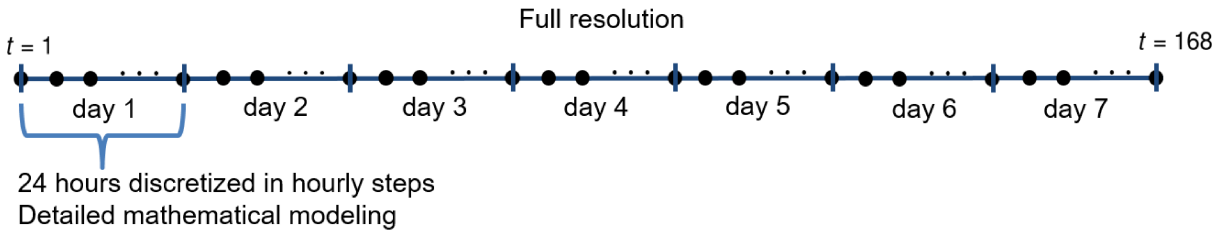

mismatch is putting the system in an unstable region, which may cause supply failures or blackouts.

Considering all components that have a massive contribution to the STGS problem can lead the resulting optimization problem computationally intractable, several strategies can be implemented aiming to turn this problem tractable in computational aspects. Some strategies perform temporal aggregation, while others utilize simplified formulations for the system components. Both cases are not mutually exclusionary and can be combined to result in a simplified version of the STGS problem. Each type of strategy has some consequences, and the details of both cases will be presented in this section.

Given the STGS problem presented in Chapter 2, and assuming a horizon with 168 hours discretized in hourly steps, i.e., $t = \{1,2,\ldots,168\}$, several model simplifications can be performed, such as presented in Chapter 3 to the HPF. On the other hand, assuming we are interested in obtaining only the day-ahead decisions (first 24 hours), including detailed formulation in all planning periods can drastically increase the problem size. Following the idea presented in Chapter 3, simplifications can be performed in other constraints, such as those related to the TUC and network models. Table 20 presents possible simplifications that can be applied to the STGS problem, where linear relaxation concerns the relaxation of the integrality constraints.

Table 20 – Simplifications that can be applied to the STGS problem.

Constraints	**Original Formulation**	**Simplifications**
HPF	Mixed-Integer Nonlinear	CH, PWL models, linear relaxation
Thermal UC	Mixed-Integer Linear	Linear relaxation, drop UC constraints
Network	Linear	Economic dispatch model

Performing model simplifications can drastically reduce the computational effort involved to solve the resulting STGS problem; however, the impacts on the day-ahead decisions due to the use of this strategy are not well defined. Therefore, when this approach is used, it is important to assess the quality of the solution. Aggregation of

variables (and constraints, when possible), is already used in certain types of optimization problems. For example, the work (SHIN; ZAVALA, 2018) uses aggregation methods to design a hierarchical architecture to solve large-scale optimization problems.

The authors (SHIN; ZAVALA, 2021) used a time aggregation (time-coarsening) strategy called diffusing-horizon (DH) to handle the tractability issues of large-scale MPC problems. This strategy aggregates variables and constraints over a coarse grid[1], reducing the size of the resulting optimization problem. In particular, in this aggregation, the temporal resolution becomes exponentially more sparse as one moves forward in time (called exponential coarsening). The DH strategy proposes an alternative way to perform a temporal aggregation based on a property of exponential decay of sensitivity (EDS) (XU, W.; ANITESCU, 2018; NA; ANITESCU, 2020), which states that the effects of parametric perturbations at a future time decay exponentially as one moves backward in time, i.e., a perturbation at the end of the period (last hours of the planning horizon) will have little impact in the early periods. The authors also showed the theoretical results for the EDS property in LP problems. They proposed several types of time coarsening, including a case called exponential coarsening (DH case), as shown in Figure 40.

Figure 40 – Different time aggregation strategies.

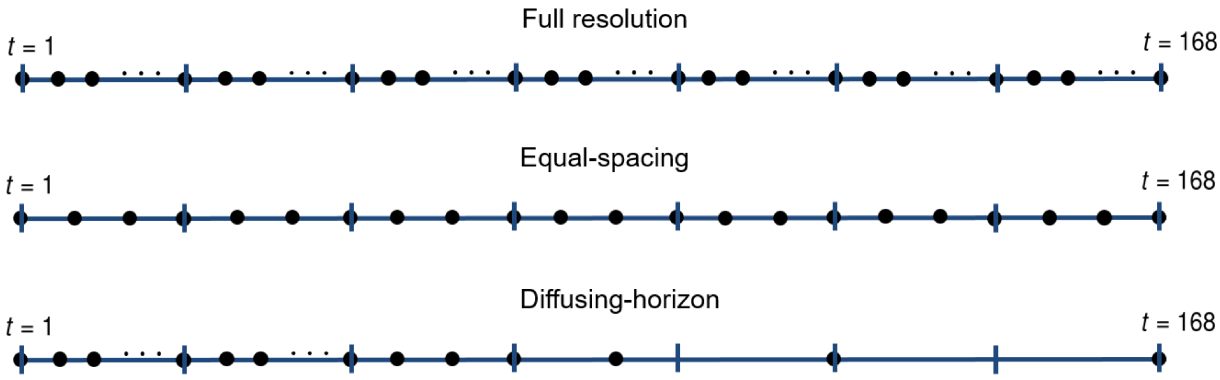

The choice of period aggregation in equal-spacing and diffusing-horizon strategy is performed as in (SHIN; ZAVALA, 2021). For both cases, assume the length of the time interval that the temporal aggregation will be performed as N, and K is the number of stages desired. Let $\{M_k\}_{k=1}^{K}$ the sequence of periods obtained after performing the temporal aggregation strategy. In the equal-spacing strategy, this sequence is built through Equation (67), and for the diffusing-horizon strategy, the points are chosen

[1] aggregation in this case consists in create an equivalent variable for all variables over the periods, e.g., if we have an aggregated stage of 3 periods and a variable V for each period (V_1, V_2, V_3), the aggregated variable V_q will represent these variables, i.e., $V_q = V_1 = V_2 = V_3$.

through Equation (68).

$$M_k = \left\lfloor \frac{N(k-1)}{K} + 1 \right\rfloor, k \in \{1,2,\ldots,K\}, \tag{67}$$

$$M_k = \max\left\{k, \left\lfloor (N+1)^{\frac{k-1}{K}} \right\rfloor\right\}, k \in \{1,2,\ldots,K\}. \tag{68}$$

To understand the application of Equations (67)-(68), consider a period of 24 hours discretized in hours, i.e., $N = 24$ and $K = 6$. Figure 41 present the resulting period aggregation for both strategies aforementioned, represented by the corresponding hour in the full resolution model.

Figure 41 – Example of different temporal aggregations performed in a period constituted of 24 hours.

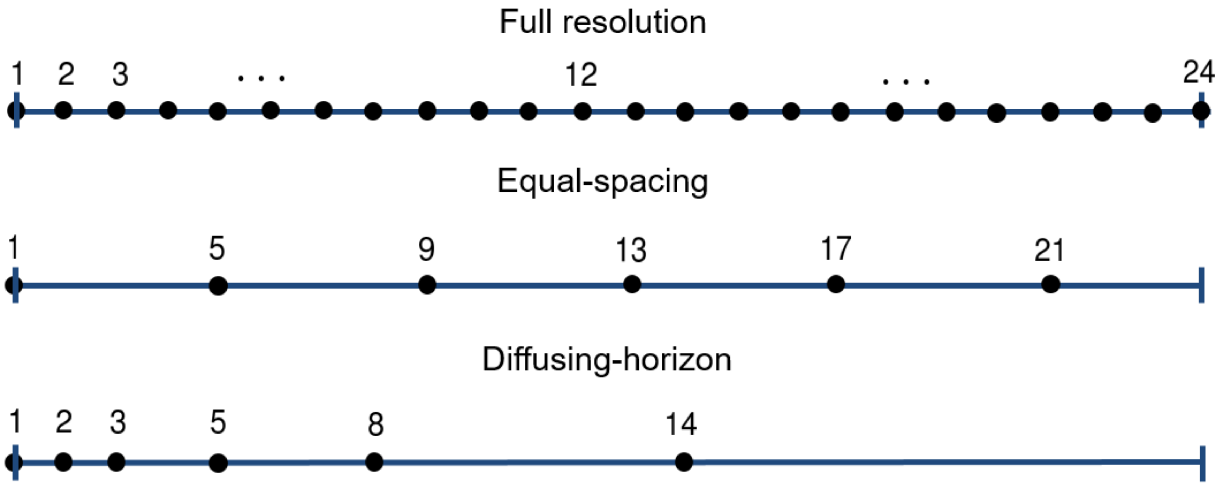

Performing temporal aggregations in the STGS problem must consider the physical constraints of components and how they will be represented in the equivalent aggregated stage. For example, assume a thermal plant with a ramp of 10 MW. Let us assume that at instant $t = 0$, the output power of this plant is $pt = 20$ MW, and the plant needs to increase the power at the maximum ramp capacity (10 MW) for the next four hours. The power output will be given as presented in Figure 42(a).

Suppose a temporal aggregation is used for the periods $t = 1,\ldots,4$, resulting in an aggregated stage with four hours. In that case, there are two possible outcomes: the first is called least cost (LC), which will assume that there is always possible to execute the ramp up at the maximum level, resulting in a power output presented in Figure 42(b). Note that this operation will not be feasible since this plant can increase only 10 MW at each period. For this case, we assume that the power output is 60 MW at all periods aggregated. In contrast, to avoid this infeasiblity, the second possible outcome, most expensive (ME), will look at an aggregated stage as a single period, resulting in an operation shown in Figure 42(c).

Figure 42 – Example of less and most expensive cases when temporal aggregation is performed, where (a) is the original constraint set, (b) is the case with the least cost, and (c) is the case with the most expensive operation.

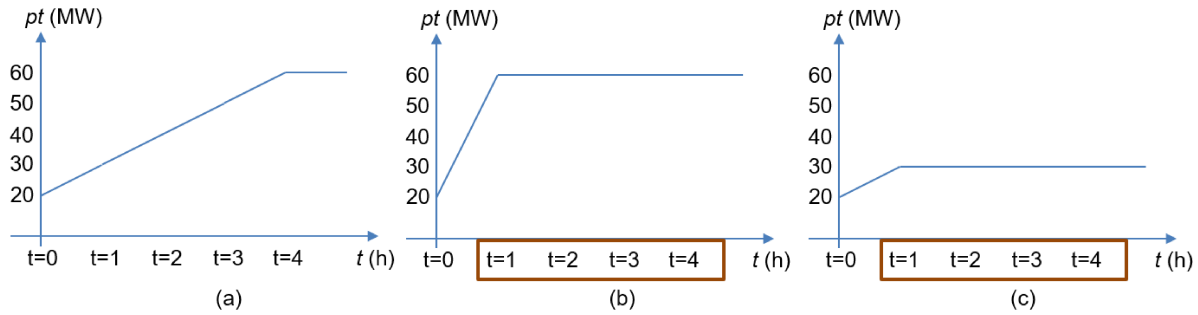

The case from Figure 42(c) is the most expensive because it is expected that the resulting decisions are the optimal, i.e., case (a). Since we are not following the given order (the power output at the final period is 30 MW instead of 60 MW), to result in a feasible operation, the remaining 30 MW needs to be supplied by another source, and it is expected that source will be at least the same cost at this plant. In aggregated stages with more than one time period, the uptime and downtime constraints for thermal plants and water balance constraints are adapted. To understand how the aggregated stage impact these equations, assume a thermal plant with minimum uptime equal to three hours and a planning horizon of eight hours, where the hours 4 to 6 are aggregated into a single stage, as shown in Figure 43. In this figure, the uptime constraint for each period of interest is represented by a block highlighted with the period.

Analyzing from hour 3 onwards, note that only for $q = 3$ does the uptime constraint includes three hours. For $q = 4$, this constraint includes three aggregated stages totaling five hours since $q = 4$ contains three hours. For $q = 5$ and $q = 6$, the resulting constraint for these stages involves more than three hours due to the aggregated stage $q = 4$. In all cases, the uptime constraint referring to the stage involves at least three hours, which is the minimum uptime required. In other words, if a solution is found for this case, it is also feasible for the original formulation where each stage comprises one hour. Finally, in this thesis, this adaptation is performed for the uptime, downtime, and water balance constraints.

5.3 COMPUTATIONAL EXPERIMENTS

This section presents computational experiments performed on the STGS problem to assess the impacts of time series aggregations and model simplification schemes proposed in this thesis. The simulations are performed considering the same STGS problem used in Chapter 4. The resulting optimization problem is solved in Gurobi

Figure 43 – Example of temporal aggregation for the thermoelectric uptime constraint.

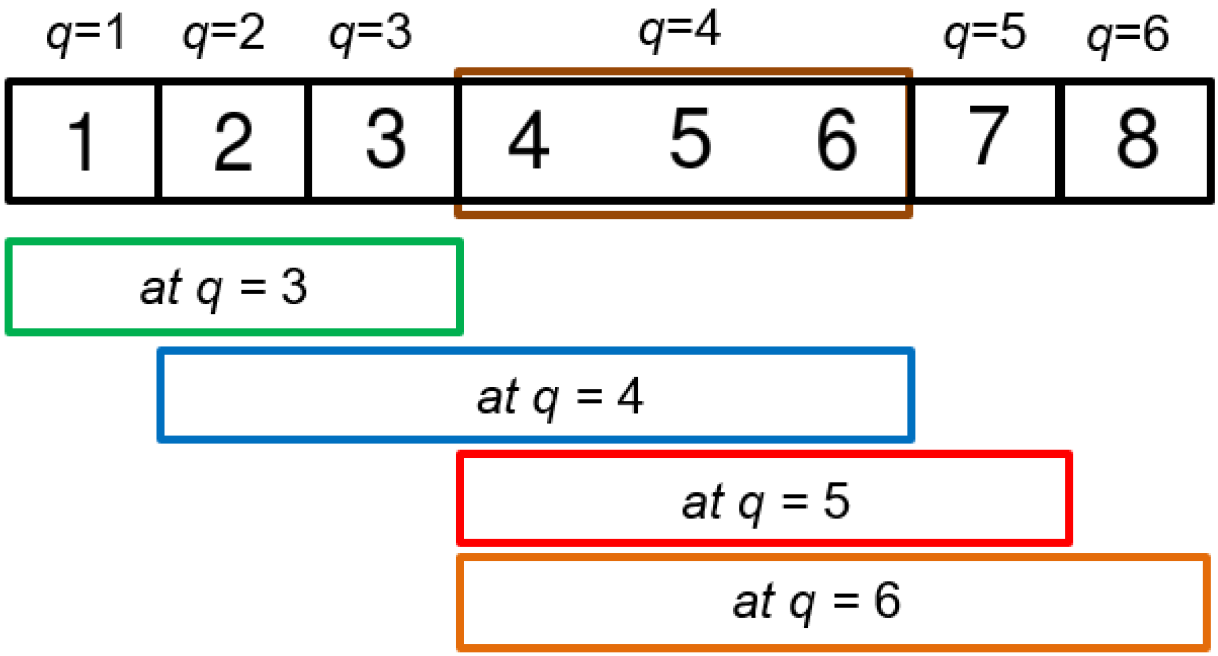

9.0.1. without employing any decomposition strategy. To create a fairness indicator, all simulations are executed four times, and the mean runtime is presented in the results.

In this thesis, the original STGS problem is called OR. Temporal aggregations performed by the k-means strategy will be termed k-means, where k is the number of clusters used. The equal spacing strategy is p-ES, where p is the size of the aggregated stage ($p = N/K$). For the diffusing-horizon strategy, labeled as m-DH, m is the same parameter as p (termed different only for convenience). We use only the CH models for HPF in the model simplifications, employ the linear relaxation for TUC, and perform the economic dispatch model for the network constraints. Since we can perform both model simplifications and temporal aggregations, several types of simulations can be performed. The parameter T divides the set of periods $\mathcal{T}$ into two subsets, $\mathcal{T}_1 = \{1, 2, \ldots, T\}$ and $\mathcal{T}_2 = \{T + 1, T + 2, \ldots, \mathrm{NT}\}$, where only in the second set model simplifications and temporal aggregations are performed (i.e., in the first set, the full representation of the optimization problem is performed). In the remaining of this section, we divide the results considering cases: (a) that performed only model simplifications, (b) in which only temporal aggregations are employed, and (c) both model simplifications and temporal aggregations are evaluated.

5.3.1 Assessing impacts of model simplifications

This subsection contains the results obtained when model simplifications are imposed. The values of T chosen are 96, 120, and 144, and the following simulations

were performed concerning the model simplifications:

- Case MS-1: HPF and TUC with linear relaxations, and network without simplifications.
- Case MS-2: HPF and TUC without simplifications, and network with economic dispatch model.
- Case MS-3: HPF and TUC with linear relaxations, and network with economic dispatch model.

The problem indicators for all simulations are shown in Table 21. For the rest of this chapter, Ncv is the number of linear variables of the resulting optimization problem, Nbv is the number of binary variables used in the model, Ncons is the number of constraints, Rt is the runtime to solve the problem, ΔRt is the reduction in the computational runtime compared with OR, Dac is the day-ahead scheduled cost, and ΔDac is the relative cost variation using OR' cost as reference. Note that there is a drastic reduction in the computational complexity as the parameter T gets lower.

Table 21 – Summary of problem statistics for simulations with model simplifications

Case	T	Ncv	Nbv	Ncons	Rt (s)	ΔRt (%)	Dac (10^6 \$)	ΔDac (%)
MS-1	144	107,478	19,770	369,505	1806	35.27	3.0106	-0.29
	120	110,718	16,530	369,505	1618	42.01	3.0241	0.15
	96	113.958	13,290	369,505	1545	44.63	3.0201	0.02
MS-2	144	92,478	23,010	330,961	1617	42.05	2.8310	-6.23
	120	80,718	23,010	292,417	1254	55.06	2.6839	-11.11
	96	68,958	23,010	253,873	761	62.63	2.4982	-17.26
MS-3	144	95,718	19,770	330,961	1748	37.35	2.8260	-6.40
	120	87,198	16,530	292,417	1052	62.30	2.6880	-10.97
	96	78,678	13,290	253,873	627	77.53	2.5166	-16.65
OR	-	104,238	23,010	369,505	2790	-	3.0194	0

Since the optimality gap is not zero, and the resulting STGS problem is a MILP that normally contains multiple solutions, to assess the quality of the solutions obtained for the day ahead, it is important to analyze some aspects. In this thesis, we evaluate the cost of the day-ahead, the thermoelectric cost operation (Dac), and the total hydro and thermal generation. Looking only for the Dac parameter, note that for case MS-1, there are small differences between all simulations compared with OR. On the other hand, cases MS-2 and MS-3, which involves the economic dispatch simplification, lead to significant differences in terms of the day-ahead scheduled decisions.

A comparison of the thermoelectric generation for T = 144 is presented in Figure 44, and for the first 24 hours is presented in Figure 45. From these figures, note that at the final of the planning horizon, there are significant differences between cases with model simplifications and OR. On the other hand, for the first 24 hours, case MS-1 and

OR has the same generation pattern (generation curve), with an average difference of 1.56% and a maximum difference of less than 8%, occurs in hour 3.

Figure 44 – Thermoelectric generation scheduled in the planning horizon with MS-1, MS-2, and MS-3 for cases with T = 144.

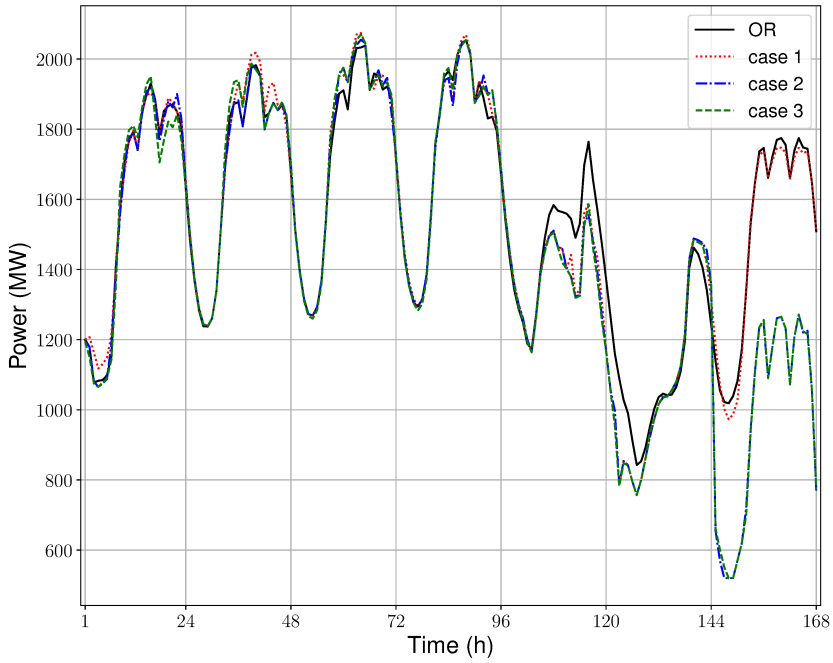

Figure 45 – Thermoelectric generation for the first 24 hours with MS-1, MS-2, and MS-3 for cases with T = 144.

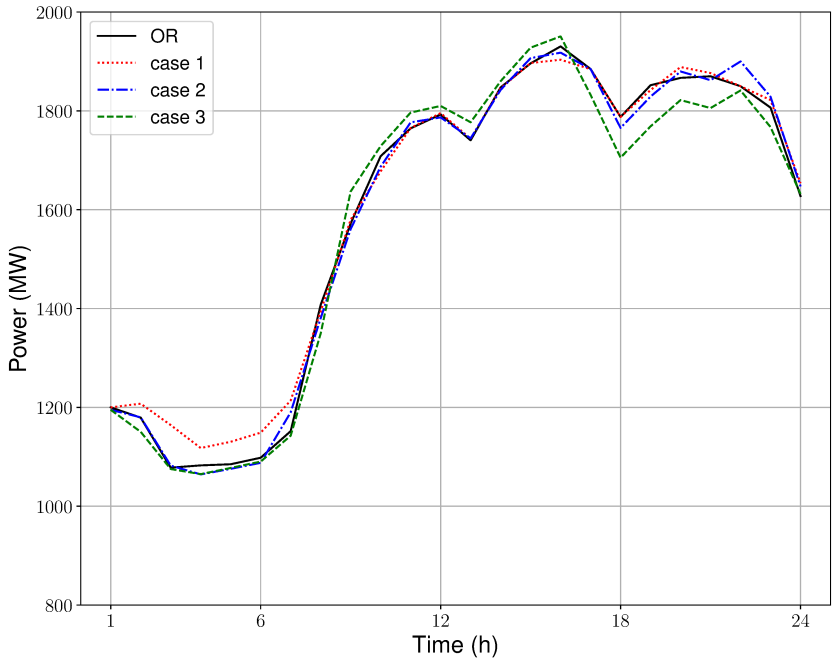

In terms of total hydro generation, the results from simulations for the first 24 hours are presented in Figure 46. Like the thermal generation, the hydro generation for case 1 presents small differences compared with OR, where the average difference equals 0.71% and the largest difference of 3% in hour 3.

Figure 46 – Hydro generation for the first 24 hours with MS-1, MS-2, and MS-3 for cases with T = 144.

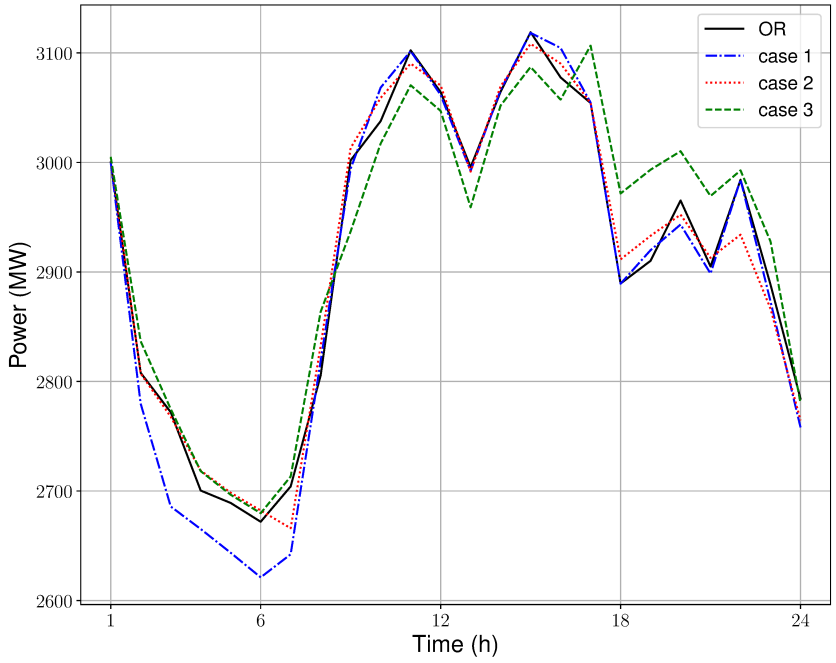

From these results, the model simplifications when case MS-1 is employed, i.e., relaxing the integrality constraints at the last periods of the planning horizon, significantly reduces the computational effort without compromising the quality of solutions obtained for the day-ahead. In fact, for cases where T = 120 and T = 96, the computational effort was reduced by 40%, and the differences for the day-ahead scheduled decisions are small, as shown in Figure 47.

Figure 47 – Thermoelectric generation for the first 24 hours with model simplifications for case MS-1.

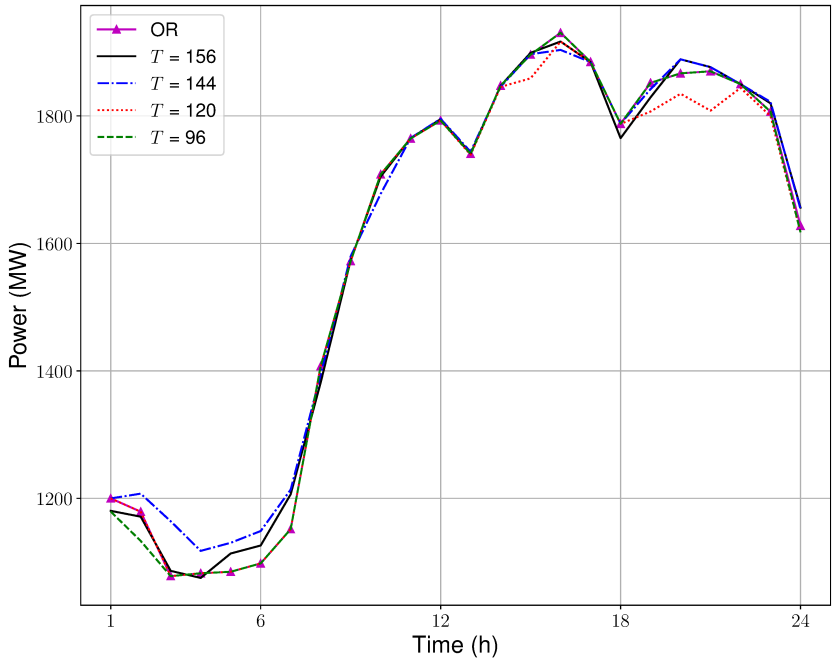

5.3.2 Assessing impacts of temporal aggregations

This subsection contains the results obtained for simulations where temporal aggregations are performed. The values of T chosen are 96, 120, and 144, and the following simulations were performed concerning the temporal aggregations:

- Case TA-1-LC: k-means with $k \in \{4, 6, 8\}$, with ramp constraints modeled by the LC model.
- Case TA-1-ME: k-means with $k \in \{4, 6, 8\}$, with ramp constraints modeled by the ME model.
- Case TA-2-LC: equal-spacing (p-ES) with $p \in \{2, 4, 6\}$, with ramp constraints modeled by the LC model.
- Case TA-2-ME: equal-spacing (p-ES) with $p \in \{2, 4, 6\}$, with ramp constraints modeled by the ME model.
- Case TA-3-LC: diffusing-horizon (m-DH) with $m \in \{2, 4, 6\}$, with ramp constraints modeled by the LC model.
- Case TA-3-ME: diffusing-horizon (m-DH) with $m \in \{2, 4, 6\}$, with ramp constraints modeled by the ME model.

The problem indicators for cases TA-1-LC and TA-1-ME are shown in Tables 22-23. Note that all simulations present a significant reduction in the computational effort, and small differences between the day-ahead costs obtained are observed when compared with case OR. Figures 48-49 present the day-ahead scheduled thermoelectric generation for cases TA-1-ME and TA-1-LC with $T = 96$. Note that the power curves obtained are approximately the same as the OR case.

Table 22 – Summary of problem statistics for simulations with temporal aggregations case TA-1-LC

k	*T*	Ncv	Nbv	Ncons	Rt (s)	ΔRt (%)	Dac (10^6 $)	ΔDac (%)
4	144	93,078	20,580	329,959	1194	57.21	3.0121	-0.24
	120	80,058	17,745	283,822	617	77.89	3.0139	-0.18
	96	68,898	15,315	244,276	507	81.83	3.0139	-0.18
6	144	96,798	21,390	343,141	1318	52.76	2.9878	-1.04
	120	86,878	19,230	307,989	904	67.60	3.0289	0.31
	96	76,338	16,935	270,640	590	79.86	3.0138	-0.18
8	144	98,038	21,660	347,535	1158	58.50	3.0176	-0.05
	120	88,738	19,635	314,580	862	69.11	2.9782	-1.36
	96	80,678	17,880	286,019	755	72.94	3.0119	-0.24
OR	-	104,238	23,010	369,505	2790	-	3.0194	0

Table 23 – Summary of problem statistics for simulations with temporal aggregations case TA-1-ME

k	*T*	Ncv	Nbv	Ncons	Rt (s)	ΔRt (%)	Dac (10^6 $)	ΔDac (%)
4	144	93,078	20,580	329,959	1110	60.22	3.0345	0.50
	120	80,058	17,745	283,822	759	72.80	3.0079	-0.38
	96	68,898	15,315	244,276	633	77.32	2.8808	-4.59
6	144	96,798	21,390	343,141	1496	46.38	2.9369	-2.73
	120	86,878	19,230	307,989	948	66.03	2.9357	-2.77
	96	76,338	16,935	270,640	656	76.49	3.0192	-0.01
8	144	98,038	21,660	347,535	1502	46.17	3.0123	-0.23
	120	88,738	19,635	314,580	918	67.10	3.0089	-0.34
	96	80,678	17,880	286,019	787	71.80	3.0110	-0.27
OR	-	104,238	23,010	369,505	2790	-	3.0194	0

Figure 48 – Thermoelectric generation for the first 24 hours for case TA-1-ME with $T = 96$.

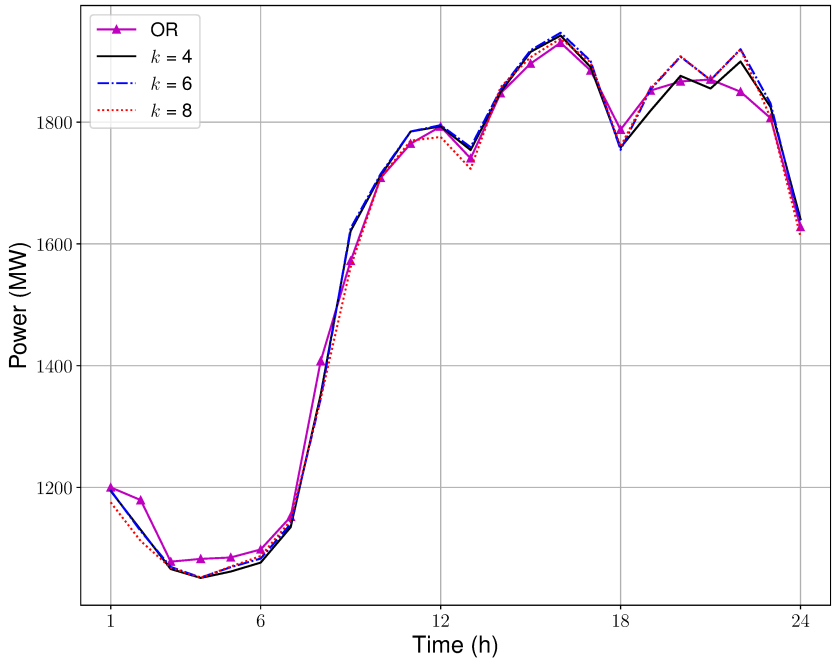

Figure 49 – Thermoelectric generation for the first 24 hours for case TA-1-LC with $T = 96$.

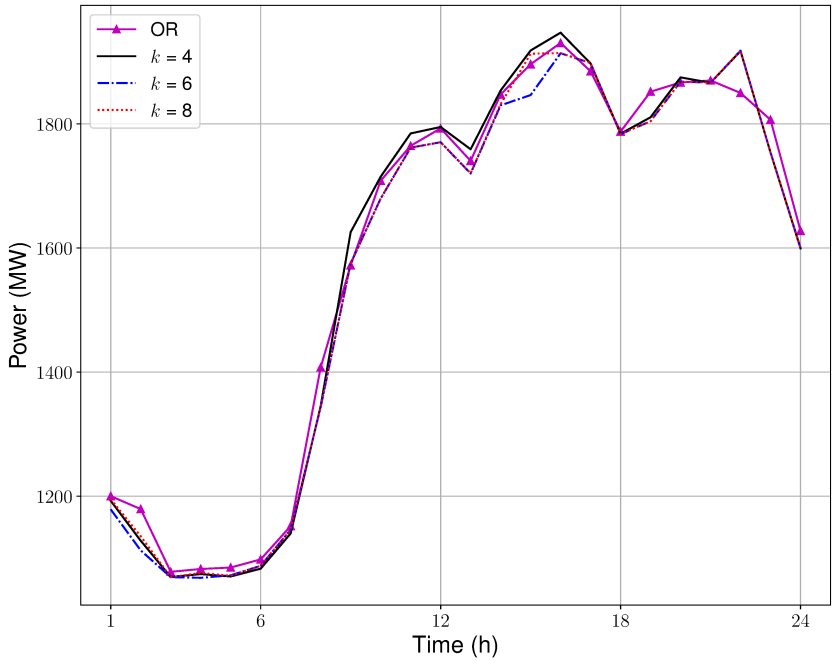

The statistics for simulations performed for cases TA-2-LC and TA-2-ME are shown in Tables 24-25. There is a significant reduction in computational effort for all

cases, and similar to cases with the k-means approach, the day-ahead costs obtained have small differences compared with OR. For example, the day-ahead thermoelectric generation for TA-2-ME and TA-2-LC with $T = 120$ is presented in Figures 50-51. In particular, case TA-2-ME with $p = 6$ and $T = 144$ presented a greater computational reduction, but this case can be assumed as an outlier.

Table 24 – Summary of statistics problem for simulations with temporal aggregations case TA-2-LC

p	T	Ncv	Nbv	Ncons	Rt (s)	ΔRt (%)	Dac (10^6 $)	ΔDac (%)
2	144	118,188	21,390	343,141	1966	29.54	3.0125	-0.22
	120	89,358	19,770	316,777	1464	47.53	3.0262	0.22
	96	81,918	18,150	290,413	1102	60.51	3.0285	0.30
4	144	93,078	20,580	329,959	1432	48.68	3.0264	0.23
	120	81,918	18,150	290,413	814	70.83	3.0277	0.27
	96	70,758	15,720	250,867	613	78.03	3.0151	-0.14
6	144	91,838	20,310	325,565	1140	59.14	2.9851	-1.13
	120	79,438	17,610	281,625	878	68.54	3.0242	0.15
	96	67,038	14,910	237,685	488	82.51	3.0252	0.19
OR	-	104,238	23,010	369,505	2790	-	3.0194	0

Table 25 – Summary of problem statistics for simulations with temporal aggregations case TA-2-ME

p	T	Ncv	Nbv	Ncons	Rt (s)	ΔRt (%)	Dac (10^6 $)	ΔDac (%)
2	144	118,188	21,390	343,141	1959	29.79	3.0194	0
	120	89,358	19,770	316,777	1332	52.26	3.0163	-0.10
	96	81,918	18,150	290,413	1455	47.85	3.0215	0.06
4	144	93,078	20,580	329,959	1521	45.49	3.0180	-0.04
	120	81,918	18,150	290,413	863	69.07	3.0083	-0.36
	96	70,758	15,720	250,867	659	76.38	2.8921	-4.21
6	144	91,838	20,310	325,565	257	90.79	3.0126	-0.22
	120	79,438	17,610	281,625	957	65.70	2.9225	-3.20
	96	67,038	14,910	237,685	605	78.32	2.8861	-4.41
OR	-	104,238	23,010	369,505	2790	-	3.0194	0

Figure 50 – Thermoelectric generation for the first 24 hours for case TA-2-ME with $T = 120$.

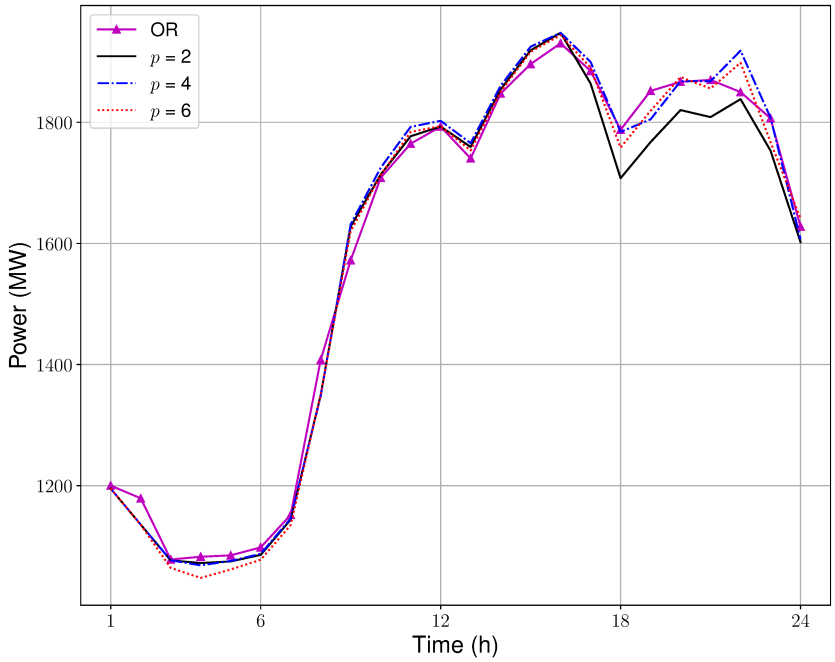

Figure 51 – Thermoelectric generation for the first 24 hours for case TA-2-LC with $T = 120$.

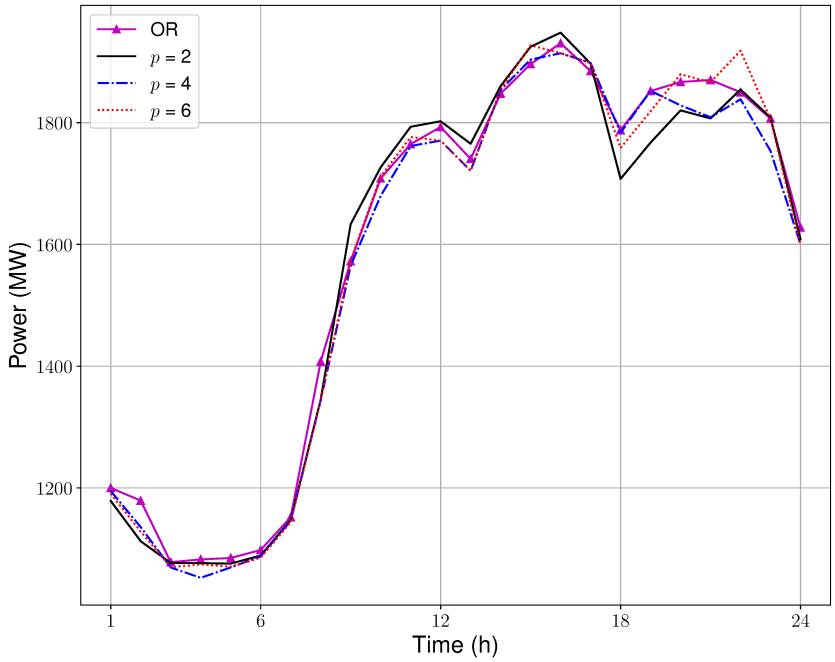

Finally, for cases TA-3-LC and TA-3-ME, the problem statistics are shown in Tables 26- 27. There is also a significant reduction in the computational effort when

compared with the OR case. Also, the day-ahead decisions presented small differences, as in Figures 52-53 for simulations with $T = 96$, cases ME and LC, respectively.

Table 26 – Summary of problem statistics for simulations with temporal aggregations case TA-3-LC

m	*T*	Ncv	Nbv	Ncons	Rt (s)	ΔRt (%)	Dac (10^6 $)	ΔDac (%)
2	144	118,188	21,390	343,141	1449	48.07	3.0143	-0.16
	120	89,358	19,770	316,777	1360	51.26	3.0172	-0.07
	96	81,918	18,150	290,413	887	68.21	3.0195	0.01
4	144	93,078	20,580	329,959	1226	56.06	3.0276	0.27
	120	81,918	18,150	290,413	820	70.61	3.0024	-0.56
	96	70,758	15,720	250,867	482	82.73	3.0065	-0.42
6	144	91,838	20,310	325,565	1353	51.51	3.0310	0.38
	120	79,438	17,610	281,625	726	73.98	3.0132	-0.20
	96	67,038	14,910	237,685	514	81.58	3.0174	-0.01
OR	-	104,238	23,010	369,505	2790	-	3.0194	0

Table 27 – Summary of problem statistics for simulations with temporal aggregations case TA-3-ME

m	*T*	Ncv	Nbv	Ncons	Rt (s)	ΔRt (%)	Dac (10^6 $)	ΔDac (%)
2	144	118,188	21,390	343,141	1554	44.31	3.0257	0.20
	120	89,358	19,770	316,777	1474	47.17	3.0330	0.45
	96	81,918	18,150	290,413	1175	57.89	3.0154	-0.13
4	144	93,078	20,580	329,959	231	91.73	2.9961	-0.77
	120	81,918	18,150	290,413	961	65.56	2.9337	-2.83
	96	70,758	15,720	250,867	536	80.79	3.0127	-0.22
6	144	91,838	20,310	325,565	1272	54.41	3.0103	-0.30
	120	79,438	17,610	281,625	885	69.28	2.9992	-0.66
	96	67,038	14,910	237,685	568	79.65	3.0132	-0.20
OR	-	104,238	23,010	369,505	2790	-	3.0194	0

Figure 52 – Thermoelectric generation for the first 24 hours for case TA-3-ME with $T = 96$.

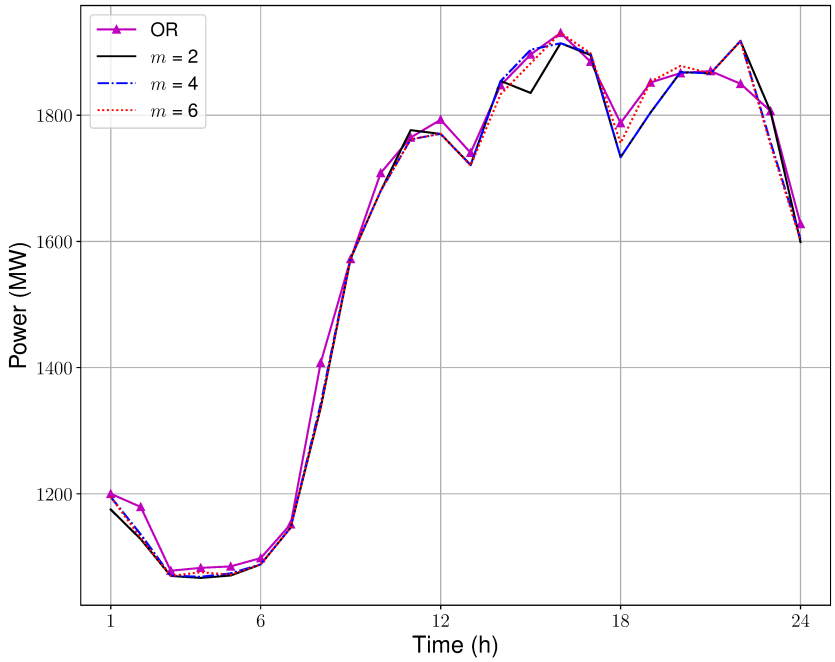

Figure 53 – Thermoelectric generation for the first 24 hours for case TA-3-LC with $T = 96$.

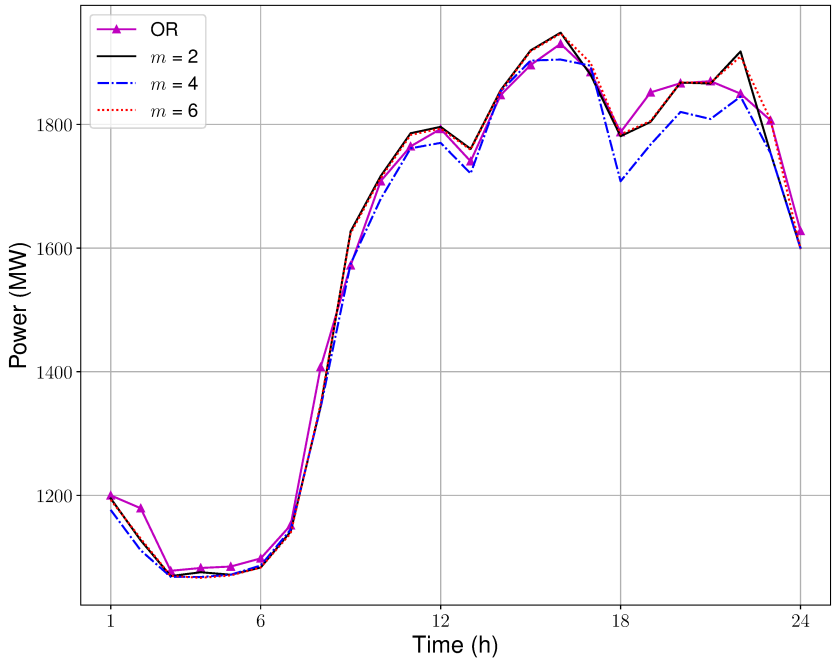

From these results, note that all types of aggregations present significant reductions in the computational effort. Furthermore, there is a relatively small impact on the

choice of representation of ramp constraints. Concerning the parameter T, note that for cases $T = 96$ and $T = 120$, the computational effort is reduced significantly in most simulations without compromising the day-ahead decisions. About the Dac, case TA-3-LC (diffusing-horizon with ramp represented by the less cost case) presented values closer to the OR case.

5.3.3 Assessing impacts of model simplifications and temporal aggregations

The results from experiments when both strategies are performed simultaneously are presented in this subsection, assuming the results obtained for simulations with model simplifications and temporal aggregations. In this case, concerning the model simplifications, the linear relaxation in the integrality constraints presented better results, being the model simplification chosen to be employed. In terms of temporal aggregations, the three types are performed since all strategies have presented interesting results. Once the ramp representation has no significant differences in simulations, we choose to use case LC in the experiments of this section. For parameter T, we decide to use $T = \{96,120\}$. The overview of the statistics for all experiments assumed is presented in Tables 28-30.

Table 28 – Summary of problem statistics for simulations with model simplifications, temporal aggregations using the k-means approach

k	T	Ncv	Nbv	Ncons	Rt (s)	ΔRt (%)	Dac (10^6 \$)	ΔDac (%)
4	120	81,273	16,530	283,822	760	72.76	3.0216	0.07
	96	70,293	13,290	244,276	422	84.88	3.0201	0.02
6	120	89,578	16,530	307,989	927	66.78	3.0097	-0.32
	96	79,983	13,290	270,640	547	80.40	3.0184	-0.03
8	120	91,843	16,530	314,580	853	69.43	3.0107	-0.28
	96	85,268	13,290	286,019	598	80.57	3.0235	0.13
OR	-	104,238	23,010	369,505	2790	-	3.0194	0

Table 29 – Summary of problem statistics for simulations with model simplifications, temporal aggregations using the equal-spacing approach

p	T	Ncv	Nbv	Ncons	Rt (s)	ΔRt (%)	Dac (10^6 \$)	ΔDac (%)
2	120	92,598	16,530	316,777	1260	54.76	3.0252	0.19
	96	86,778	13,290	290,413	897	67.85	3.0163	-0.10
4	120	83,538	16,530	290,413	891	68.07	3.0055	-0.46
	96	73,188	13,290	250,867	658	76.42	3.0122	-0.23
6	120	80,518	16,530	281,625	615	77.96	3.0323	0.42
	96	68,658	13,290	237,685	426	84.74	3.0085	-0.36
OR	-	104,238	23,010	369,505	2790	-	3.0194	0

Table 30 – Summary of problem statistics for simulations with model simplifications, temporal aggregations using the diffusing-horizon approach

m	*T*	Ncv	Nbv	Ncons	Rt (s)	ΔRt (%)	Dac (10^6 $)	ΔDac (%)
2	120	92,598	16,530	316,777	1057	62.12	3.0156	-0.12
	96	86,778	13,290	290,413	747	73.23	3.0251	0.18
4	120	83,538	16,530	290,413	827	70.36	3.0103	-0.30
	96	73,188	13,290	250,867	512	81.65	3.0064	-0.43
6	120	80,518	16,530	281,625	729	73.88	3.0306	0.37
	96	68,658	13,290	237,685	409	85.35	3.0323	0.42
OR	-	104,238	23,010	369,505	2790	-	3.0194	0

As expected, there is a reduction in the computational effort compared with cases without model simplifications, and the day-ahead scheduled decisions are closer to the case OR, as can be viewed in Figure 54 for the case with $T = 120$ with different temporal aggregations strategies. From these results, we can conclude that combined model simplifications and temporal aggregations is a valid approach to be employed in STGS problems.

Figure 54 – Thermoelectric generation for the first 24 hours for cases with model simplifications and temporal aggregations with $T = 120$.

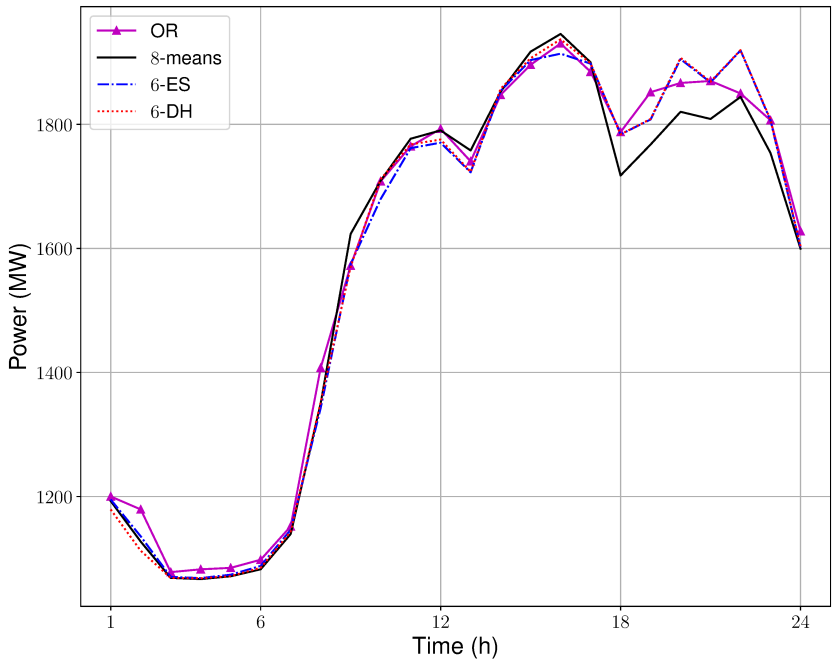

5.4 FINAL CONSIDERATIONS

This chapter assesses the computational effort involved in solving an STGS problem. It is assumed that the STGS problem is solved daily by the system operator in a rolling horizon scheme, where the goal is to obtain the day-ahead scheduled decisions.

Since the planning horizon is normally greater than one day, the STGS is a large-scale MILP optimization problem that is usually hard to be solved. Therefore, strategies to reduce the computational effort are commonly employed, including temporal aggregations.

Inspired by the recent exponential decay of sensitivity in LP problems, in this thesis we employed different temporal aggregations, including the diffusing-horizon strategy and model simplifications to deal with the computational complexity of the STGS problem. The results obtained from experiments performed on a modified version of the IEEE-118 bus system show that when we employ model simplifications and temporal aggregations after a certain period of the planning horizon, small perturbations in the day-ahead scheduled decisions are observed. Still, the reduction in the computational effort is significant, showing the potential use of these strategies in other large-scale optimization problems or STGS problems with larger power systems instances. Also, an analysis on how the dual variables are affected by this type of strategy is an interesting topic that requires attention.

6 CONCLUSIONS

The STGS problem determines which generating units will be active and how much power they will produce for a day-ahead operation and over a one-week planning horizon. The STGS solution is used for several systems operation purposes, especially as a reference point for real-time operation and determining the day-ahead spot prices. Despite being well-studied and utilized worldwide, the STGS still poses a considerable challenge because it needs to be solved rapidly. Specifically, the STGS problem is a large-scale, nonlinear, and nonconvex mixed-integer optimization problem. The STGS is typically simplified and formulated as a MILP problem, but even this reformulation can be intractable to modern, off-the-shelf optimization solvers. Such simplifications as the linear formulation of power flow and linear approximations for the HPF can impact the results obtained, possibly creating divergences in the values implemented in the real-time operation, which is not desirable.

In this context, hydropower offers unique flexibility features, and an adequate representation is crucial for overcoming operation challenges. For systems with hydro predominance, models with great details for the HPF are attractive. However, simplifications of HPF modeling are necessary due to the computational burden. The plant-based HPF piecewise linear approach is the most common simplification presented for real-life cases. In this case, the GUs of a plant are aggregated and represented by a single equivalent generator. Although this approach significantly reduces the size and complexity of the STGS, several operating issues are not considered adequately, especially the forbidden zones and the nonlinearities of the GUs. In this thesis, we present a new approach that considers the nonlinearities and forbidden zones of the HPF via aggregation of the GUs and piecewise mixed-integer linear approximations in an innovative way, where the PWL formulation makes it possible to control the approximation error. From the results obtained from simulations performed in the IEEE-118 bus, we observe that the PCH and PWL models are an interesting alternative to represent the HPF since both models precisely handle the operation in forbidden zones, achieving an overall average error of less than 6% for all simulations. The increase in computational time is an issue that needs more investigation in large-size systems, although decomposition techniques and parallel processing are natural options in this context. Also, depending on the accuracy required, a particular HPF model can be chosen, enabling an STGS problem where each hydro has a specific type of formulation presented in this thesis.

To handle the computational effort to solve the STGS problem, in this thesis, we used a temporal decomposition strategy provided by DDiP. The classical DDiP is based on nested Benders decomposition, and a pre-solve step is initially applied. A study of the size of stages is presented, aiming to find the best trade-off between the computational effort involved in solving each SP and the convergence of DDiP. Next, a novel

contribution constituted on overlap constraints is presented, and criteria for choosing the type of constraints that will belong to the overlap for the STGS problem are discussed. The simulations are performed considering an STGS problem with a one-week planning horizon and a modified version of the IEEE-118 bus system, and from the results obtained, we show that the DDiP can obtain solutions with an optimality gap of less than 0.5% way faster than solving the STGS without decomposition, showing the potential of the DDiP, especially for large-size problems. When the overlap constraints are introduced, despite the computational effort to solve each SP increases, the convergence of the DDiP accelerates, indicating a new possibility that can be applied to other types of temporal decomposition strategies.

This thesis' third contribution concerns assessing the computational effort involved in solving an STGS problem. The STGS problem is normally solved every day by the system operator in a rolling horizon scheme, where the target is to obtain the day-ahead scheduled decisions. Temporal aggregations are usually employed to reduce the computational effort involved in solving the STGS problem. Inspired by the recent results of the exponential decay of sensitivity in LP problems, in this thesis, we employed different temporal aggregations, including the diffusing-horizon strategy, and model simplifications to deal with the computational complexity of the STGS problem. The simulations are performed considering a one-week planning horizon and a modified version of the IEEE-118 bus system to assess the day-ahead scheduled decisions for the strategies presented in this thesis. The results show that small perturbations in the day-ahead scheduled decisions are observed when we apply model simplifications and temporal aggregations after a certain period of the planning horizon. Still, computational effort reduction is generally greater than 40%, showing the potential use of these strategies in other large-scale optimization problems. Concerning model simplifications, the linear relaxation of the integrality constraints presented the best results, and about temporal aggregations, both k-means, equal-spacing, and diffusing-horizon strategies presented satisfactory results.

Finally, future works can be listed as follows:

- In terms of HPF formulations, a natural extension is to insert the several formulations presented in this thesis in a large-scale problem, where each formulation for HPF is decided using the accuracy criteria. The inclusion of spillage in all plant-based HPF models is a natural extension. The mixed-integer models can be inserted using a PWL formulation for the spillage active region using at least one binary variable. To increase the precision, bidimensional PWL models can be used, but this case requires more investigation once the computational effort can be increased drastically. A combination with bidimensional PWL formulations and SOS-2 or logarithm formulations can provide a good trade-off for this case.

- In terms of the DDiP applied to the STGS problem, natural extensions use parallel processing strategies to create a scheme where the different temporal decomposition is employed to provide valid cuts for specific SPs. Also, the convergence of each SP is directly related to the optimality gap used, and another possibility is to study the impacts of the optimality gap used. In the pre-solve strategy, despite we explore only the linear relaxation, there are other possibilities to explore, such as temporal decomposition. Suppose we employ temporal decomposition in the pre-solve step. In that case, the cuts are still valid for the DDiP iterative scheme for the corresponding SP, which enables a new possibility for a large-scale problem. Suppose, in the pre-solve step, the resulting problem is a relaxed mixed-integer version of the original problem. In that case, multiple solutions for different optimality gaps can be used to generate valid cuts. Also, the DDiP strategy employed in this thesis is from classical BD. For schemes containing a low number of SPs, the modern BD approach is an interesting strategy that can be employed. Finally, in this thesis, we didn' t employ a cut selection strategy. Since the DDiP is a recent topic in the scientific community, this is an open area to explore. As an example, techniques of machine learning can be used to select which cuts will be inserted at a specific iteration.

- In terms of temporal aggregations and model simplifications applied to the STGS problem, a natural extension is to apply the same strategies in a large-scale system and analyze the impacts on the day-ahead scheduled decisions. Considering the STGS problem is a mixed-integer, where there is no definition of shadow prices, one common approach is to fix the binary variables and consider these as continuous, and solve the STGS in the linear version to obtain these prices. One interesting and challenging approach is verifying how the temporal aggregations impact the shadow prices considering the decisions obtained for the mixed-integer version of the STGS problem. Also, other types of model simplifications, such as the network flow model instead of the economic dispatch model for the network constraints are a possibility.

- All the studies performed in this thesis can be combined. For example, a large-scale STGS problem where advanced formulations for the HPF are employed in the first days of the planning horizon, using model simplifications and temporal aggregations, solved by the DDiP is a possibility to be explored.

REFERENCES

ALEMANY, J.; MAGNANO, F. Benders Decomposition Applied to Security Constrained Unit Commitment: Initialization of the Algorithm. **International Journal of Electrical Power & Energy Systems**, v. 66, p. 53–66, Mar. 2015.

AMJADY, N.; ANSARI, M. R. Hydrothermal Unit Commitment with AC Constraints by a New Solution Method Based on Benders Decomposition. **Energy Conversion and Management**, v. 65, p. 57–65, Jan. 2013.

ANSARI, M. R.; AMJADY, N.; VATANI, B. Stochastic Security-constrained Hydrothermal Unit Commitment Considering Uncertainty of Load Forecast, Inflows to Reservoirs and Unavailability of Units by a New Hybrid Decomposition Strategy. **IET Generation, Transmission & Distribution**, v. 8, n. 12, p. 1900–1915, Dec. 2014.

BAHL, B.; KÜMPEL, A.; SEELE, H.; LAMPE, M.; BARDOW, A. Time-Series Aggregation for Synthesis Problems by Bounding Error in the Objective Function. **Energy**, v. 135, p. 900–912, 2017.

BAI, Y.; ZHONG, H.; XIA, Q.; KANG, C.; XIE, L. A Decomposition Method for Network-Constrained Unit Commitment with AC Power Flow Constraints. **Energy**, v. 88, p. 595–603, Aug. 2015.

BALAKRISHNAN, A.; GRAVES, S. C. A Composite Algorithm for a Concave-cost Newtork Flow Problem. **Networks**, p. 175–202, 1989.

BARBIR, Frano; ULGIATI, Sergio. **Sustainable Energy Production and Consumption: Benefits, Strategies and Environmental Costing**. [S.l.]: Springer, 2008.

BELLONI, A.; LIMA, A. L. D. S.; MACEIRA, M. E. P.; SAGASTIZÁBAL, C. A. Bundle Relaxation and Primal Recovery in Unit Commitment Problems: The Brazilian Case. **Annals of Operations Research**, v. 120, p. 21–44, Apr. 2003.

BENDERS, J. F. Partitioning Procedures for Solving Mixed-Variables Programming Problems. **Numerische Mathematik**, v. 4, n. 1, p. 238–252, 1962.

BENÍTEZ, I.; QUIJANO, A.; DÍEZ, J-L.; DELGADO, I. Dynamic Clustering Segmentation Applied to Load Profiles of Energy Consumption from Spanish

Customers. **International Journal of Electrical Power & Energy Systems**, v. 55, p. 437–448, 2014.

BESTUZHEVA, Ksenia et al. **The SCIP Optimization Suite 8.0**. [S.l.], Dec. 2021.

BIRGE, J. R. Decomposition and Partitioning Methods for Multistage Stochastic Linear Programs. **Operations Research**, v. 33, n. 5, p. 989–1007, 1985.

BONNANS, J.-F; GILBERT, J. C.; LEMARECHAL, C.; SAGASTIZÁBAL, C. **Numerical Optimization: Theoretical and Practical Aspects**. 2. ed. [S.l.]: Springer, 2006.

BORGHETTI, A.; D'AMBRÓSIO, C. D.; LODI, A.; MARTELLO, S. An MILP Approach for Short-term Hydro Scheduling and Unit Commitment with Head-dependent Reservoir. **IEEE Trans. on Power Systems**, v. 23, n. 3, p. 1115–1124, Aug. 2008.

BORGHETTI, A.; FRANGIONI, A.; NUCCI, C. A. Lagrangian Heuristics Based on Disaggegated Bundle Methods for Hydrothermal Unit Commitment. **IEEE Transactions on Power Systems**, v. 18, n. 1, p. 313–323, Feb. 2003.

BRITO, B. H.; FINARDI, E. C.; TAKIGAWA, F. Y. K. Mixed-integer Nonseparable Piecewise Linear Models for the Hydropower Production Function in the Unit Commitment Problem. **Electric Power Systems Research**, v. 182, p. 106234, May 2020.

CATALAO, J. P. S.; MARIANO, S. J. P.; MENDES, V. M. F.; FERREIRA, L. A. F. Scheduling of Head-sensitive Cascaded Hydro Systems: A Nonlinear Approach. **IEEE Trans. on Power Systems**, v. 24, n. 1, p. 337–346, Feb. 2009.

CATALAO, J. P. S.; POUSINHO, H. M. I.; MENDES, V. M. F. Hydro Energy Systems Management in Portugal: Profit-based Evaluation of a Mixed-integer Nonlinear Approach. **Energy**, v. 36, n. 1, p. 500–507, Jan. 2011.

CATALAO, J. P. S.; POUSINHO, H. M. I.; MENDES, V. M. F. Mixed-integer Nonlinear Approach for the Optimal Scheduling of a Head-dependent Hydro Chain. **Electric Power Systems Research**, v. 80, n. 8, p. 935–942, Aug. 2010.

COLONETTI, B.; FINARDI, E. C. Stochastic Hydrothermal Unit Commitment Models via Stabilized Benders Decomposition. **Electr Eng**, v. 103, p. 2197–2211, Feb. 2021.

CONEJO, A. J.; CASTILLO, E.; MINGUEZ, R.; GARCIA-BERTRAND, R. **Decomposition Techniques in Mathematical Programming**. [S.l.]: Springer, 2006.

DINIZ, A. L.; COSTA, F. S.; MACEIRA, M. E. P.; SANTOS, T. N.; SANTOS, L. C. B.; CABRAL, R. N. Short/Mid-Term Hydrothermal Dispatch and Spot Pricing for Large-Scale Systems-the Case of Brazil. In: 2018 POWER SYSTEMS COMPUTATION CONFERENCE (PSCC), p. 1–7. DOI: 10.23919/PSCC.2018.8442897.

DINIZ, A. L.; MACEIRA, M. E. P. A Four-dimensional Model of Hydro Generation for the Short-term Hydrothermal Dispatch Problem Considering Head and Spillage Effects. **IEEE Trans. on Power Systems**, v. 23, n. 3, p. 1298–1308, Aug. 2008.

DINIZ, A. L.; SOUZA, T. M. Short-term Hydrothermal Dispatch With River-level and Routing Constraints. **IEEE Trans. on Power Systems**, v. 29, n. 5, p. 2427–2435, Sept. 2014.

DOUGLAS, D. H.; PEUCKER, T.K. Algorithms for the Reduction of the Number of Points Required to Represent a Digitized Line or its Caricature. **Can. Cartogr.**, p. 112–122, 1973.

DUNNING, I.; HUCHETTE, J.; LUBIN, M. JuMP: A Modeling Language for Mathematical Optimization. **SIAM Rev.**, v. 59, n. 2, p. 295–320, Jan. 2017.

FAZLOLLAHI, S.; BUNGENER, S. L.; MANDEL, P.; BECKER, G.; MARÉCHAL, F. Multi-Objectives, Multi-Period Optimization of District Energy Systems: I. Selection of Typical Operating Periods. **Computers & Chemical Engineering**, v. 65, p. 54–66, 2014.

FAZLOLLAHI, S.; MARÉCHAL, F. Multi-Objective, Multi-Period Optimization of Biomass Conversion Technologies Using Evolutionary Algorithms and Mixed Integer Linear Programming. **Applied Thermal Engineering**, v. 50, n. 2, p. 1504–1513, 2013.

FINARDI, E. C.; LOBATO, R. D.; MATOS, V. L.; SAGASTIZÁBAL, C. A.; TOMASGARD, A. Stochastic Hydro-thermal Unit Commitment via Multi-level Scenario Tress and Bundle Regularization. **Optim Eng**, v. 21, n. 2, p. 393–426, June 2020.

FINARDI, E. C.; SILVA, E. L. Solving the Hydro Unit Commitment Problem via Dual Decomposition and Sequential Quadratic Programming. **IEEE Trans. on Power Systems**, v. 21, n. 2, p. 835–844, May 2006.

FLAMM, B.; EICHLER, A.; WARRINGTON, J.; LYGEROS, J. Two-Stage Dual Dynamic Programming with Application to Nonlinear Hydro Scheduling. **IEEE Trans. on Control Systems Technology**, v. 29, n. 1, p. 96–107, Jan. 2021.

FRANGIONI, A.; GENTILE, C.; LACALANDRA, F. Solving Unit Commitment Problems with General Ramp Constraints. **International Journal of Electrical Power & Energy Systems**, v. 30, n. 5, p. 316–326, June 2008.

FU, Y.; LI, Z.; WU, L. Modeling and Solution of the Large-Scale Security-Constrained Unit Commitment. **IEEE Trans. on Power Systems**, v. 28, n. 4, p. 3524–3533, Nov. 2013.

GEISSLER, B.; MARTIN, A.; MORSI, A. **Using Piecewise Linear Functions for Solving MINLPs**: The IMA Volumes in Mathematics and its Applications. New York: Springer Science + Business, 2012. v. 154, p. 287–314.

GENTILE, C.; MORALES-ESPAÑA, G.; RAMOS, A. A Tight MIP Formulation of the Unit Commitment Problem with Start-up and Shut-down Constraints. **EURO Journal on Computational Optimization**, v. 5, n. 1-2, p. 177–201, Mar. 2017.

GEOFFRION, A. M. Generalized Benders Decomposition. **J Optim Theory Appl**, v. 10, p. 237–260, Oct. 1972.

GUEDES, L. S. M.; MAIA, P. M.; LISBOA, A. C.; VIEIRA, D. A. G.; SALDANHA, R. R. A Unit Commitment Algorithm and a Compact MILP Model for Short-term Hydropower Generation Scheduling. **IEEE Trans. on Power Systems**, v. 32, n. 5, p. 3381–3390, Sept. 2017.

GUROBI. **Gurobi - The Fastest Solver**. [S.l.], 2022. Available from: `http://www.gurobi.com`. Visited on: 7 Feb. 2021.

HAMANN, A.; HUG, G.; ROSINSKI, S. Real-time Optimization for the Mid-Columbia Hydropower System. **IEEE Trans. on Power Systems**, v. 32, n. 1, p. 157–165, Jan. 2017.

HEDMAN, K. W.; FERRIS, M. C.; O'NEIL, R. P.; FISHER, E. B.; OREN, S. S. Co-Optimization of Generation Unit Commitment and Transmission Switching with N-1 Reliability. **IEEE Trans. on Power Systems**, v. 25, n. 2, p. 1052–1063, May 2010.

HUCHETTE, J.; VIELMA, J. P. **Nonconvex Piecewise Linear Functions: Advanced Formulations and Simple Modeling Tools**. [S.l.: s.n.], 2019. arXiv: 1708.00050 [math.OC].

IEEE. **IEEE 118-bus data**. [S.l.], 2022. Available from: http://www.motor.ece.iit.edu/data/. Visited on: 17 May 2022.

JIA, J.; GUAN, X. MILP Formulation for Short-term Scheduling of Cascaded Reservoirs with Head Effects. In: 2ND INTERNATIONAL CONFERENCE ON ARTIFICIAL INTELLIGENCE, MANAGEMENT SCIENCE and ELECTRONIC COMMERCE (AIMSEC), p. 4061–4064.

JILIN, C.; MIN, Z.; ZHONGHUA, G.; WEIJIANG, Q.; YONG, C.; WEIXI, W. The Application of Douglas-Peucker Algorithm in Collaborative System for Power Grid Operation Mode Calculation. In: MATEC WEB CONF., p. 03041.

KOCH, K.; HILLER, B.; PFETSCH, M. E.; SCHEWE, L. **Evaluating Gas Network Capacities**. [S.l.]: SIAM, 2015.

KONG, J.; SKJELBRED, H. I.; FOSSO, O. B. An Overview on Formulations and Optimization Methods for the Unit-based Short-term Hydro Scheduling Problems. **Electric Power Systems Research**, v. 178, p. 106027, Jan. 2020.

KORUK, B.; DEY, S. S.; SUN, X. A. Strong SOCP Relaxations for the Optimal Power Flow Problem. **Operations Research**, v. 64, n. 6, p. 1177–1196, Nov. 2016.

KUMAR, R.; WENZEL, M. J.; ELBSAT, M. N.; RISBECK, M. J.; DREES, K. H.; ZAVALA, V. M. Dual Dynamic Programming for Multi-Scale Mixed-Integer MPC. **Computers & Chemical Engineering**, v. 148, p. 107265, May 2021.

LARA, C. L.; MALLAPRAGADA, D. S.; PAPAGEORGIOU, D. J.; GROSSMAN, I. E. Deterministic Electric Power Infrastructure Planning: Mixed-integer Programming Model and Nested Decomposition Algorithm. **European Journal of Operational Research**, v. 271, n. 3, p. 1037–1054, Dec. 2018.

LARA, C. L.; SIIROLA, J. D.; GROSSMAN, I. E. Eletric Power Infrasctructure Planning Under Uncertainty: Stochastic Dual Dynamic Integer Programming (SDDiP) and Parallelization Scheme. **Optim. Eng.**, v. 21, n. 4, p. 1243–1281, Dec. 2020.

LI, X.; LI, T.; WEI, J.; WANG, G.; YEH, W. W.-G. Hydro Unit Commitment via Mixed Integer Linear Programming: A Case Study of the Three Gorges Project China. **IEEE Trans. on Power Systems**, v. 29, n. 3, p. 1232–1241, May 2014.

LIU, J.; LAIRD, C. D.; SCOTT, J. K.; WATSON, J.-P; CASTILLO, A. Global Solution Strategies for the Network-Constrained Unit Commitment Problem with AC Transmission Constraints. **IEEE Trans. on Power Systems**, v. 34, n. 2, p. 1139–1150, Mar. 2019.

LLOYD, S. P. Least Squares Quantization in PCM. **IEEE Transactions on Information Theory**, v. 28, n. 2, p. 129–137, 1982.

MACEIRA, M.E.P.; PENNA, D.D.J.; DINIZ, A.L.; PINTO, R.J.; MELO, A.C.G.; VASCONCELLOS, C.V.; CRUZ, C.B. Twenty Years of Application of Stochastic Dual Dynamic Programming in Official and Agent Studies in Brazil-Main Features and Improvements on the NEWAVE Model. In: 2018 POWER SYSTEMS COMPUTATION CONFERENCE (PSCC), p. 1–7. DOI: 10.23919/PSCC.2018.8442754.

MARCHAND, A.; GENDREAU, M.; BLAIS, M.; EMIEL, G. Fast Near-optimal Heuristic for the Short-term Hydro-Generation Planning Problem. **IEEE Trans. on Power Systems**, v. 33, n. 1, p. 227–235, Jan. 2018.

MAVROTAS, G.; DIAKOULAKI, D.; FLORIOS, K.; GEORGIOU, P. A Mathematical Programming Framework for Energy Planning in Service' s Sector Building Under Uncertainty in Load Demand: The Case of a Hospital in Athens. **Energy Policy**, v. 36, n. 7, p. 2415–2429, 2008.

MOLZAHN, D. K.; HISKENS, I. A. A Survey of Relaxations and Approximations of the Power Flow Equations. **Found. Trends Electr. Energy Systems**, v. 4, n. 1-2, p. 1–221, 2019.

MURILLO-SANCHEZ, C.; THOMAS, R. J. Thermal Unit Commitment Including Optimal AC Power Flow Constraints. In: PROCEEDINGS OF THE THIRTY-FIRST HAWAII INTERNATIONAL CONFERENCE ON SYSTEM SCIENCES, p. 81–88.

NA, S.; ANITESCU, M. Exponential Decay in the Sensitivity Analysis of Nonlinear Dynamic Programming. **SIAM Journal on Optimization**, v. 30, n. 2, p. 1527–1554, 2020.

NA, S.; ANITESCU, M.; KOLAR, M. **A Fast Temporal Decomposition Procedure for Long-horizon Nonlinear Dynamic Programming**. [S.l.: s.n.], 2021. arXiv: 2107.11560 [math.OC].

NA, S.; SHIN, S.; ANITESCU, M.; ZAVALA, V. M. **On the Convergence of Overlapping Schwarz Decomposition for Nonlinear Optimal Control**. [S.l.: s.n.], 2021. arXiv: 2005.06674 [math.OC].

NAHMMACHER, P.; SCHMID, E.; HIRTH, L.; KNOPF, B. Carpe Diem: A Novel Approach to Select Representative Days for Long-Term Power System Modeling. **Energy**, v. 112, p. 430–442, 2016.

NASRI, A.; KAZEMPOUR, S. J.; CONEJO, A. J.; GHANDHARI, M. Network-Constrained AC Unit Commitment Under Uncertainty: A Benders' Decomposition Approach. **IEEE Trans. on Power Systems**, v. 31, n. 1, p. 412–422, Jan. 2016.

NICK, M.; ALIZADEH-MOUSAVI, O.; CHERKAOUI, R.; PAOLONE, M. Security Constrained Unit Commitment with Dynamic Thermal Line Rating. **IEEE Trans. on Power Systems**, v. 31, n. 3, p. 2014–2025, May 2016.

O'NEILL, R. P. Computational Issues in ISO Market Models. In: WORKSHOP ON ENERGY SYSTEMS and OPTIMIZATION.

ONS. **Operador Nacional do Sistema Elétrico**. [S.l.], 2021. Available from: http://www.ons.org.br/. Visited on: 20 Jan. 2021.

PAREDES, L. S. A. M.; SOARES, S. Using Semidefinite Relaxation to Solve the Day-ahead Hydro Unit Commitment Problem. **IEEE Trans. on Power Systems**, v. 30, n. 5, p. 2695–2705, Sept. 2015.

PEREIRA, M. V. F. Optimal Scheduling of Hydrothermal Systems - An Overview. **IFAC Proceedings Volumes**, v. 18, n. 7, p. 1–9, 1985.

PEREIRA, M. V. F. Optimal Stochastic Operations Scheduling of Large Hydroelectric Systems. **International Journal of Electrical Power & Energy Systems**, v. 11, n. 3, p. 161–169, 1989.

PEREIRA, M. V. F.; PINTO, L. M. V. G. Multi-stage Stochastic Optimization Applied to Energy Planning. **Mathematical Programming**, v. 52, n. 1, p. 359–375, 1991.

PEREIRA, M. V. F.; PINTO, M. V. G. Stochastic Optimization of a Multireservoir Hydroelectric System: A Decomposition Approach. **Water Resour. Res.**, v. 21, n. 6, p. 779–792, June 1985.

PHILPOTT, A. B.; GUAN, Z. On the convergence of stochastic dual dynamic programming and related methods. **Operations Research Letters**, v. 36, n. 4, p. 450–455, 2008.

PINA, A.; SILVA, C. A.; FERRÃO, P. High-resolution Modeling Framework for Planning Electricity Systems with High Penetration of Renewables. **Applied Energy**, v. 112, p. 215–223, 2013.

PINA, A.; SILVA, C. A.; FERRÃO, P. Modeling Hourly Electricity Dynamics for Policy Making in Long-Term Scenarios. **Energy Policy**, v. 39, p. 4692–4702, 2011.

PINEDA, S.; MORALES, J. M. Chronological Time-Period Clustering for Optimal Capacity Expansion Planning with Storage. **IEEE Transactions on Power Systems**, v. 33, n. 6, p. 7162–7170, 2018.

RAHMANIANI, R.; CRAINIC, T. G.; GENDREAU, M.; REI, W. The Benders Decomposition Algorithm: A Literature Review. **European Journal of Operational Research**, v. 259, n. 3, p. 801–817, 2016.

RAZAVI, S.-E; NEZHAD, A. E.; MAVALIZADEH, H.; RAEISI, F.; AHMADI, A. Robust Hydrothermal Unit Commitment: A Mixed-integer Linear Framework. **Energy**, v. 165, p. 593–602, Dec. 2018.

SANTOS, T. N.; DINIZ, A. L. A New Multiperiod Stage Definition for the Multistage Benders Decomposition Approach Applied to Hydrothermal Scheduling. **IEEE Trans. on Power Systems**, v. 24, n. 3, p. 1383–1392, Aug. 2009.

SANTOS, T. N.; DINIZ, A. L.; SABIOA, C. H.; CABRAL, R. N.; CERQUEIRA, L. F. Hourly Pricing and Day-ahead Dispatch Setting in Brazil: The Dessem Model. **Electric Power System Research**, v. 189, n. 1, p. 106709, Aug. 2020.

SCUZZIATO, M. R.; FINARDI, E. C.; FRANGIONI, A. Comparing Spatial and Scenario Decomposition for Stochastic Hydrothermal Unit Commitment Problems. **IEEE Trans. Sustain. Energy**, v. 9, n. 3, p. 1307–1317, July 2018.

SEGUIN, S.; COTE, P.; AUDET, C. Self-scheduling Short-term Unit Commitment and Loading Problem. **IEEE Trans. on Power Systems**, v. 31, n. 1, p. 133–142, Jan. 2016.

SHAHIDEHPOUR, M.; DING, T.; MING, Q.; HUANG, C.; WANG, Z.; DU, P. Multi-Period Active Distribution Network Planning Using Multi-Stage Stochastic Programming and Nested Decomposition by SDDIP. **IEEE Trans. on Power Systems**, v. 36, n. 3, p. 2281–2292, May 2021.

SHIN, S.; ZAVALA, V. M. Diffusing-Horizon Model Predictive Control. **IEEE Trans. on Automatic Control**, Dec. 2021.

SHIN, S.; ZAVALA, V. M. Multi-Grid Schemes for Multi-Scale Coordination of Energy Systems. **Energy Markets and Responsive Grids**, p. 195–222, 2018.

SUNDAR, K.; NAGARAJAN, H.; LUBIN, M.; ROALD, L.; MISRA, S.; BENT, R.; BIENSTOCK, D. Unit Commitment with N-1 Security and Wind Uncertainty. In: 2016 POWER SYSTEMS COMPUTATION CONFERENCE, p. 1–7.

TAWARMALANI, M.; SAHINIDIS, N. V. A Polyhedral Branch-and-cut Approach to Global Optimization. **Mathematical Programming**, p. 225–249, 2005.

TEJADA-ARANGO, D. A; WOGRIN, S.; CENTENO, E. Representation of Storage Operations in Network-Constrained optimization Models for Medium- and Long-Term Operations. **IEEE Trans. on Power Systems**, v. 33, n. 1, p. 386–396, 2018.

TONG, B.; ZHAI, Q.; GUAN, X. An MILP Based Formulation for Short-term Hydro Generation Scheduling with Analysis of the Linearization Effects on Solution Feasibility. **IEEE Trans. on Power Systems**, v. 28, n. 4, p. 3588–3599, Nov. 2013.

VIELMA, J. P. Mixed Integer Linear Programming Formulation Techniques. **Society for Industrial and Applied Mathematics Review**, v. 57, n. 1, p. 3–57, Feb. 2015.

VIELMA, J. P.; AHMED, S.; NEMHAUSER, G. Mixed Integer Models for Nonseparable Piecewise-Linear Optimization: Unifying Framework and Extensions. **Operations Research**, v. 58, n. 2, p. 303–315, Apr. 2010.

WOGRIN, S.; DUEÑAS, P.; DELGADILLO, A.; RENESES, J. A New Approachto Model Load Levels in Electric Power Systems With High Renewable Penetration. **IEEE Trans. on Power Systems**, v. 29, n. 5, p. 2210–2218, 2014.

WOGRIN, S.; GALBALLY, D.; RENESES, J. Optimizing Storage Operations in Medium- and Long-Term Power Systems Models. **IEEE Trans. on Power Systems**, v. 31, n. 4, p. 3129–3138, 2016.

WU, L.; SHAHIDEHPOUR, M. Accelerating the Benders Decomposition for Network-Constrained Unit Commitment Problems. **Energy Systems**, v. 1, n. 3, p. 339–376, Aug. 2010.

XU, W.; ANITESCU, M. Exponentially Accurate Temporal Decomposition for Long-Horizon Linear-Quadratic Dynamic Optimization. **SIAM Journal on Optimization**, v. 28, n. 3, p. 2541–2573, 2018.

XU, Y.; DONG, Z. Y.; ZHANG, R.; XUE, Y.; HILL, D. J. A Decomposition-Based Practical Approach to Transient Stability-Constrained Unit Commitment. **IEEE Trans. on Power Systems**, v. 30, n. 3, p. 1455–1464, May 2015.

ZIMMERMAN, R. D.; MURILLO-SANCHEZ, C. E.; THOMAS, R. J. MATPOWER: Steady-State Operations, Planning, and Analysis Tools for Power Systems Research and Education. **IEEE Trans. on Power Systems**, v. 26, n. 1, p. 12–19, Feb. 2011.

ZOU, J.; AHMED, S.; SUN, X. A. Multistage Stochastic Unit Commitment Using Stochastic Dual Dynamic Integer Programming. **IEEE Trans. on Power Systems**, v. 34, n. 3, p. 1814–1823, May 2019.

ZOU, J.; AHMED, S.; SUN, X. A. Stochastic Dual Dynamic Integer Programming. **Mathematical Programming**, v. 175, n. 1-2, p. 461–502, May 2019.

APPENDIX A – DATA OF MODIFIED IEEE 118-BUS SYSTEM

This appendix contains the data of the modified IEEE 118-bus system used in the simulations of this thesis. Concerning the thermoelectric costs, demand factor for each bus, and network, all these data are the same from the IEEE-118 system (IEEE, 2022). The modifications performed were replacing 14 thermoelectric plants for 15 hydro plants and the load curve for a planning horizon of 168 hours. The load curve of the system is shown in Figure 55, and the values of the total demand of the system (P) for 168 hours are presented in Table 31. All data belonging to this system can be found at `https://github.com/kennyvinente/scucdata`.

Figure 55 – Demand curve of modified IEEE-118 system.

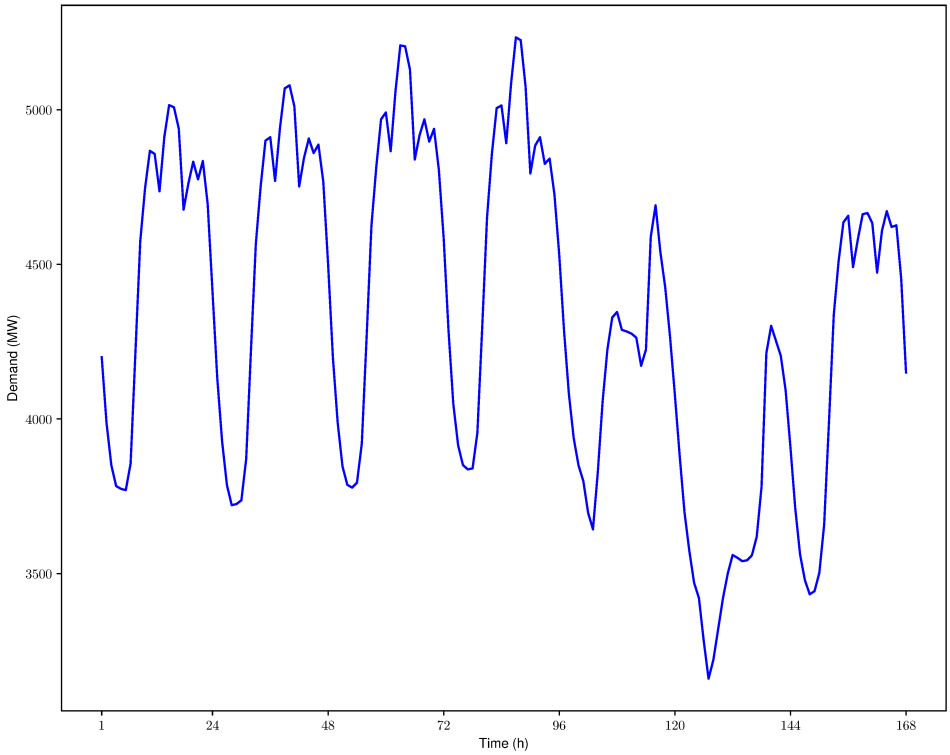

Source: Author.

The thermoelectric (g) removed from the IEEE-118 bus system and their respective bus location are presented in Table 32, obeying the respective labeled number from the original system.

For the hydro plants (h), their data are presented in Tables 33-41. It is important to note that the polynomials referring to the Hill curves are fictitious since this information has industrial property secrecy. All hydro plants have the same type of GUs. In Table 33, LRV means that the hydro plant has a large reservoir, while ROR means the hydro is a run of river, and SINF concerns if the spillage influences the tailrace level. The

Table 31 – Hourly load data

t	P (MW)	t	P (MW)	t	P (MW)	t	P (MW)	t	P (MW)
1	4200	37	4770	73	4288	109	4288	145	3711
2	3987	38	4939	74	4049	110	4283	146	3562
3	3850	39	5069	75	3915	111	4276	147	3479
4	3783	40	5079	76	3851	112	4263	148	3433
5	3774	41	5011	77	3837	113	4172	149	3443
6	3770	42	4752	78	3840	114	4224	150	3502
7	3856	43	4844	79	3955	115	4589	151	3658
8	4213	44	4907	80	4295	116	4691	152	3989
9	4574	45	4860	81	4650	117	4539	153	4337
10	4746	46	4887	82	4855	118	4426	154	4510
11	4867	47	4768	83	5005	119	4266	155	4636
12	4857	48	4502	84	5014	120	4079	156	4657
13	4736	49	4199	85	4892	121	3882	157	4491
14	4912	50	3987	86	5085	122	3699	158	4581
15	5015	51	3846	87	5234	123	3574	159	4662
16	5008	52	3787	88	5225	124	3470	160	4666
17	4939	53	3778	89	5076	125	3421	161	4633
18	4677	54	3794	90	4794	126	3282	162	4473
19	4762	55	3920	91	4884	127	3160	163	4608
20	4832	56	4263	92	4911	128	3221	164	4672
21	4775	57	4264	93	4825	129	3322	165	4621
22	4834	58	4813	94	4842	130	3421	166	4626
23	4695	59	4969	95	4726	131	3501	167	4453
24	4412	60	4991	96	4530	132	3560	168	4150
25	4130	61	4866	97	4284	133	3551		
26	3927	62	5060	98	4081	134	3540		
27	3786	63	5208	99	3938	135	3543		
28	3721	64	5205	100	3850	136	3559		
29	3725	65	5130	101	3799	137	3619		
30	3737	66	4839	102	3696	138	3780		
31	3871	67	4918	103	3643	139	4213		
32	4226	68	4969	104	3827	140	4301		
33	4566	69	4897	105	4056	141	4252		
34	4752	70	4938	106	4225	142	4204		
35	4900	71	4806	107	4328	143	4093		
36	4911	72	4585	108	4346	144	3909		

Source: Author.

inflow data is referred to each day, i.e., for any instant of time of that day, the inflow is the same.

Table 32 – Thermoelectric removed from IEEE 118-bus system

g	bus	g	bus
5	12	17	40
7	18	18	42
10	25	21	54
11	26	23	56
14	32	25	61
15	34	28	66
16	36	53	113

Source: Author.

Table 33 – Hydroelectric data

h	name	bus	$\overline{\mathbf{php}}$ (MW)	$\overline{\mathbf{q}}$ (m^3/s)	$\underline{\mathbf{q}}$ (m^3/s)	$\overline{\mathbf{S}}$ (m^3/s)	$\lvert\mathcal{J}\rvert$	SINF	type
1	Promissão	12	265	431	297.4	8620	3	yes	LRV
2	Barra Bonita	18	140	189	118.2	3780	4	yes	LRV
3	N. Avanhandava	25	375	477	331.8	8620	3	yes	ROR
4	Jupiá	26	605	596	298	50128	5	yes	ROR
5	Bariri	32	144	257	182.2	4136	3	yes	ROR
6	Monjolinho	34	74	71	50.9	6755	2	yes	ROR
7	Quebra Queixo	36	120	38	27.2	5000	3	yes	LRV
8	São José	40	56	144	102.3	11700	2	yes	ROR
9	Passo São João	42	78	163	115	11570	2	yes	ROR
10	Passo Fundo	54	226	51	36.4	2250	2	no	LRV
11	Pedra do Cavalo	56	160	90	63.6	12000	2	yes	LRV
12	Balbina	59	250	255	168	5800	5	yes	LRV
13	Garibaldi	61	186	167	118.7	17360	3	yes	LRV
14	Foz do Chapecó	66	855	489	348.3	62190	4	no	ROR
15	Ibitinga	113	133	234	165.5	4680	3	yes	ROR

Source: Author.

Table 34 – Coefficients of hydroelectric forebay level polynomials

h	$\mathbf{F}_0$	$\mathbf{F}_1$	$\mathbf{F}_2$	$\mathbf{F}_3$	$\mathbf{F}_4$
1	369.6938	-5.249989E-4	1.08299E-6	-1.6016E-10	7.927737E-15
2	432.7839	0.0149645	-6.70742E-6	1.75977E-9	-1.69823E-13
3	358	0	0	0	0
4	280	0	0	0	0
5	427.5	0	0	0	0
6	174.9	3.587054	-0.03450381	1.553922E-4	-2.620451E-7
7	503.9448	0.541329	-0.00196869	3.08552E-6	0
8	154.67	0	0	0	0
9	118.5711	0.1861556	-0.001278737	3.841826E-6	0
10	580.3909	0.0221501	-1.41343E-5	6.344678E-9	-1.15472E-12
11	65.90313	0.03003821	-7.557153E-6	1.168574E-9	-7.571734E-14
12	36.95247	0.001339282	-5.455607E-8	1.446067E-12	-1.554142E-17
13	693.2867	0.03963221	0	0	0
14	244.7873	0.01345915	-1.927264E-10	8.457124E-14	-1.387779E-17
15	404	0	0	0	0

Source: Author.

Table 35 – Coefficients of hydroelectric tailrace level polynomials

h	$\mathbf{G}_0$	$\mathbf{G}_1$	$\mathbf{G}_2$	$\mathbf{G}_3$	$\mathbf{G}_4$
1	358.0039	-2.40967E-4	5.598189E-7	-1.2308E-10	8.030587E-15
2	427.5408	-8.052159E-4	3.08062E-6	-1.3497E-9	1.90171E-13
3	323.085	0.004314847	-2.13336E-6	5.67896E-10	-5.37797E-14
4	253.441	5.786598E-4	1.44023E-8	-1.41555E-12	2.609049E-17
5	403.9468	4.802749E-4	1.55539E-6	-8.13472E-10	1.21667E-13
6	264.9243	0.002269349	3.017191E-7	-1.656882E-10	1.758906E-14
7	426.0178	0.008268859	-2.409649E-5	3.49374E-8	-1.806209E-11
8	130.6639	0.002290688	-2.354779E-7	1.855546E-11	-5.689697E-16
9	97.55073	0.006214246	-5.315673E-6	3.541552E-9	-9.312565E-13
10	335.0999	0.008166667	-5.666669E-6	0	0
11	4.14481	0.005542674	-5.100707E-6	2.870954E-9	-6.078898E-13
12	22.57763	0.007527882	-4.957306E-6	2.01131E-9	-3.0082E-13
13	659.9229	0.001509382	1.604493E-8	-7.742374E-11	1.447932E-14
14	210.7079	0.001545053	-1.58656E-7	1.221691E-11	-3.688747E-16
15	379.348	0.00225722	1.96279E-7	-3.23657E-10	5.8838E-14

Source: Author.

Table 36 – Coefficients of GU yield polynomials referring to hydro *h*

h	$\mathbf{I}_0$	$\mathbf{I}_1$	$\mathbf{I}_2$	$\mathbf{I}_3$	$\mathbf{I}_4$	$\mathbf{I}_5$
1	0.358727	0.002413	0.013761	3.18E-5	-5.2E-6	-4.5E-4
2	0.358727	0.005503	0.014696	7.74E-5	-2.7E-5	-5.2E-4
3	0.358727	0.00218	0.010207	2.13E-5	-4.2E-6	-2.5E-4
4	0.358727	0.001745	0.013378	2.23E-5	-2.7E-6	-4.3E-4
5	0.358727	0.004047	0.015045	5.83E-5	-1.5E-5	-5.4E-4
6	0.358727	0.014649	0.005679	7.96E-5	-1.9E-4	-7.7E-5
7	0.358727	0.027371	0.002956	7.75E-5	-6.6E-4	-2.1E-5
8	0.358727	0.007223	0.014999	1.04E-4	-4.6E-5	-5.4E-4
9	0.358727	0.006381	0.011531	7.04E-5	-3.6E-5	-3.2E-4
10	0.358727	0.020394	0.001375	2.68E-5	-3.7E-4	-4.5E-6
11	0.358727	0.011557	0.003249	3.59E-5	-1.2E-4	-2.5E-5
12	0.358727	0.004079	0.01253	4.89E-5	-1.5E-5	-3.8E-4
13	0.358727	0.006228	0.007963	4.75E-5	-3.4E-5	-1.5E-4
14	0.358727	0.002127	0.006681	1.36E-5	-4.0E-6	-1.1E-4
15	0.358727	0.014427	0.014427	6.14E-5	-1.8E-5	-5.0E-4

Source: Author.

Table 37 – Coefficients of GU penstock losses referring to hydro *h*

h	$\mathbf{D}$
1	2.636290E-6
2	5.571512E-6
3	2.16346E-6
4	8.334928E-7
5	3.0114E-6
6	3.420351E-6
7	2.873912E-3
8	2.797067E-5
9	1.204411E-5
10	2.801422E-3
11	2.716049E-4
12	5.843906E-6
13	3.478073E-5
14	7.106464E-6
15	5.420410E-6

Source: Author.

Table 38 – Reservoir data

h	*h* in downstream	τ (hours)	$\overline{\mathbf{V}}$ (hm^3)	$\underline{\mathbf{V}}$ (hm^3)
1	3	1	7408	5280
2	5	2	3135	569
3	4	3	2738.5	2340.5
4	-	-	3353.75	2450
5	15	1	544.2	485.29
6	14	1	150.553	139.573
7	-	-	136.63	111.12
8	9	0	188.1	165.53
9	-	-	102.4	77.5
10	6	1	1588.61	184
11	-	-	3134	2187
12	-	-	20006.22	9711.9
13	14	1	296	232
14	-	-	1501.8	1427.5
15	1	1	983.16	926.91

Source: Author.

Table 39 – Initial conditions of hydro plants

h	$\mathbf{V}_0$ (%)	$\mathbf{Q}_0$	$\mathbf{S}_0$
1	36.91	0	0
2	58.81	0	0
3	94.74	0	0
4	87.35	0	0
5	59.97	0	0
6	100	0	0
7	99.57	0	0
8	78	0	0
9	87.88	0	0
10	65.15	0	0
11	90.27	0	0
12	43.01	0	0
13	49.83	0	0
14	74.73	0	0
15	47.50	0	0

Source: Author.

Table 40 – Inflow data (m^3/s)

h	day 1	day 2	day 3	day 4	day 5	day 6	day 7
1	586.96	525.24	464.06	341.52	222	343.87	369.99
2	553.50	373.56	307.08	308.06	311.46	280.86	277
3	344.89	181.85	158.7	162.7	186.85	163.7	246
4	4173.38	4128.5	5497.08	4344.15	4035.38	4302.19	4845
5	392.95	247.42	244.52	256.32	245.62	281.81	334.48
6	32	88.04	90.13	92.64	37.92	102.51	99.6
7	139.53	150.07	140.65	134.69	112.98	110.6	108.75
8	347.52	280.58	229.55	208.9	208.19	227.1	329.71
9	346.09	349.91	258.44	279.53	257.81	255.81	282.99
10	36.34	27.66	29.89	32.77	31.07	47.93	59.04
11	28.98	28.84	24.87	20.14	19.64	17.81	15.4
12	1434.28	1917.5	1683.59	1405.55	1359.91	1209.63	1455.81
13	220.45	212.61	183.6	145.06	142.55	198.97	248.07
14	650.78	1038.69	832.13	545.3	360.52	915.17	1064.74
15	469	429.46	357.15	321.58	227.97	353.85	349.69

Source: Author.

Table 41 – Coefficients of FCF

h	**M0**	**M0**
1	671.581944	671.581944
2	515.5	515.5
3	909.284722	909.284722
4	171.833333	100.236111
5	658.694444	658.694444
6	1789.930555	1789.930555
7	1606.820659	1264.943923
8	329.7768055	329.776805
9	431.874444	431.874444
10	7370.934027	7370.934027
11	3044.671875	3044.671875
12	11.713305	11.713305
13	1240.063888	1240.063888
14	1457.719444	1457.719444
15	668.360069	668.360069
M1	2.102811E8	2.100363E8

Source: Author.

APPENDIX B – MILP FORMULATION FOR THE PRODUCT BETWEEN A CONTINUOUS AND A BINARY VARIABLE

This appendix presents a MILP formulation for a product between a continuous variable x and a binary variable u. If x is bounded below by zero and above by $\overline{x}$, then the product $y = x \cdot u$ can be reformulated as:

$$y \leq \overline{x} \cdot u \tag{69}$$

$$y \leq x \tag{70}$$

$$y \geq x - (1-u)\overline{x} \tag{71}$$

$$y \geq 0 \tag{72}$$

If x is limited by $[\underline{x}, \overline{x}]$, and assuming $\overline{x}$ to be positive, the product $y = x \cdot u$ can be reformulated as:

$$\min\{0, \underline{x}\} \leq y \leq \overline{x} \tag{73}$$

$$\underline{x}u \leq y \leq \overline{x}u \tag{74}$$

$$x - (1-u)\overline{x} \leq y \leq x - (1-u)\underline{x} \tag{75}$$

$$y \leq x + (1-u)\overline{x} \tag{76}$$